Międzyuczelniany Wydział Biotechnologii
Uniwersytetu Gdańskiego
i Gdańskiego Uniwersytetu Medycznego

ROZPRAWA DOKTORSKA

mgr Karolina Zdrojewska

Biochemiczna i funkcjonalna charakterystyka polimerazy DNA kodowanej przez bakteriofaga vB_EfaS-271

Biochemical and functional characterization of the DNA polymerase encoded by bacteriophage vB_EfaS-271

Praca przedstawiona
Radzie Dyscypliny Biotechnologia Uniwersytetu Gdańskiego
celem uzyskania stopnia doktora
w dziedzinie nauk ścisłych i przyrodniczych
w dyscyplinie naukowej biotechnologia

Promotorzy: dr hab. Michał R. Szymański, prof. UG
Laboratorium Biologii Strukturalnej
Międzyuczelniany Wydział Biotechnologii UG i GUMed

prof. dr hab. Alicja Węgrzyn
Centrum Terapii Fagowej
Uniwersytecki Ośrodek Badań Stosowanych i Międzyobszarowych

GDAŃSK 2026

Dokument zanonimizowany za pomocą UG DLP Anonimizator, 2026-10-08 12:13:43

Międzyuczelniany Wydział Biotechnologii
Uniwersytetu Gdańskiego i Gdańskiego Uniwersytetu Medycznego

mgr Karolina Zdrojewska

Biochemiczna i funkcjonalna charakterystyka polimerazy DNA kodowanej przez bakteriofaga vB_EfaS-271

Biochemical and functional characterization of the DNA polymerase encoded by bacteriophage vB_EfaS-271

Praca przedstawiona
Radzie Dyscypliny Biotechnologia Uniwersytetu Gdańskiego
celem uzyskania stopnia doktora
w dziedzinie nauk ścisłych i przyrodniczych
w dyscyplinie naukowej biotechnologia

Promotorzy: dr hab. Michał R. Szymański, prof. UG
Laboratorium Biologii Strukturalnej
Międzyuczelniany Wydział Biotechnologii UG i GUMed

prof. dr hab. Alicja Węgrzyn
Centrum Terapii Fagowej
Uniwersytecki Ośrodek Badań Stosowanych i Międzyobszarowych

GDAŃSK 2026

This doctoral dissertation was made possible thanks to funding from the following projects:

1. The EMBO Installation Grant (4129) awarded to dr. hab. Michał R. Szymański by the European Molecular Biology Organization



2. NCN OPUS 23 UMO-2022/45/B/NZ1/02680 awarded to prof. Alicja Węgrzyn



3. NAWA, The Bekker programme BPN/BEK/2023/1/00313/DEC/1 awarded to Karolina Zdrojewska



Rozumowi nie ufam samowładnie – ale, kochając ludzi, nie uważam za zbrodnię ich rozumieć.

- Cyprian Kamil Norwid, Pisma wybrane, Listy

I would like to thank Dr hab. Michał R. Szymański for his valuable comments, which helped me refine the research methodology, as well as for his consultations at various stages of this work.

I would like to thank Prof. Dr hab. Alicja Węgrzyn for her substantive support and for the kindness I could always rely on throughout the course of this work.

I would also like to thank Prof. Roberto Galletto from Washington University in St. Louis, USA, for the opportunity to complete a one-year research stay under his supervision, and for introducing me to the methods and techniques that became a part of this work.

I would like to thank the team at Laboratory of Structural Biology for their help, willingness to share knowledge, and the friendly working atmosphere every day.

I would like to thank my family and friends for their support and belief in me throughout this time.

To my husband, Paweł, I owe a special thank you – for his everyday support, patience and for always being someone I could count on.

Table of Contents

1. Streszczenie 9

2. Abstract 11

3. List of abbreviations 13

4. Introduction 15

4.1. DNA replication and polymerase function 15

4.2. Isothermal amplification: current enzyme limitations 21

4.3. Cold-adapted enzymes - mechanisms and examples 29

4.4. Bacteriophages as sources of DNA polymerases 31

4.5. Discovery and uniqueness of DNA polymerase Efa 33

5. Aims of the Thesis 35

6. Materials and methods 36

6.1. Construction of Efa expression plasmids 36

6.2. Protein overproduction 36

6.3. Protein purification 44

6.3.1. Analytical size-exclusion chromatography 45

6.4. Circular dichroism (CD) spectroscopy 45

6.5. Preparation of DNA substrates 46

6.6. DNA polymerase and exonuclease activity assays 49

6.7. Kinetic analysis 49

6.8. Temperature-dependence studies 51

6.9. Primer extension at low temperature 51

6.10. X-ray crystallography 52

6.10.1. Apoenzyme protein crystallization 52

6.10.2. Bioinformatic identification of the DEDD exonuclease motif 52
6.10.3. Holoenzyme protein crystallization 53
6.11. AlphaFold prediction of Efa as a molecular replacement model 54
6.12. X-ray diffraction data collection and structure determination 54
6.12.1. Apoenzyme structure determination 54
6.12.2. Holoenzyme complex structures 55
6.12.3. Model building, refinement and validation 55
6.13. Bioinformatic analyses of the N-terminal region 56
6.14. Molecular graphics and analysis in ChimeraX 56
7. Results 57
7.1. Protein overproduction and purification 57
7.2. Polymerase and exonuclease activities 58
7.3. Cold-adapted activity 63
7.4. Structural characterization 66
7.4.1. Apo-enzyme crystal structure 66
7.4.2. Prediction of residues responsible for 3′→5′ exonuclease activity 67
7.4.3. Ternary holo-enzyme complexes (engaged vs. loose N-terminal conformation). 72
7.5. N-terminal domain: bioinformatic identification, creating the Efa Δ27-124 construct and functional analysis 76
7.5.1. Bioinformatic identification 76
7.5.2. Construction of the Efa Δ27-124 mutant 77
7.5.3. Functional characterization of the Efa ΔN variant 78
7.5.4. Performance on structured hairpin templates 81
7.6. Kinetic analysis 82

7.6.1. Pre-steady-state burst kinetics 84
7.6.2. Single-turnover kinetics at low temperature 86
7.6.3. Apparent dCTP dependence and the role of the N-terminus 97
8. Discussion 101
8.1. Biotechnological relevance of a cold-active polymerase 101
8.2. Comparative assessment with classical polymerase 102
8.3. Mechanistic insight: N-terminal SSB-like function 103
8.4. Implications for engineering new isothermal enzymes 106
8.5. Study limitations 107
8.6. Future directions 108
8.7. Concluding remarks 109
9. References 110
10. Scientific Meetings and Trainings 123
11. Scholarships and Fellowships 125
12. Lists of Publications 126
13. List of patent applications 127

1. Streszczenie

Większość polimeraz DNA traci wydajność katalityczną wraz ze spadkiem temperatury poniżej 20°C. Stanowi to fundamentalne ograniczenie dla metod diagnostyki izotermalnej, zwłaszcza przeznaczonych do zastosowań terenowych, które powinny funkcjonować bez aktywnego ogrzewania. Niniejsza praca rozpoczęła się od odkrycia w genomie bakteriofaga vB_EfaS-271, wyizolowanego ze ścieków w Gdańsku, genu kodującego nieopisaną wcześniej polimerazę DNA z rodziny B, nazwaną Efa. Enzym ten wykazał wyjątkowo wysoką aktywność w niskich temperaturach. Testy wydłużania startera potwierdziły wydajną syntezę DNA w zakresie od -5 do 50°C. Bezpośrednie porównania przeprowadzone w temperaturze -10°C wykazały, że Efa syntetyzuje produkt pełnej długości. Natomiast polimerazy T4, T7 oraz Pol I z *E. coli* pozostają praktycznie nieaktywne. Wyniki te doprowadziły do postawienia istotnego pytania mechanistycznego: jakie adaptacje molekularne umożliwiają polimerazie Efa prowadzenie syntezy DNA w warunkach, w których większość polimeraz przestaje funkcjonować?

Pierwszych wskazówek dostarczyły analiza sekwencji aminokwasowej oraz predykcja struktury białka. Efa posiada typowy dla polimeraz z rodziny B rdzeń katalityczny obejmujący domeny dłoni, palców, kciuka oraz domenę egzonukleazową 3'→5'. Jednocześnie zawiera dodatkową domenę N-końcową (reszty 27-124), tworzącą fałd OB (*oligonucleotide-binding fold*), który jest motywem strukturalnym charakterystycznym dla białek wiążących jednoniciowe DNA. Przykładami takich białek są bakteryjne białka SSB (*single-stranded DNA-binding proteins*) czy eukariotyczne białka RPA (*replication protein* A). W celu określenia funkcji tej domeny skonstruowano wariant delecyjny Efa ΔN, pozbawiony regionu N-końcowego. W temperaturze 10°C polimeraza typu dzikiego wbudowywała nukleotydy w warunkach pojedynczego cyklu katalitycznego (*single-turnover*) ze stałą szybkości obserwowanej wynoszącej 27,3 s^{-1}, podczas gdy aktywność wariantu Efa ΔN była ponad 500-krotnie niższa (0,05 s^{-1}). Różnice te były szczególnie widoczne podczas syntezy na matrycach zawierających struktury typu spinki do włosów. Polimeraza typu dzikiego skutecznie wydłużała starter przez obszary o strukturze drugorzędowej, wytwarzając produkt pełnej długości, natomiast wariant delecyjny zatrzymywał syntezę w miejscu rozpoczęcia struktury spinki do włosów.

Krystalografia rentgenowska pozwoliła wyjaśnić strukturalne podstawy tej adaptacji do niskich temperatur. Strukturę apoenzymu wyznaczono z rozdzielczością 2,3 Å, ujawniając obecność N-końcowego fałdu OB położonego nad rdzeniem polimerazy. Analiza kompleksów trójskładnikowych z matrycą starterową wykazała występowanie dwóch odmiennych stanów konformacyjnych. W pierwszym z nich domena OB oddziałuje z sześcionukleotydowym jednoniciowym końcem 5′ poprzez kontakty z udziałem reszt K53, Y74, R79 i F105. W drugim stanie, obserwowanym przy czteronukleotydowym końcu jednoniciowym, domena odchyla się o około 4 Å i obraca o 22°. Zmiany konformacyjne bezpośrednio przekładają się na właściwości kinetyczne enzymu. W obecności długich jednoniciowych końców polimeraza typu dzikiego charakteryzowała się szybkim wbudowywaniem pojedynczego nukleotydu, natomiast skrócenie końca do czterech nukleotydów powodowało ~130-krotny spadek wartości k_{obs}, upodabniając zachowanie enzymu do obserwowanego dla wariantu Efa ΔN. Analiza Arrheniusa wykazała ponadto, że związanie domeny N-końcowej z jednoniciowym DNA wiąże się z inną pozorną zależnością temperaturową obserwowanej szybkości reakcji w badanych warunkach.

Podsumowując, uzyskane wyniki wspierają model, w którym Efa, według naszej wiedzy, jest pierwszą pochodzącą od bakteriofaga zimnoaktywną polimerazą DNA z rodziny B scharakteryzowaną na poziomie strukturalnym. Wykazano, że jej N-końcowy fałd OB pełni funkcję zintegrowanego modułu przypominającego białka SSB, stabilizując jednoniciowe DNA oraz przyspieszając przyłączanie nukleotydów w niskich temperaturach. Architektura ta, łącząca klasyczny rdzeń polimerazy z dodatkową domeną wiążącą DNA, która w sposób dynamiczny oddziałuje z matrycą zależnie od długości jednoniciowego końca, stanowi naturalny model dla projektowania wielodomenowych polimeraz o pożądanych właściwościach temperaturowych. Unikalne cechy polimerazy Efa czynią ją obiecującą platformą do opracowania niskotemperaturowych metod amplifikacji izotermalnej zdolnych do działania w temperaturze otoczenia bez specjalistycznych urządzeń grzewczych, co może istotnie zwiększyć dostępność diagnostyki molekularnej w warunkach ograniczonych zasobów.

2. Abstract

Most DNA polymerases lose catalytic efficiency as temperature drops below 20°C, creating a fundamental barrier for field-deployable isothermal diagnostics that must operate without active heating. This work began with a gene found in the genome of bacteriophage vB_EfaS-271, isolated from Gdańsk sewage, encoding a previously uncharacterized B-family DNA polymerase designated Efa. The enzyme proved remarkably cold-active: primer extension assays showed robust DNA synthesis from -5°C to 50°C. Direct comparisons at -10°C revealed that Efa generates a full-length product, whereas T4, T7, and *E. coli* Pol I remain essentially inactive. This raised a compelling mechanistic question: what molecular adaptations allow Efa to catalyze DNA synthesis when most polymerases cease to function?

Sequence analysis and structural prediction provided the first clue. Efa possesses a canonical B-family polymerase core (palm, fingers, thumb, and 3' to 5' exonuclease domains) but carries an unexpected N-terminal extension (residues 27-124) that folds into an oligonucleotide-binding (OB) fold, a motif normally found in single-stranded DNA-binding proteins such as bacterial SSB or eukaryotic RPA. To probe its function, we generated a truncated variant, Efa ΔN, lacking this domain. At 10°C, wild-type Efa incorporated nucleotides under single-turnover conditions with an observed rate constant of 27.3 s^{-1}, whereas Efa ΔN was more than 500 times slower (0.05 s^{-1}). On structured hairpin templates, wild-type Efa extended through secondary structure to produce full-length product, while the truncated mutant accumulated exclusively at the stall site.

X-ray crystallography revealed the structural basis of this cold adaptation. The apoenzyme structure at 2.3-Å resolution showed the N-terminal OB-fold perched above the polymerase core. Ternary complexes with primer-template DNA captured two distinct conformational states: an engaged state, in which the OB-fold clamps a 6-nucleotide 5-prime overhang through contacts involving K53, Y74, R79, and F105, and a loose state (with a 4-nucleotide overhang), in which the domain swings away by 4 Ångströms and rotates by 22 degrees. This structural switching translates directly into kinetic control. On long overhangs, wild-type Efa displayed rapid single-nucleotide incorporation. Shortening the overhang to 4 nucleotides reduced k_{obs} by approximately 130-fold, collapsing its behavior to that of the truncated

mutant. Arrhenius analysis showed that N-terminal engagement was associated with a different apparent temperature dependence of the observed reaction under the conditions tested.

Together, these data support a model in which Efa is, to our knowledge, the first structurally characterized cold-active B-family polymerase from a bacteriophage and reveal that its N-terminal OB-fold functions as an integrated SSB module that stabilizes single-stranded DNA and accelerates nucleotide addition at low temperature. This modular architecture, a conventional polymerase core coupled to an accessory DNA-binding domain that dynamically engages the template depending on overhang length, provides a natural blueprint for engineering multi-domain polymerases with tailored temperature profiles. Efa's unique properties position it as a promising platform for developing low-temperature isothermal amplification technologies that could operate at ambient temperature without specialized heating equipment, expanding access to molecular diagnostics in resource-limited settings.

3. List of abbreviations

Å	Ångström
A	Amplitude (pre-steady-state kinetics)
A	Pre-exponential factor (temperature-dependence experiments)
A280	Absorbance at 280 nm
dATP	Deoxyadenosine triphosphate
CD	Circular dichroism
dCTP	2′-Deoxycytidine-5′-triphosphate
DNA	Deoxyribonucleic acid
dNTP(s)	Deoxyribonucleoside triphosphate(s)
DTT	Dithiothreitol
ε_{280}	Extinction coefficient at 280 nm
E_a	Activation energy
EDTA	Ethylenediaminetetraacetic acid
Efa ΔN	Efa DNA polymerase variant lacking residues 27-124
Efa DEDD	Efa DNA polymerase D137A E139A D188A D281A
FAM	6-Carboxyfluorescein (fluorescent label)
Flsn	Fluorescein (fluorescent label)
HDA	Helicase-dependent amplification
HEPES	4-(2-hydroxyethyl)-1-piperazineethanesulfonic acid
IA	Isothermal amplification
IPTG	Isopropyl β-d-1-thiogalactopyranoside
ipTM	Inter-chain predicted TM score
$K_{D,app}$	Apparent equilibrium dissociation constant
kDa	Kilodalton
k_{max}	Maximal observed incorporation rate
KleLF	Klenow fragment
k_{obs}	Observed rate constant
k_{ss}	Steady-state rate constant
LAMP	Loop-mediated isothermal amplification

LB	Lysogeny broth
MDA	Multiple displacement amplification
MWCO	Molecular weight cutoff
Ni-NTA	Nickel-nitrilotriacetic acid (affinity resin)
nt	Nucleotide(s)
OB-fold	Oligonucleotide-binding fold
OD_{600}	Optical density at 600 nm
PAGE	Polyacrylamide gel electrophoresis
PCR	Polymerase chain reaction
PDB	Protein Data Bank
pLDDT	Predicted local distance difference test
PMSF	Phenylmethylsulfonyl fluoride
POC	Point-of-care
pTM	Predicted TM score
RCA	Rolling-circle amplification
R_{free}	Free R-factor
RMSD	Root mean square deviation
RPA (method)	Recombinase polymerase amplification
RPA (protein)	Replication protein A
R_{work}	working R-factor
SDS	Sodium dodecyl sulphate
SDS-PAGE	Sodium dodecyl sulphate – polyacrylamide gel electrophoresis
SEC	Size exclusion chromatography
SSB	Single-stranded binding protein
ssDNA	Single-stranded DNA
SUMO	Small ubiquitin-like modifier (fusion tag)
TCEP	Tris(2-carboxyethyl) phosphine hydrochloride
T_m	Melting temperature
UV	Ultraviolet
WT	Wild-Type

4. Introduction

4.1. DNA replication and polymerase function

DNA replication is the foundation of cellular inheritance (Diffley, 1994; Hoeben & Uil, 2013; Kelman & Kelman, 2014). Its precise regulation ensures that each daughter cell inherits a precise copy of the genetic instructions specified by the parental genome. This process is coordinated by the replisome, a multiprotein complex that includes replicative polymerases, helicases, primases, clamp loaders, ligases and topoisomerases (Benkovic et al., 2001; Bertolin et al., 2025; Kitao et al., 2018). These components perform distinct but coordinated functions: helicases unwind the parental DNA duplex, primases synthesize RNA or DNA primers, clamp loaders and sliding clamps promote the stable association and processivity of DNA polymerase, ligases seal remaining nicks, and topoisomerases relieve torsional stress generated during DNA unwinding. Within this complex, DNA polymerase uses the parental DNA template and synthesizes a complementary strand by selecting nucleotides and catalyzing phosphodiester bond formation. This activity is essential for accurate duplication and transmission of genetic information (Ekundayo & Bleichert, 2019; Garcia-Diaz & Bebenek, 2007).

DNA polymerases are grouped into seven families (**Table 1**) (Feng et al., 2020; Ishino et al., 1998; Kannan et al., 2024; Yamtich & Sweasy, 2010; W. Yang, 2005). Families A, B, and C include the principal replicative polymerases of eukaryotes and bacteria: eukaryotic replicases (Pol alpha, delta, epsilon) belong to family B, bacterial replicative polymerases to families A (Pol I) and C (Pol III), and archaeal replicases to families B and D (Tahirov et al., 2009). Families X and Y are predominantly involved in DNA repair and translesion synthesis, respectively, while reverse transcriptases catalyze RNA-templated DNA synthesis (Garcia-Diaz & Bebenek, 2007; Kuznetsova et al., 2022). However, functional specialization is not absolute across families: family A includes repair polymerases (Pol theta) alongside replicases, and family Y members participate in damage tolerance pathways that interface with replication fork restart (Sale et al., 2012). Many DNA polymerases adopt a canonical ‘right-hand’ architecture with fingers, palm and thumb domains (**Fig.1**), but the degree of

structural conservation varies. Families A and B share the Klenow fold, while families X and C instead adopt the Pol beta fold, and family D polymerases possess a distinct double-psi beta-barrel fold not found in other families (Raia et al., 2019; Sauguet et al., 2016). This structural divergence reflects the independent evolutionary origins of the polymerase families, even though the core chemistry of nucleotide incorporation remains broadly conserved.

Table 1. Families of DNA polymerases (based on Morcinek-Orłowska et al., 2022)

Family	*Polymerase*	*Organism*	*Main function*	*Proofreading (3′-5′ exo)*
A	Pol I	Bacteria	Okazaki fragment processing, gap filling, long-patch BER	Yes (intrinsic)
B	T4 DNA pol	Virus (T4 phage)	Phage genome replication	Yes (intrinsic)
C	Pol III (DnaE)	Bacteria	Chromosomal replication	Yes (epsilon/ DnaQ subunit)
D	Pol D	Archaea	Chromosomal replication	Yes (DP1 subunit)
X	Pol beta	Eukaryota	Short-patch BER	Generally absent
Y	Pol eta	Eukaryota	TLS past cyclobutane pyrimidine dimers	Generally absent
RT	Telomerase (TERT)	Eukaryota	Telomere extension (RNA-dependent)	Generally absent

A single nucleotide incorporation cycle proceeds through a series of discrete steps. The polymerase first binds the primer-template DNA, forming a stable binary complex. Upon binding the correct dNTP, the fingers domain rotates inward and adopts a closed conformation that positions the nucleotide for catalysis a process known as induced fit. The chemical step, phosphoryl transfer, proceeds through a two-metal-ion mechanism in most polymerases and involves two divalent metal ions, typically Mg^{2+}. They are coordinated by conserved carboxylate residues in the palm domain (Brautigam & Steitz, 1998; Steitz, 1999).

In the best-characterized examples of this mechanism, metal A helps activate the primer 3′-hydroxyl for nucleophilic attack on the α-phosphate of the incoming dNTP, while metal B stabilizes the pyrophosphate leaving group and helps position the substrate (Gao & Yang, 2016). This catalytic architecture is broadly conserved across polymerase families, though the precise coordination geometry and the number of catalytically relevant metal ions can vary. Additional metal ions have been implicated in the active sites of some polymerases (Joyce & Benkovic, 2004). Following pyrophosphoryl transfer, pyrophosphate is released, the fingers reopen, and the polymerase translocates by one base pair to reset the active site for the next cycle (K. A. Johnson, 2010).

Within this classification, B-family polymerases are of particular interest. Many replicative B-family polymerases share a characteristic multi-domain organization comprising palm, fingers, and thumb domains that form the polymerase active site. In a subset of these enzymes, the polymerase core is accompanied by an N-terminal domain and a 3'→5' exonuclease domain responsible for proofreading. (Joyce & Benkovic, 2004; Tahirov et al., 2009). In polymerases that retain this activity, the exonuclease domain contains a conserved DEDD motif (four acidic residues) that coordinates two metal ions to excise misincorporated nucleotides. Communication between the exonuclease and polymerase active sites enables efficient switching between synthesis and proofreading modes. Well-studied B-family members include eukaryotic replicative polymerases alpha, delta, and epsilon; archaeal Pol B; and bacteriophage polymerases such as phi29 and T4. These last two serve as models for understanding processive DNA synthesis and protein-primed replication (Blanco et al., 1989; Reha-Krantz, 2010).

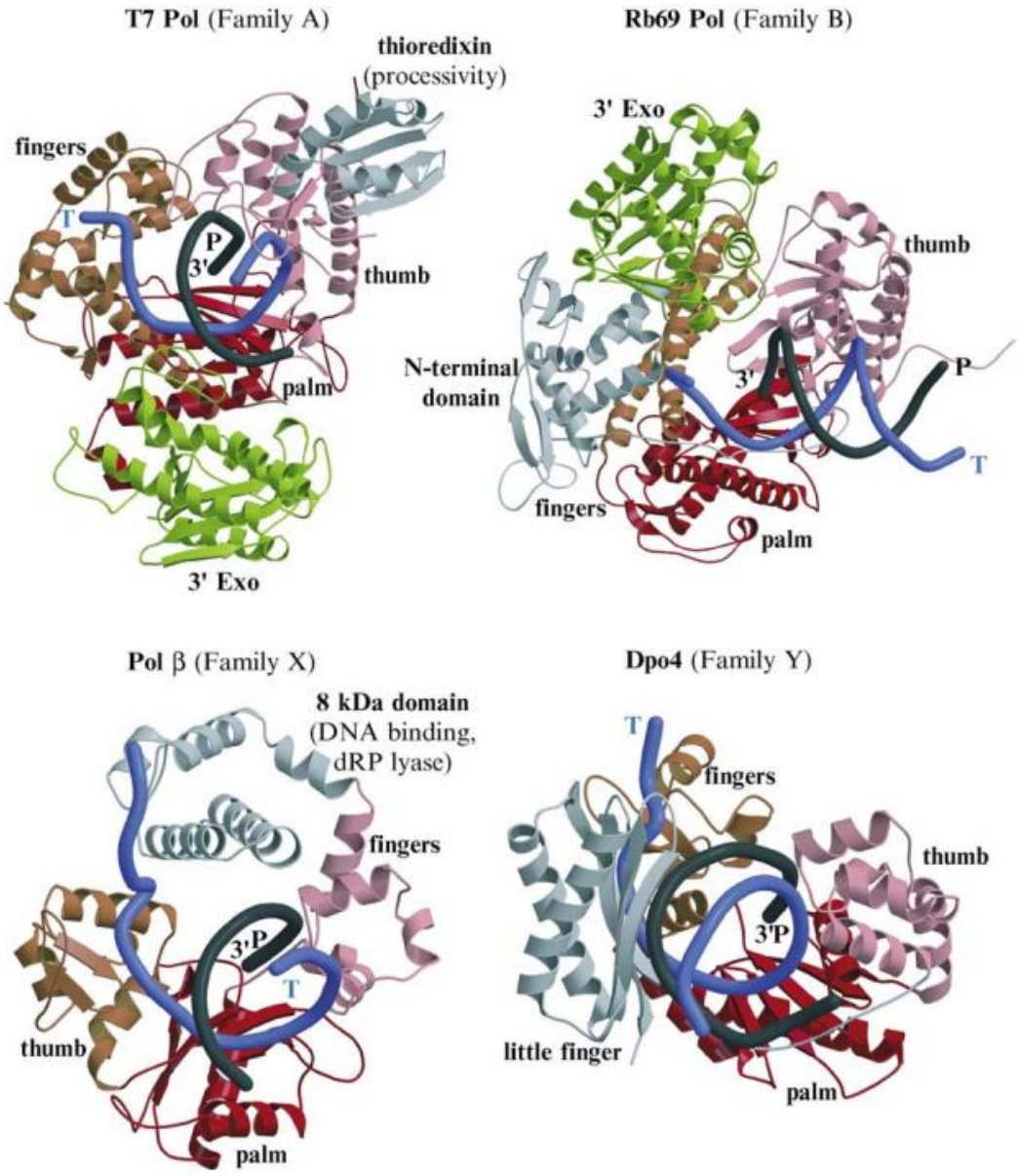


Figure 1. Structures of different members of the DNA polymerase families (based on Bebenek & Kunkel, 2004)

Replicative DNA polymerases are distinguished by their fidelity, which enables the precise incorporation of complementary nucleotides into the synthesized strand (Eckert & Kunkel, 1991; K. A. Johnson, 2010). Such accuracy derives from two synergistic mechanisms. First, the polymerase active site acts as a geometric filter, recognizing a correct hydrogen-bond pattern (Dodd et al., 2020). Second, many high-fidelity polymerases have an inherent 3′→5′ exonuclease domain that excises misincorporated nucleotides during proofreading,

dramatically reducing the net error rate (often by 10- to 100-fold). The polymerase and exonuclease active sites are physically separated by approximately 30-40 Å within the protein. Proofreading requires the primer terminus to shuttle from the polymerase site to the exonuclease site. A mismatched terminal base pair destabilizes the primer at the polymerase active site, favoring melting of the last one to three nucleotides and threading of the resulting single-stranded overhang into the exonuclease site, where the misincorporated residue is excised (Dodd et al., 2020). The excised primer terminus then returns to the polymerase site to resume DNA synthesis. This partitioning between sites is governed by the thermodynamic stability of the terminal base pair, providing a built-in kinetic checkpoint that couples error detection to strand transfer (Betancurt-Anzola et al., 2025).

Another key property for effective replication is processivity (Cohan & Frappier, 2021; Y. Wang, 2004). It allows polymerase to synthesize long DNA fragments without dissociating from the template. It might be enhanced by accessory factors, such as sliding clamps (e.g., PCNA in eukaryotes or the β-clamp in bacteria) (Cohan & Frappier, 2021; Czarnecki & Traktman, 2017; González-Magaña & Blanco, 2020; Simonsen et al., 2024). They tether the polymerase to DNA, enabling rapid, uninterrupted synthesis (Roske & Yeeles, 2024).

For many replicative DNA polymerases, either the induced-fit conformational change or product release is rate-limiting. Both steps are often temperature-sensitive (Brown & LiCata, 2013; Rentergent et al., 2016). As temperature decreases, polymerases may increasingly populate inactive conformational states even while remaining bound to DNA. It might reduce the fraction of catalytically competent enzyme (Rentergent et al., 2016). This temperature dependence has been most directly studied in Pol I family members. The Klenow fragment loses up to 73% of its catalytically active population at 5°C as a result of unproductive binding and conformational trapping (Rentergent et al., 2016). Similarly, cold-sensitive mutants of Klentaq have been mapped to hinge residues in the fingers domain that gate the conformational cycle (Wu et al., 2015). These findings are relevant to understanding how polymerases from psychrophilic organisms maintain catalytic activity at low temperatures, where the energetic cost of the rate-limiting conformational change becomes a significant barrier to turnover (Xue et al., 2021)

The maintenance of genome stability relies on a precise equilibrium between the fidelity and processivity of polymerases. When errors are not corrected by cellular proofreading, they may become established mutations (Buchel et al., 2023; Zhou & Kunkel, 2022). This may increase the risk of disease if essential genes are affected (Aoi, 2016; Cui et al., 2020; Topilow et al., 2022). Insufficient processivity may stall the replication fork, triggering DNA damage responses and elevating the risk of chromosomal instability (Kaszubowski and Trakselis, 2022). Consequently, identifying the molecular factors that regulate polymerase activity remains a central objective in both basic and translational research. Advances in this area have facilitated the rational engineering of polymerases, which are now essential for a wide array of biotechnological applications, including PCR, next-generation sequencing, and synthetic biology (Betancurt-Anzola et al., 2025; Oliveira et al., 2021; M. Wang et al., 2023; Zhao et al., 2015).

4.2. Isothermal amplification: current enzyme limitations

Since Kary Mullis's discovery in 1985, the Polymerase Chain Reaction (PCR) has become a gold standard technique for DNA amplification (Kaunitz, 2015). Its speed, reliability, and versatility (Oliveira et al., 2021) support a broad range of applications. It is widely used for drug development and the primary diagnosis of viral, bacterial, or genetic diseases (Gayet-Ageron et al., 2013; Inata et al., 2018; Kumar et al., 2025; Martinez et al., 2014; Nicolini et al., 2004). The use of this technique enables vaccine development and the generation of genetically engineered animal models, both of which are crucial for medical progress. Moreover, its influence extends beyond medicine and molecular biology to agriculture and livestock farming, where it facilitates the efficient production of high-quality meat, milk, and crops (Gavrilov et al., 2022; Oliveira et al., 2021).

Despite its broad acceptance, PCR has a fundamental limitation: it requires precise thermocycling, which in turn depends on costly, specialized equipment (**Fig. 2**).

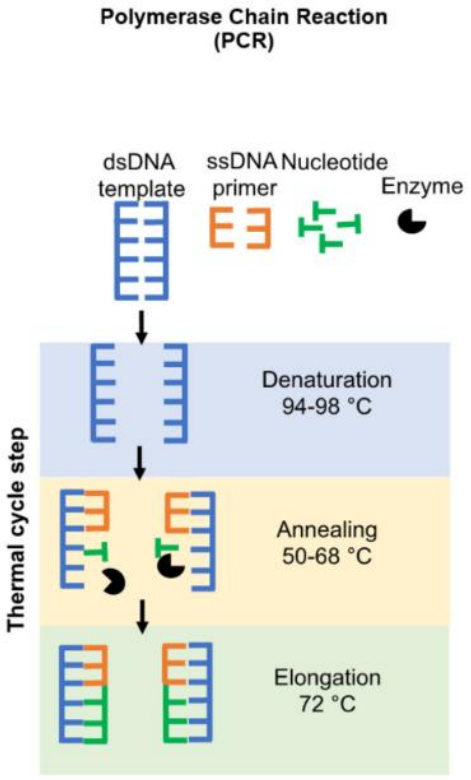


Figure 2. Overview of PCR reaction (based on Boonbanjong et al., 2022). Amplification proceeds in the 5′ to 3′ direction.

This constraint has motivated the development of cheaper, more flexible nucleic acid amplification strategies that do not rely on temperature cycling (Analytical Methods Committee, 2014). Isothermal amplification (IA) methods mimic the intracellular environment of DNA replication by maintaining a constant reaction temperature (typically 30-65 °C) (Boonbanjong et al., 2022; Zhao et al., 2015). They exploit enzymatic activities that replace the denaturation, annealing, and extension cycles of PCR. Compared with PCR, many IA techniques generate longer amplicons, achieve higher amplification efficiency and yield, display markedly reduced sensitivity to sample-derived inhibitors, and require fewer preparation steps (Oliveira et al., 2021). Prominent examples include Helicase-Dependent Amplification (HDA) (**Fig. 3A**) (Gavrilov et al., 2022), Recombinase Polymerase Amplification (RPA) (**Fig. 3B)** (Tan et al., 2022), and Loop-mediated Isothermal Amplification (LAMP) (**Fig. 3C)** (N. Yang et al., 2024). HDA and RPA rely on a DNA polymerase and single-stranded-binding proteins (**Table 2**). HDA additionally requires a

helicase to unwind duplex DNA, whereas RPA uses a recombinase to promote primer-template pairing. LAMP amplifies DNA at a constant temperature using a strand-displacing DNA polymerase and a set of four to six primers that recognize multiple regions of the target sequence, making it highly specific, rapid, and well-suited for point-of-care and field-based detection (Lai et al., 2024; Park, 2022; Shukla et al., 2023). Commercial kits based on these platforms, e.g., BioHelix's HDA reagents and TwistDx's RPA system, are already employed for pathogen detection in environmental, water, food, and clinical samples (Gavrilov et al., 2022; Tan et al., 2022; M. Wang et al., 2023). The combination of IA with microfluidic and nanotechnological components further improves sensitivity, reproducibility, speed, and cost-effectiveness, while decreasing contamination risk and enabling truly portable diagnostic devices.

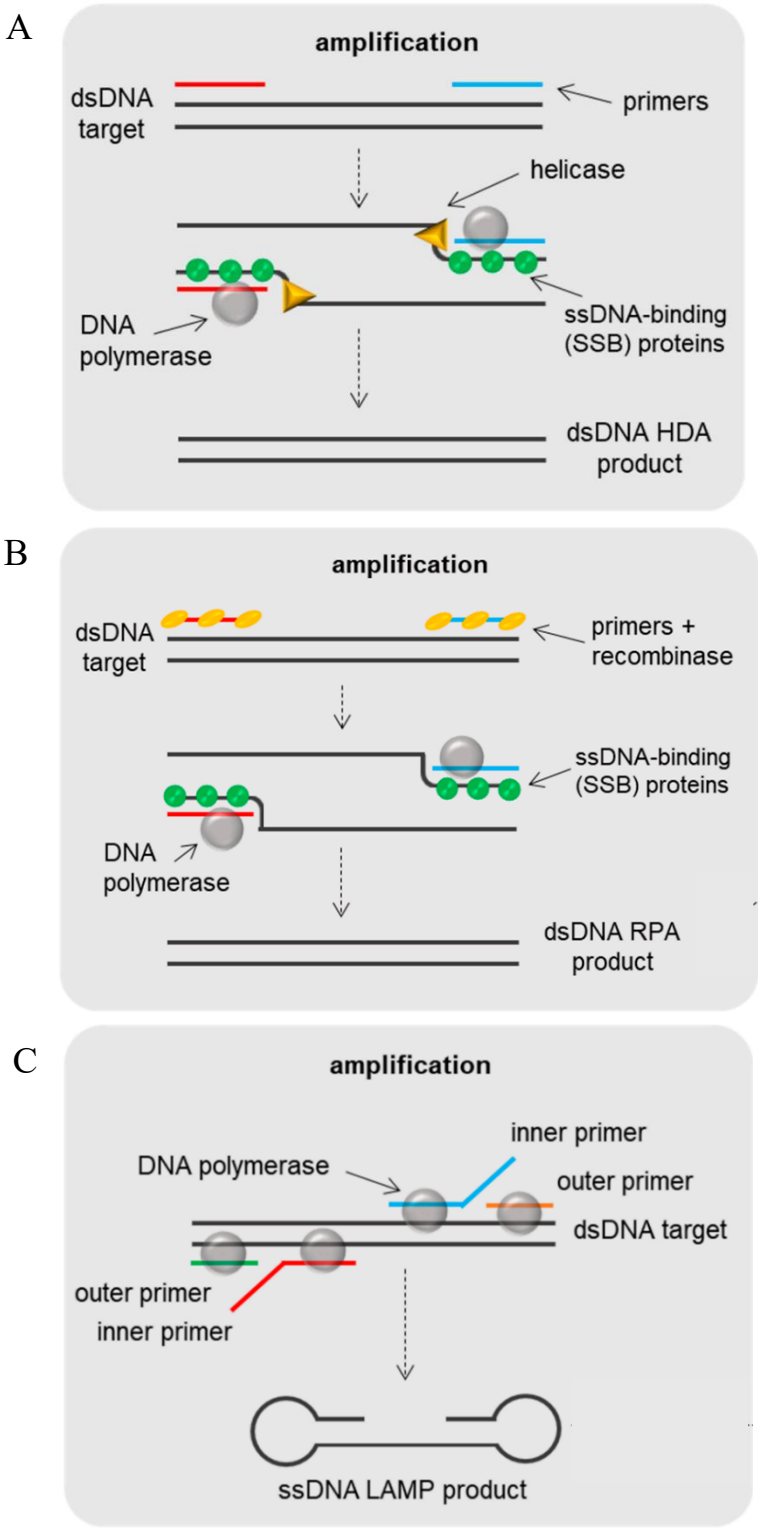


Figure 3. Examples of isothermal amplification techniques include **(A)** Helicase-dependent amplification, **(B)** Recombinase Polymerase Amplification, and **(C)** Loop-mediated Isothermal Amplification (based on Leonardo et al., 2021)

Nevertheless, the performance of isothermal assays is essentially limited by the temperature range over which the employed DNA polymerases remain active (**Table 2**) (Boonbanjong et al., 2022; Oliveira et al., 2021).

Enzymes can be classified according to their optimal temperature as: psychrophilic (below 25 °C) (Collins & Feller, 2023; Parvizpour et al., 2021), mesophilic (20-45 °C), and thermophilic (above 60°C). Thermophilic polymerases, such as Pfu, dominate PCR, and mesophilic enzymes, like φ29 DNA polymerase, which possesses strong strand-displacement activity, are widely used in isothermal applications (Mannier & Yoon, 2022; Soroka et al., 2021). However, mesophilic polymerases lose catalytic efficiency as temperature drops, rendering them unsuitable for low-temperature amplification. Psychrophilic DNA polymerases, therefore, represent a promising solution to this gap. Discovering polymerases that retain high activity at low temperatures would expand the operational window of diagnostic assays. It would eliminate the requirement for specialized heating equipment, and enable nucleic-acid detection in extreme environments: from Arctic field sites to space missions (Collins & Feller, 2023; Xu et al., 2024; Xue et al., 2021). Moreover, low-temperature amplification offers an additional advantage. Many nucleases that degrade DNA are most active at moderate temperatures. Conducting reactions at reduced temperatures may reduce the activity of many contaminating nucleases (Xue et al., 2021). At the same time, a cold-adapted polymerase continues to synthesize DNA efficiently, preserving sample stability, an especially valuable feature when handling limited or difficult-to-collect specimens where repeat sampling is impractical (Xue et al., 2021; W. Yang, 2011).

While PCR remains indispensable, the development and deployment of psychrophilic DNA polymerases are essential to overcome the equipment dependence and nuclease sensitivity of current nucleic acid amplification technologies.

Table 2. Comparison of RPA, HDA, and LAMP methods.

Method	*Operating temperature range*	*Core enzymatic components*	*Typical reaction time*	*Main advantages*	*Main limitations*
RPA	37 °C-42°C (mesophilic)	Recombinase-mediated primer targeting, single-strand-binding protein, strand-displacing polymerase (often a thermostable version of Bacillus subtilis Pol I)	20-40 min	Very rapid; low-temperature incubation reduces sample degradation; tolerant to many inhibitors; compatible with multiplexing (Lobato & O'Sullivan, 2018; Tan et al., 2022)	Enzyme supply is patented (commercial kits can be costly); activity drops sharply below ~ 30 °C, limiting true ambient-temperature use (Cobzariu, Lobo-Castañón and Miranda-Castro, 2023); stringent reaction-buffer requirements can affect assay robustness (Oliveira, Veigas and Baptista, 2021)

Method	*Operating temperature range*	*Core enzymatic components*	*Typical reaction time*	*Main advantages*	*Main limitations*
LAMP	60 °C-65°C (moderately thermophilic)	Bst DNA polymerase (strand-displacing), 4-6 primers recognizing 6-8 distinct target regions	≤ 60 min (often 30 min with loop primers)	Extremely high amplification efficiency (up to 10^{9}-fold in < 1 h); high specificity due to multiple primer binding sites; visual read-outs (turbidity, colorimetry) enable equipment-free detection (Suther et al., 2022; N. Yang et al., 2024)	Primer design is complex and time-consuming; susceptibility to non-specific amplification (primer-dimer artifacts) (Oliveira, Veigas and Baptista, 2021); requires a stable 60-65°C heat source, which raises power consumption for point-of-care (POC) devices (Cobzariu, Lobo-Castañón and Miranda-Castro, 2023)

Method	*Operating temperature range*	*Core enzymatic components*	*Typical reaction time*	*Main advantages*	*Main limitations*
HDA	~65°C (thermophilic)	Helicase (e.g., UvrD or T7 helicase) to unwind DNA, strand-displacing polymerase (often Bst)	30-120 min (depending on target)	No need for an initial denaturation step; works directly on double-stranded DNA; relatively simple reagent mix (Cobzariu, Lobo-Castañón and Miranda-Castro, 2023)	Lower amplification speed compared with RPA/LAMP; helicase activity can be inhibited by complex sample matrices; temperature still requires modest heating (~ 65 °C) (Oliveira, Veigas and Baptista, 2021)

The global burden of infectious diseases disproportionately affects resource-limited settings, where access to centralized laboratory infrastructure remains scarce (Mabey et al., 2004; Yager et al., 2008). While PCR-based diagnostics offer unparalleled sensitivity, their reliance on thermal cycling equipment and stable power supplies restrict deployment to well-equipped laboratories. This limitation has driven the development of point-of-care (POC) nucleic acid tests that are rapid, affordable, and equipment-minimal (Niemz et al., 2011; Urdea et al., 2006).

Isothermal amplification technologies have emerged as leading candidates for POC molecular diagnostics precisely because they operate at a single temperature, eliminating the need for thermal cyclers (Oliveira et al., 2021; Zhao et al., 2015). However, the mesophilic and thermophilic enzymes underpinning current isothermal methods impose their own thermal requirements. RPA operates optimally at 37-42°C and LAMP at 60-65°C, both still above ambient temperature in many field settings (Boonbanjong et al., 2022). This means that POC devices must incorporate heating elements, which consume battery power, add cost, and increase device complexity.

An enzyme that catalyzes DNA amplification at low temperatures, ideally in the 0-15°C range, would eliminate the thermal cycling requirement inherent to standard PCR. Such a psychrophilic polymerase would reduce the energy footprint of the amplification step, simplify reagent stabilization for warm-climate transport and storage, and lower the barrier to deploying diagnostic devices in resource-limited or field settings (Xu et al., 2024; Xue et al., 2021). These considerations provide the practical motivation for discovering and characterizing cold-active DNA polymerases.

4.3. Cold-adapted enzymes - mechanisms and examples

Cold-adapted (psychrophilic) enzymes have evolved to sustain high catalytic rates in environments where thermal energy is severely limited, such as polar seas, deep-ocean vents, alpine soils, and cold habitats (Collins & Feller, 2023; Feller & Gerday, 2003; Oliveira et al., 2021). The low ambient temperatures impose a kinetic barrier that most mesophilic enzymes

cannot overcome. Psychrophiles, therefore, rely on structural strategies that increase conformational dynamics and lower the activation energy of the chemical step (Lonhienne et al., 2000; Sočan et al., 2019). Comparative analyses of crystal structures and molecular-dynamics simulations have repeatedly shown that psychrophilic enzymes possess a larger proportion of flexible surface loops, a reduced number of stabilizing salt bridges and hydrogen-bond networks, and a more loosely packed hydrophobic core compared with their mesophilic or thermophilic homologs (Åqvist et al., 2017; Siddiqui & Cavicchioli, 2006; Zecchinon et al., 2001). These alterations diminish the rigidity of the protein scaffold, allowing the enzyme to sample catalytically competent conformations even when thermal motion is minimal (Matinja et al., 2022; Nowak & Otzen, 2024).

Several psychrophilic DNA polymerases have been characterized to date, including a DNA polymerase from the psychrophilic archaeon *Cenarchaeum symbiosum,* PIPI form *Psychromonas ingrahamii*, and the PWT-WT and FWT-WT polymerases from *Psychrobacillus* strains (Schleper et al., 1997; Y. Sun et al., 2024; Xue et al., 2021). Among these enzymes, PIPI has been particularly well described with respect to its temperature-dependent polymerization activity. In primer extension assays, PIPI displays markedly higher activity than the mesophilic Klenow fragment (KleLF) at temperatures below 37°C. It outperforms Taq polymerase by more than 10-fold at 30°C, confirming the classic cold-adaptation phenotype of high catalytic efficiency at low thermal energy. Remarkably, when the reaction is performed at -19°C in a glycerol-stabilized buffer, a clear full-length extension product appears after 7 h of incubation, whereas KleLF fails to generate any detectable product even after 23 h. The hallmark adaptations of cold-active enzymes are increased surface and loop flexibility, reduced electrostatic interactions, a looser hydrophobic core, and altered oligomeric states, and each structural manifestation is linked to its functional consequence. Although these features plausibly account for PIPI's ability to remain active at -19 °C, to my knowledge, no high-resolution structure of this polymerase has been solved. Its precise molecular adaptations remain unknown (Xue et al., 2021). The limited number of known psychrophilic polymerases, combined with the absence of structural data for PIPI, underscores a major gap in our understanding of cold-adapted DNA replication. To address this, attention has increasingly turned to new sources of enzymatic diversity. Among these,

bacteriophages stand out as a vast and underexplored reservoir of nucleic-acid-processing enzymes.

4.4. Bacteriophages as sources of DNA polymerases

Bacteriophages constitute one of the largest reservoirs of nucleic-acid-processing enzymes on the planet. Analysis of environmental viromes has revealed that a substantial fraction of phage genomes encodes their own DNA polymerases. Many viruses must replicate their genomes autonomously rather than relying exclusively on host enzymes (Keown et al., 2022; Morcinek-Orłowska et al., 2022; Weigel & Seitz, 2006). Surveys of sequenced phage genomes indicate that DNA polymerase genes are remarkably widespread. Over 25% of known dsDNA phages carry a family A DNA polymerase gene alone, making it one of the most prevalent replication-associated genes in the virosphere (Nasko et al., 2018; Wommack et al., 2015). This underscores how common replication-associated machinery is in viral genomes and supports the view that bacteriophages represent a vast, largely untapped source of characterized polymerases.

Beyond sheer numbers, phage-encoded polymerases often display biochemical properties adapted to their hosts' ecological niches. Viruses that infect thermophilic, halophilic, or otherwise extremophilic bacteria frequently encode polymerases that remain active at temperatures above 70°C, in saturated NaCl solutions, or under high-pressure conditions (Han et al., 2023; Y. Sun et al., 2025). These adaptations arise because the viral replication apparatus must function under the same physicochemical constraints that govern host DNA metabolism. Consequently, phage polymerases provide a natural library of enzymes with altered temperature optima, ion preferences, and substrate specificities that are difficult to obtain by rational protein engineering alone.

Among phage-encoded B-family polymerases, the best characterized is the phi29 DNA polymerase from Bacillus subtilis phage phi29. It exhibits exceptional processivity (greater than 70 kb) and strong strand-displacement activity, making it a cornerstone of multiple displacement amplification (MDA) and rolling-circle amplification (RCA) (Blanco et al., 1989; Esteban et al., 1993; Paez, 2004). Phi29 operates optimally at 30°C and retains activity at temperatures as low as 20°C, yet its mesophilic character limits utility below this range.

Other phage-derived polymerases, such as those from T4 and T7, offer high fidelity and rapid synthesis but share a similar mesophilic temperature optimum (Reha-Krantz, 2010; Y. Wang, 2004). These observations underscore a gap. No B-family polymerase from a bacteriophage source has been shown to maintain robust activity at or below 0°C. The identification of such an enzyme would expand the known temperature range of phage replication machinery and open new avenues for cold-active biotechnology.

The present thesis focuses on a previously uncharacterized DNA polymerase gene of the vB_EfaS-271 bacteriophage. Bioinformatic analysis places this polymerase, Efa, within the B family of polymerases, a group already known for high processivity (e.g., φ29 DNAP) (Han et al., 2023; Topka-Bielecka et al., 2020). The genomic context of *efa*, flanked by genes encoding a helicase, an endonuclease, and a primase, is consistent with a compact replication module. It has been described for many lytic phages that encode a near-complete replication toolkit (Topka-Bielecka et al., 2020). Whether this module can function independently of host factors remains to be tested experimentally (**Fig.4**).

Systematic exploration of such phage-derived enzymes promises to uncover novel catalytic motifs, altered fidelity determinants, and unique metal-ion dependencies. They can be repurposed for biotechnological applications such as isothermal amplification, long-read sequencing, and synthetic biology scaffolds (Y. Sun et al., 2025).

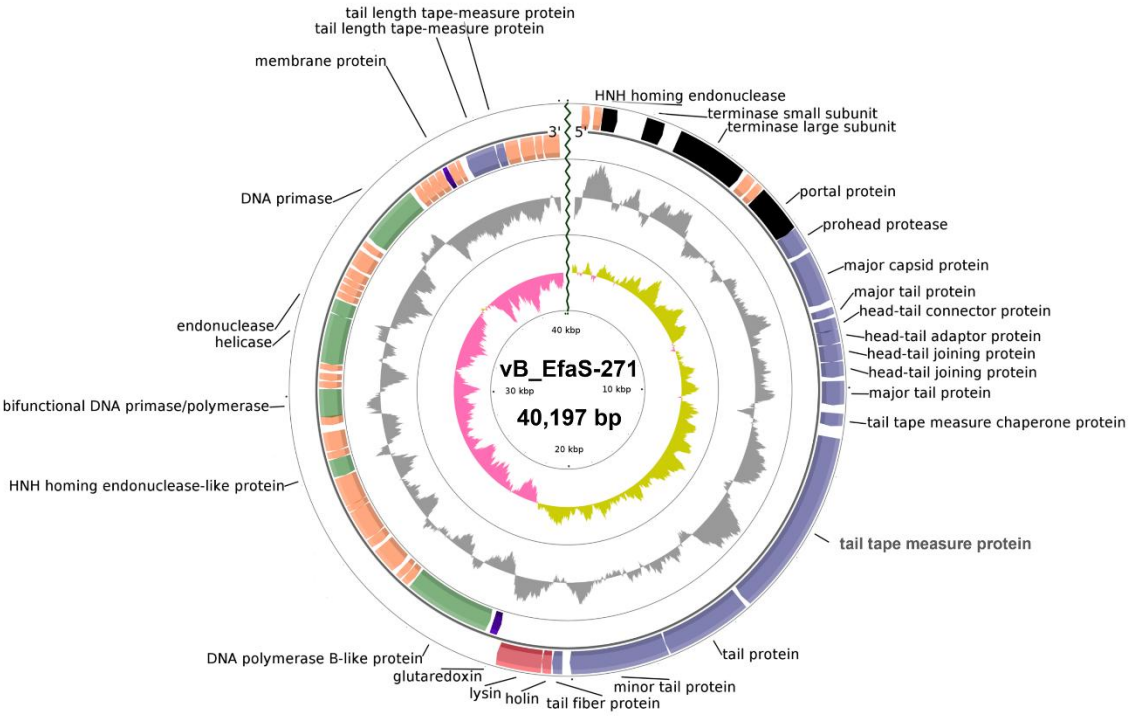


Figure 4. Genome of bacteriophage vB_EfaS-271(GenBank: MT520979.1)

4.5. Discovery and uniqueness of DNA polymerase Efa

The DNA polymerase Efa was initially identified by bioinformatic analysis of the vB_EfaS-271 phage genome. Sequence inspection revealed that the *efa* gene encodes a protein with the canonical domain organization of a B-family DNA polymerase, an exonuclease domain, followed by palm, fingers, and thumb domains (Topka-Bielecka et al., 2020, 2021).

B-family DNA polymerases are the dominant replicative polymerases in archaea and eukarya, and several phage-encoded members of this family have been characterized in detail (Braithwaite & Ito, 1993). While the canonical architecture of these enzymes is well understood, structural variations have been reported in phage-encoded homologs, including N-terminal extensions of unknown functions (Xue et al., 2021). Whether such extensions contribute to catalysis, DNA binding, or enzyme stability has not been systematically explored. Moreover, although a number of cold-adapted DNA polymerases have been

described from psychrophilic organisms, the structural basis for sub-zero catalytic activity in phage-encoded enzymes remains poorly understood (Y. Sun et al., 2024; Xue et al., 2021). These gaps motivated the present study.

This doctoral project set out to perform an integrated biochemical, kinetic and structural characterization of the Efa DNA polymerase and to assess its potential as a low-temperature amplification enzyme.

5. Aims of the Thesis

The identification of a gene encoding DNA polymerase Efa in the genome of vB_EfaS-271, together with its low sequence identity to other known polymerases, motivated further investigation of this enzyme. During the initial biochemical and biophysical characterization, Efa unexpectedly displayed substantial DNA synthesis activity at low temperature. This thesis therefore aims to characterize the biochemical, kinetic, and structural properties of Efa and to determine the molecular basis of its observed low-temperature activity. The study evaluates the enzyme's catalytic properties, temperature dependence, and structural organization, including the contribution of its N-terminal domain to DNA synthesis. It also seeks to identify the structural and kinetic features that may underline Efa's activity at low temperatures and to assess its potential for low-temperature DNA amplification applications.

The specific objectives were:

1. **Biochemical characterization -** determining the purity, secondary structure content, and thermal stability of recombinant Efa DNA polymerase (CD, thermal melt).
2. **Enzymatic activity profiling -** quantifying DNA 5′→3′ polymerase and 3′→5′ exonuclease activities over a temperature range (-10°C to 30°C) and comparing them to those of standard DNA polymerases (T4, T7, Pol I).
3. **Role of the N-terminal domain -** generating an N-terminal truncated mutant (Efa ΔN) and assessing how the N-terminal "SSB-like" region influences substrate binding, kinetics, and low-temperature performance.
4. **Structural elucidation** - solving high-resolution crystal structures of the apo-enzyme and holo-enzyme ternary complexes (DNA with 4-nt and 6-nt overhangs); mapping catalytic-site residues and N-terminal interactions with the nucleic-acid substrate.
5. **Bioinformatic analysis** - comparing the N-terminal sequence and structure of Efa DNA polymerase with known single-strand-binding proteins across viruses, bacteria, and eukaryotes.

6. Materials and methods

6.1. Construction of Efa expression plasmids

Plasmids bearing genes encoding the wild-type Efa DNA polymerase (Efa WT; residues 1-763) (**Fig. 5A**), the exonuclease-deficient mutant Efa DEDD (D137A E139A D188A D281A; residues 1-763) (**Fig. 5B**), and the N-terminal deletion mutant Efa ΔN (residues Δ27-124) (**Fig. 5C**) were used in this study. The WT Efa expression construct used for protein purification in the experiments presented in Figs. 7, 9, 10, and 12 was generated by Joanna Morcinek-Orłowska. The remaining constructs were codon-optimized for *Escherichia coli* expression and cloned into the pET28 vector with an N-terminal His_6-tag followed by a SUMO cleavage site. Constructs were synthesized by EPOCH Life Science and all plasmids were verified by Sanger sequencing performed by EPOCH Life Science. The constructs are summarized in **Table 3**. Plasmids were introduced into *Escherichia coli* Rosetta (DE3) pLysS (Novagen, Cat. No. 70956-3) cells by heat-shock at 42°C. Briefly, 100 µL of chemically competent cells were mixed with 100 ng of plasmid DNA, incubated on ice for 30 min, heat-shocked at 42°C for 90s, and recovered in 1 mL of lysogeny broth (LB) medium at 37°C for 1h with shaking at 150 rpm. Cells were plated on LB agar supplemented with 50 µg/mL kanamycin (BioShop, Cat. No. KAN201) and 34 µg/mL chloramphenicol (Merck, Cat. No. C0378-25G) and incubated at 37°C overnight.

6.2. Protein overproduction

A single colony was used to inoculate 10 mL of LB broth supplemented with 50 µg/mL kanamycin and 34 µg/mL chloramphenicol and grown overnight at 37°C with shaking at 150 rpm. This pre-culture was diluted 1:100 into 1000 mL of fresh LB medium with the same antibiotics and grown at 37°C with shaking at 150 rpm until the optical density at 600 nm (OD_{600}) reached 0.6. Protein expression was induced by the addition of isopropyl-β-D-thiogalactopyranoside (IPTG; A&A Biotechnology, Cat. No. 2003-25) to a final concentration of 0.5 mM, and the cells were incubated for an additional 5 h at 37 °C with shaking at 150 rpm. Cells were harvested by centrifugation at 3 000 × g (rotor: Beckman JLA 10.500) for 10 min at 4°C. Cell pellets were flash-frozen in liquid nitrogen and stored at -

80°C pending purification. This protocol was used for all three constructs (Efa WT, Efa DEDD, Efa ΔN).

Table 3. List of Efa polymerase variants generated for functional analysis

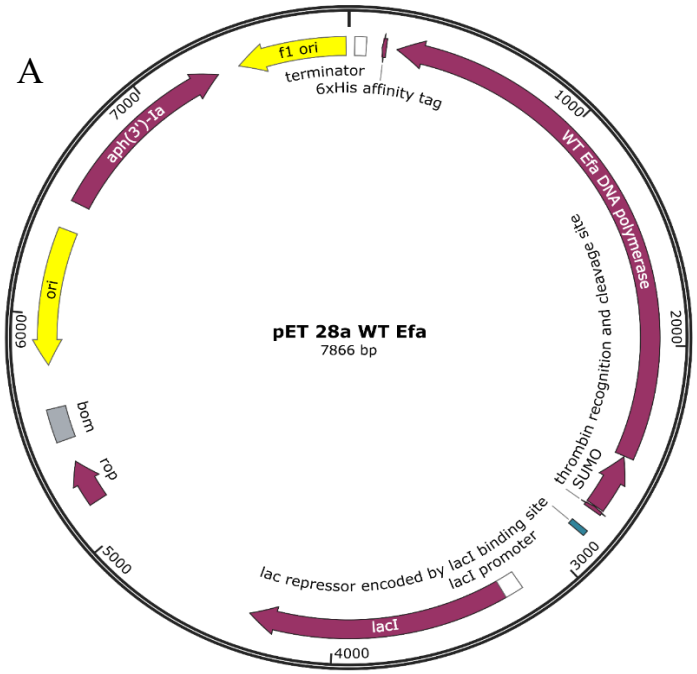
Construct ID	*Encoded protein*	*Mutations or deletion*	*Vector backbone and features*	*Tag, fusion and cleavage-site arrangement*	*Cloning method*	*Construct source*	*Sequence verification*	*Comments*
WT Efa, in-house construct	WT Efa DNA polymerase, residues 1-763	None	pET-28a	6xHis tag, SUMO region	Restriction-enzyme-free assembly	Constructed in-house by Joanna Morcinek-Orłowska, PhD	The complete *efa* coding sequence was verified by Sanger sequencing. No unintended nucleotide substitutions were detected.	Construct was used to prepare experiments from figures 7, 9, 10, and 12

Construct ID	*Encoded protein*	*Mutations or deletion*	*Vector backbone and features*	*Tag, fusion and cleavage-site arrangement*	*Cloning method*	*Construct source*	*Sequence verification*	*Comments*
GS75031-1, Construct180	WT Efa, residues 1-763	None	pET-28a	6xHis tag, SUMO region	NdeI/ EcoRI-based cloning	EPOCH Life Science	The complete *efa* coding sequence was verified by Sanger sequencing. No unintended nucleotide substitutions were detected.	-

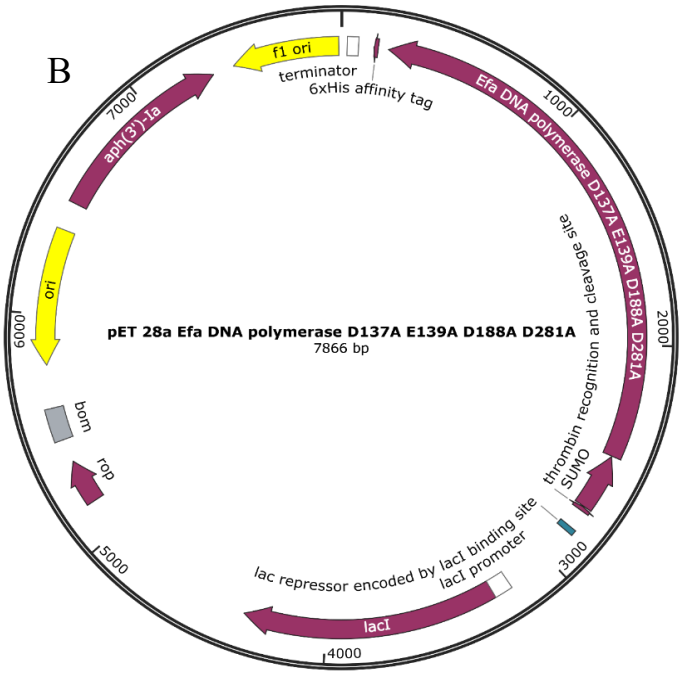
Construct ID	*Encoded protein*	*Mutations or deletion*	*Vector backbone and features*	*Tag, fusion and cleavage-site arrangement*	*Cloning method*	*Construct source*	*Sequence verification*	*Comments*
GS75031-2	Efa DEDD (exonuclease-deficient DNA polymerase), residues 1-763	D137A, E139A, D188A, and D281A	pET-28a	6xHis tag, SUMO region	NdeI/ EcoRI-based cloning	EPOCH Life Science	The complete *efa* coding sequence was verified by Sanger sequencing. No unintended nucleotide substitutions were detected.	-

Construct ID	*Encoded protein*	*Mutations or deletion*	*Vector backbone and features*	*Tag, fusion and cleavage-site arrangement*	*Cloning method*	*Construct source*	*Sequence verification*	*Comments*
GS75577-1	Efa ΔN DNA polymerase. Residues 1-26, and 125-763	Internal deletion of residues 27-124	pET-28a	6xHis tag, SUMO region	NdeI/ EcoRI-based cloning	EPOCH Life Science	The complete *efa* coding sequence was verified by Sanger sequencing. No unintended nucleotide substitutions were detected.	-

A


f1 ori
terminator
6xHis affinity tag
1000
WT Efa DNA polymerase
thrombin recognition and cleavage site
SUMO
2000
3000
lac repressor encoded by lacI binding site
lacI promoter
lacI
4000
5000
bom
rop
6000
ori
7000
aph(3')-Ia
pET 28a WT Efa
7866 bp

B


f1 ori
terminator
6xHis affinity tag
1000
Efa DNA polymerase D137A E139A D188A D281A
thrombin recognition and cleavage site
SUMO
2000
3000
lac repressor encoded by lacI binding site
lacI promoter
lacI
4000
5000
bom
rop
6000
ori
7000
aph(3')-Ia
pET 28a Efa DNA polymerase D137A E139A D188A D281A
7866 bp

C

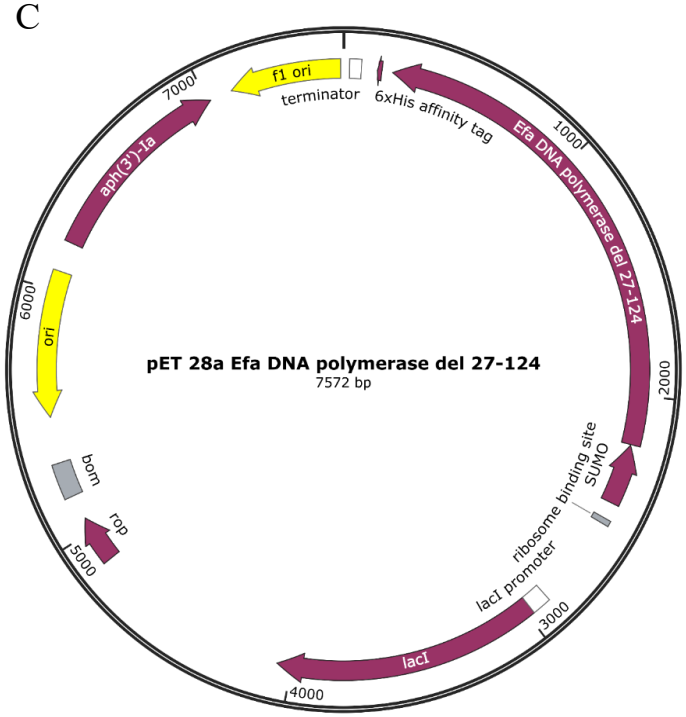


Figure 5. Schematic maps of the three Efa expression plasmids generated by EPOCH Life Science

Circular maps of **(A)** pEfa WT, (**B**) pEfa D137A, E139A, D188A, D281A, **(C)** pEfa Δ27-124 are shown. The WT construct used for protein production in the experiments presented in Figures 7, 9, 10, and 12 was generated separately in-house by Joanna Morcinek-Orłowska using a restriction-enzyme-free assembly method and is not represented in panels A-C. The EPOCH-generated constructs were codon optimized for expression in *E. coli* and synthesized in the pET-28a. The synthetic *efa* gene was inserted into the vector after digestion with NdeI and EcoRI, creating compatible 5′ and 3′ overhangs allowing directional cloning of the insert. All three plasmids were visualized and exported as circular diagrams using SnapGene (v2.5).

6.3. Protein purification

Bacterial cultures expressing the recombinant Efa DNA polymerase gene were resuspended in lysis buffer (50 mM Tris-HCl, pH 7.5; 300 mM NaCl; 5 % glycerol; 0.2 mM TCEP; 5 mM imidazole; 1 mg mL^{-1} lysozyme; 1 mM PMSF) at 10 mL per gram of wet cell mass. Cells were disrupted by sonication for 5 min in a pulse mode of 3s on/ 5s off at an amplitude of 18%. The lysate was clarified by centrifugation at 45,000 × g for 60 min at 4 °C in a Beckman (JA-20) rotor. The clarified supernatant was loaded onto a HisTrap HP column (Cytiva, 5 mL, Cat. No. 17524801) pre-equilibrated with the A buffer (50 mM Tris-HCl, pH 7.5; 300 mM NaCl; 5 % glycerol; 0.2 mM TCEP; 5 mM imidazole). The column was washed with 10 column volumes (CV) of buffer A. Bound protein was eluted with buffer B containing 50 mM Tris-HCl (pH 7.5), 300 mM NaCl, 5% glycerol, 0.2 mM TCEP, and 500 mM imidazole. Eluted fractions were analyzed by SDS-PAGE using the PageRuler^{TM} Prestained Plus Protein Ladder (Thermo Fisher Scientific, Cat. No. 26619) as a molecular-weight standard. Fractions containing Efa were pooled. All recombinant Efa constructs were expressed with an N-terminal SUMO-His_6 tag. The tag was cleaved by Ulp1 protease to yield native Efa without a residual affinity tag

The pooled eluate was treated with Ulp1 protease at a 1:100 molar ratio (Ulp1: Efa fusion) to cleave the SUMO-His6 tag. The reaction was incubated overnight at 4°C and dialyzed against the SEC buffer (50 mM Tris-HCl, pH 7.5; 200 mM NaCl; 5% glycerol; 1 mM TCEP) using membrane with molecular weight cutoff (MWCO) of 30 kDa (Millipore, Cat. No. UFC9030). The sample volume was 40 mL, and the dialysis buffer was replaced three times over 12 h at 4°C. After dialysis, the sample was reapplied to a HisTrap HP column (Cytiva, 5 mL, Cat. No. 17524801) pre-equilibrated with buffer A. This second affinity-chromatography step was used to separate tag-free Efa from uncleaved Efa-SUMO-His_6. These His-tag-containing species were retained on the column, while tag-free Efa passes through the column and is collected in flow-through. The flow-through was concentrated to 1 mL using Amicon Ultra centrifugal filter with a 30 kDa MWCO (Millipore, Cat. No. [redacted]). The concentrated sample was subjected to size-exclusion chromatography on a HiLoad 16/600 Superdex 200 pg column (GE Healthcare, Cat. No. 17-1069-01) pre-

equilibrated with SEC buffer. The column was operated at a flow rate of 0.5 mL min^{-1} and 0.5 mL fractions were collected. Elution profiles were monitored at 260 and 280 nm by UV absorbance. Peak fractions were verified by SDS-PAGE, pooled, and dialyzed into the storage buffer (50 mM Tris-HCl, pH 7.5; 200 mM NaCl; 40 % glycerol; 1 mM TCEP; 0.1 mM EDTA) for 4h at 4°C with three buffer exchanges using a 30 kDa MWCO membrane. The final preparation was aliquoted, flash-frozen in liquid nitrogen, and stored at -80 °C. Protein concentration was determined by absorbance at 280 nm using extinction coefficients calculated from the amino acids sequence with ProtParam tool (Gasteiger et al., 2005): $\varepsilon_{280} = 96\,275\ M^{-1}\ cm^{-1}$ (full-length Efa DNA polymerase) or $\varepsilon_{280} = 82\,295\ M^{-1}\ cm^{-1}$ (Efa Δ27-124), derived from the contributions of Trp, Tyr and Cys residues using the method of Pace et al. (1995). The A_{260}/A_{280} ratio of the final preparation was between 0.52-0.6.

6.3.1. Analytical size-exclusion chromatography

Monomeric state of Efa was verified by size-exclusion chromatography (SEC) on a Superdex 200 Increase 10/300 GL column (Cytiva) equilibrated with buffer containing 50 mM Tris-HCl (pH 7.5), 200 mM NaCl, 5% glycerol and 1 mM TCEP at a flow rate of 0.5 mL min^{-1}, and protein was injected at a concentration of approximately 1 mg mL^{-1} in a volume of 100µL. Elution was monitored by absorbance at 280 nm and 260 nm. The column was calibrated with gel filtration molecular weight standards (Bio-Rad, Cat. No. 1511901): thyroglobulin (670 kDa), γ-globulin (158 kDa), ovalbumin (44 kDa), myoglobin (17 kDa), and vitamin B12 (1.35 kDa).

6.4. Circular dichroism (CD) spectroscopy

CD sample preparation was performed by the author, measurements and data analysis were performed by dr. hab. Rafał Dutkiewicz. CD measurements were carried out using a J-1500 spectropolarimeter (JASCO) and a 1-mm quartz cuvette at 20 °C. Protein samples (2.5 µM) in CD buffer (20 mM potassium phosphate, pH 8.0; 140 mM KCl) were prepared from stock solutions whose concentrations were determined spectrophotometrically at 280 nm using extinction coefficients calculated with the ProtParam tool (Gasteiger et al. 2005) based on the method of Pace et al. (1995). Spectra were recorded from 190 nm to 260 nm

with a 1 nm step size, a 1 nm bandwidth, a scan speed of 50 nm min^{-1}, and a data pitch of 0.1 nm. Each spectrum represents an average value of three consecutive scans. The corresponding buffer spectrum, acquired under identical conditions, was subtracted to obtain baseline-corrected curves.

For thermal stability studies, the ellipticity at 208 nm was monitored while the temperature was increased from 0°C to 90°C at 0.5 °C min^{-1} using the instrument's Peltier temperature controller. Samples were allowed to equilibrate at the initial temperature for at least 5 min prior to the ramp. Melting temperatures (T_m) were obtained from the inflection point of the unfolding curve using Spectra Manager v2.0 (JASCO).

6.5. Preparation of DNA substrates

All oligonucleotides were obtained from Metabion International AG (Germany) (**Table 4**). They were purified using HPLC. For duplex formation, complementary strands were mixed in the annealing buffer (20 mM Tris-HCl, pH 8.0; 0.1 mM EDTA) at a total concentration that gave a 1.2: 1 molar ratio of unlabeled to fluorescently labeled strand. The mixture was heated to 95°C for 5 min, then slowly cooled to room temperature to complete annealing.

Table 4. Oligonucleotides employed in the present work.

Oligo name	*Sequence*
Primer strands (P)	
MRS#273	5'-Flsn-GCG GAC TGC TTA C-3' (13-mer)
KZ_Prmr-2	5'-FAM-TCG GAC TGC TTA*C-3' (13-mer)
MRS#274	5'-Flsn-GCG GAC UGC UUA C-3' (13-mer)
MRS#297	5'-GAC CAC GGC CA-ddC-3' (12-mer)
Template strands (T)	
MRS#275	5'-ATA AGC AGT TCA GGT AAG CAG TCC GC-3' (26-mer)
KZ_Tmpl-1_1	5'-ATA AGC AGT TCA GGT AAG CAG TCC GA-3' (26-mer)
KZ_template_4nt_overhang	5'-TCA GGT AAG CAG TCC GA-3' (17-mer)
MRS#276	5'-AUA AGC AGU UCA GGU AAG CAG UCC GC-3' (26-mer)
MRS#298	5'-AAC TGT GGC CGT GGT C-3' (16-mer)
MRS#339	5'-GCG AGA AAA ACG ACG ATA AGC AGT TCA GGT AAG CAG TCC GC-3' (41-mer)
MRS#401	5'-AGA ACT GTG GCC GTG GTC-3' (18-mer)
MRS#427	5'-AAGTGTAACACTTGTATACAAGTGTTACACTTTTTTTTTTTTTTTGTAAGCAGT-3' (54-mer)
MRS#438	5'-TGCCTCTACACACTCTCTGACACATCTATCCCTTTTTTTTTTTTTGTAAGC-3' (50-mer)

Marker (M) 80-5nt	
MRS#35	5'-CTAGT-Flsn-3' (5-mer)
MRS#34	5'-ACAGTCTAGT-Flsn-3' (10-mer)
MRS#33	5'-CGTAATACAGTCTAGT-Flsn-3' (16-mer)
MRS#32	5'-CACGTAATACAGTCTAGT-Flsn-3' (18-mer)
MRS#116	5'-CGCACGTAATACAGTCTAGT-Flsn-3' (20-mer)
MRS#36	5'-TT-CGCACGTAATACAGTCTAGT-Flsn-3' (22-mer)
MRS#37	5'-TTTTTTT-CGCACGTAATACAGTCTAGT-Flsn-3' (27-mer)
MRS#38	5'-TTTTTTTTTTTTTTT-CGCACGTAATACAGTCTAGT-Flsn-3' (35-mer)
MRS#125	5′-ACT AGA CTG TAT TAC GTG CGG TAT GGC ACT GGC CCT CGT TTT CG-Flsn-3′ (44-mer)
MRS#52	5'-TTTTTTTTTTTTTTTTTTTTTTTTTTTTT-CGCACGTAATACAGTCTAGT-Flsn-3' (50-mer)
MRS#39	5'-TTTTTTTTTTTTTTTTTTTTTTTTTTTTTTTTTTTTTTTTTTTTTTTTTTTTTTTT-CGCACGTAATACAGTCTAGT-Flsn-3' (80-mer)

Abbreviations: Flsn - fluorescein label, FAM- 6-carboxyfluorescein label, * - phosphorothioate linkages

6.6. DNA polymerase and exonuclease activity assays

Protein-concentration-dependent primer-extension assays were performed in 20 µL of the HK140 buffer (20 mM HEPES, pH 7.5; 140 mM KCl; 5 % v/v glycerol; 1 mM TCEP) at 30 °C. Each reaction contained 50 nM fluorescein-labeled primer-template pair, 0.39-100 nM Efa or its variants, 500 µM dNTPs, and 5 mM $MgCl_2$. The substrate, dNTPs, and MgCl2 were preincubated at 30°C for 1 min before the reaction, while Efa or its variants were preincubated separately under the same conditions. Reactions were initiated by adding the enzyme to the substrate mixture and were incubated for 5 min at 30 °C. To terminate the reactions, 20 µL of the STOP buffer (86 % formamide, 50 mM EDTA, pH 8.0, 1× TBE) was added, followed by heating at 95°C for 5 min. Exonuclease assays were carried out under identical conditions but without dNTPs. Reaction products were resolved electrophoretically in 20% denaturing polyacrylamide gels (8 M urea, 1× TBE) at 40 W for 50 min. Fluorescein-labeled size markers of defined lengths (**Table 4**) were run alongside reaction products to assign polymerase-extended and exonuclease-degraded bands. Gels were scanned for fluorescence on a Typhoon imager (Cytiva) and quantified with ImageJ software (https://imagej.net/ij/index.html). Background subtraction was performed by measuring signal intensity in a blank lane adjacent to each sample. Product, substrate, and degradation bands were assigned based on migration relative to the size markers (**Table 4**). Band intensities were integrated over the lane width and normalized to the total signal in each lane. All assays were performed in three independent biological replicates. Data are presented as mean ± standard deviation.

6.7. Kinetic analysis

Kinetic experiments were performed in the Galletto laboratory (Department of Biochemistry and Molecular Biophysics, Washington University in Saint Louis, School of Medicine). Enzyme activity was measured with 13-nt primer/ 26-nt template duplexes in HEPES-KCl buffer (20 mM HEPES, pH 7.5; 300 mM KCl; 5 % glycerol; 1 mM TCEP) containing 10 mM $MgCl_2$ and the appropriate dNTP concentration. Prior to the reaction, enzyme (Efa WT and Efa ΔN mutant), DNA substrate and dNTPs were pre-incubated in Mg^{2+} free buffer for 5 min at room temperature. The reaction was initiated by the addition of

$MgCl_2$ to start catalysis. Measurements were performed using a Kintek rapid-quench-flow apparatus (RQF-3). For measurements, approximately 20 μL of each reaction solution was manually introduced into the mixing assembly of the apparatus. After the run was started, the instrument mixed the two solutions, initiating reaction. The two solutions were combined at a 1:1 ratio. The resulting reaction mixture was then propelled through the reaction pathway by buffer delivered from two 5 mL syringes. At defined time points, the reaction was terminated by introducing stop buffer from a third 5 mL syringe. The stop buffer contained 50 mM EDTA.

Pre-steady-state burst experiments were conducted by mixing 100 nM Efa DNA polymerase (or the Efa ΔN mutant) with $MgCl_2$ and quenching at intervals from 0 to 5 s. Quenching time points were specifically optimized to each experiment to capture the initial rate accurately. Reactions were stopped with 50 mM EDTA and analyzed by denaturing PAGE. Single-turnover experiments were performed with the enzyme in excess (1 μM) over DNA (100 nM) at dCTP concentrations ranging from 5 to 1000 μM. Product formation was monitored as described above. Band intensities were quantified using ImageJ, converted to the concentration of product formed $[P]/[E]$, and fitted to single-exponential or double-exponential functions to obtain observed rate constants (k_{obs}) and amplitudes. The number of exponential terms was chosen for each trace individually. A double exponential was applied when the curve visibly deviated from single-exponential behavior and the goodness of fit (R^2) improved substantially upon inclusion of the second term. Because the experiments were performed under single-turnover conditions (enzyme in excess over DNA), the amplitude is not expected to depend on dCTP concentration. At intermediate dCTP concentrations the unconstrained amplitude approached ~0.9, while at low and high dCTP the amplitude and k_{obs} were strongly correlated, preventing reliable simultaneous estimation of both parameters. The amplitude was therefore constrained to $A = 0.9$, and this constraint was applied to all fits. For double-exponential fits, the rate constant of the first phase was used in all subsequent analyses. To determine the apparent dependence of the observed rate on dCTP concentration, plots of k_{obs} versus dCTP concentration were fitted to a hyperbolic equation using nonlinear regression, yielding an apparent dissociation constant ($K_{D,app}$). $K_{D,app}$ is an apparent dCTP concentration parameter derived from the k_{obs} versus [dCTP] dependence and should not be interpreted as a direct measure of equilibrium nucleotide

binding. All kinetic parameters, including 95% confidence intervals and fitting errors, were calculated using OriginLab (OriginLab Corporation). Reported errors represent the standard error of the fit. Experiments were independently repeated three times using the same protein preparation. Traces from all three replicates were globally fit to a shared model.

6.8. Temperature-dependence studies

Single-turnover reactions were conducted at 10 °C, 20 °C, and 30°C with the same substrate and enzyme concentrations as in Section 6.7. In all temperature-dependent experiments, the enzyme, DNA and 200 μM dCTP were pre-incubated at target temperature for 5 min in Mg^{2+} free buffer before initiating the reaction by addition of $MgCl_2$. Observed rate constant (k_{obs}) was extracted from the exponential fits for each temperature. An Arrhenius plot of ln k_{obs} versus $1/T$ (where T is the absolute temperature in Kelvin) was constructed for each substrate length. The activation energy (E_a) and the pre-exponential factor (A) were determined from the slope ($-E_a/R$) and intercept ($\ln A$) obtained by linear regression in OriginLab. Arrhenius plots were used to estimate apparent activation energies and pre-exponential factors from the observed rate constants. Because only three temperature points were analyzed, the resulting parameters should be interpreted as estimates of the temperature dependence of the observed process rather than as direct measurements of the activation energy of a specific elementary step. Reported errors represent the standard error of the fit. Experiments were independently repeated three times using the same protein preparation.

6.9. Primer extension at low temperature

Reactions were assembled in a final volume of 20 μL containing 50 nM of a 13-nt 5′-fluorescein-labeled primer annealed to its complementary 41-nt template, 500 μM dNTPs, and the appropriate enzyme (Efa DNA polymerase, T4 DNA polymerase (Thermo Fisher Scientific, Cat. No. EP0062), T7 DNA polymerase (Thermo Fisher Scientific, Cat. No. EP0081), or *E. coli* DNA Pol I (Thermo Fisher Scientific, Cat. No. EP0042). The reaction mixture was supplemented with 1 nM enzyme when incubated at 30°C (the optimal temperature for Efa). For the experiments performed at -10°C, the enzyme concentration was set to 50 nM. Reactions were carried out in HK140 buffer (20 mM HEPES, pH 7.5; 140 mM

KCl; 40 % v/v glycerol; 1 mM TCEP) and incubated in a calibrated dry block heater at either 30°C or -10°C. Aliquots (10 µL) were withdrawn at 0, 5, 10, and 15 min, mixed with an equal volume of STOP buffer (86 % formamide, 50 mM EDTA, pH 8.0, 1× TBE), and heated at 95°C for 5 min to terminate the reactions. Reaction products were separated electrophoretically in 20% denaturing polyacrylamide gels (8 M urea, 1× TBE) run at 40 W for 50 min. Fluorescently labeled DNA fragments were detected with a Typhoon fluorescence imager (Cytiva) and quantified using ImageJ. Experiments were independently repeated three times using the same protein preparation.

6.10. X-ray crystallography

Crystallization experiments were carried out in 96-well IntelliPlates (Art Robbins Instruments, Cat. No. 102-0001-20) at ambient temperature using a Mosquito liquid-handling robot (TTP Labtech). Drops were set up by mixing protein solution with reservoir solution in two ratios, 1 : 1 (200 nL + 200 nL) and 2 : 1 (400 nL + 200 nL), and equilibrated against 70 µL of reservoir at 18 °C. Seven commercial sparse-matrix screens: MORPHEUS I-III, JCSG Plus, HELIX (Molecular Dimensions), INDEX, and Crystal 41 (Hampton Research), were screened, and crystal growth was inspected periodically by light microscopy.

6.10.1. Apoenzyme protein crystallization

The Efa protein (pET28 WT Efa) at a concentration of 45 mg mL^{-1} yielded rod-shaped crystals in a condition containing 0.085 M sodium formate and 12 % (w/v) PEG 3350. After three days of growth, crystals were harvested and transferred to mother liquor supplemented with 12.5 % (v/v) glycerol and 12.5 % (v/v) MPD as cryoprotectant. Crystals were then flash-cooled in liquid nitrogen for subsequent X-ray diffraction analysis.

6.10.2. Bioinformatic identification of the DEDD exonuclease motif

To identify the residues forming the 3′→5′ exonuclease active site, the exonuclease region of Efa (residues 124-328) was aligned with the exonuclease domains of well-characterized B-family DNA polymerases. The reference sequences used were RB69 DNA polymerase (PDB ID: 1WAF), KOD DNA polymerase (PDB ID: 1WNS) and Pfu DNA polymerase (PDB ID: 2JGU). Multiple sequence alignments were generated with

Clustal Omega (EMBL-EBI, version 1.2.4) using default parameters including the Gonnet substitution matrix, a gap opening penalty of 6 bits, and a gap extension penalty of 1 bit. The alignment was inspected for the conserved D-E-D-D catalytic tetrad. Motif boundaries were assigned based on conservation of the four acidic residues (Asp, Glu, Asp, Asp) in the aligned exonuclease regions, with reference to the published exonuclease domain boundaries of RB69 DNA polymerase. Based on this analysis, an exonuclease-deficient mutant (Efa D137A E139A D188A D281A) was designed and synthesized by EPOCH Life Science and used in the crystallographic experiments described below.

6.10.3. Holoenzyme protein crystallization

DNA substrates were prepared by annealing equimolar oligonucleotides (MRS#297/ MRS#298 or MRS#297/ MRS#401) in the TE buffer (20 mM Tris, pH 8.1, 0.1 mM EDTA). The mixture was heated to 95°C for 5 min and then cooled slowly to room temperature, yielding a duplex concentration of 700 µM. Protein-DNA complexes were assembled by mixing the duplex with Efa DEDD (construct pET28 Efa D137A E139A D188A D281A) at a protein: DNA molar ratio of approximately 1: 1.25 (final protein concentration 100 µM, final DNA concentration 125 µM) in a buffer containing 20 mM HEPES, pH 7.5, 140 mM KCl, 5 % (v/v) glycerol, 1 mM TCEP, together with 20 mM $MgCl_2$ and 2 mM dATP. After a 5-minute incubation at 20 °C, the mixtures were clarified by centrifugation at 15,000 × g for 15 min at 4 °C. For the D137A E139A D188A D281A mutant in complex with a 12-mer/18-mer duplex, crystals were obtained in the “Divalents II” condition of the Morpheus II screen (Molecular Dimensions, Cat. No. MD2-100-231) (2 mM each of $MnCl_2 \cdot 4H_2O$, $CoCl_2 \cdot 6H_2O$, $NiCl_2 \cdot 6H_2O$ and Zn $(CH_3COO)_2 \cdot 2H_2$ O, together with a 30 % (v/v) precipitant mix 7 composed of 20 % (w/v) PEG 8000 and 40 % (v/v) 1,5-pentanediol). Plate-shaped crystals appeared after three days, were transferred to mother liquor containing 12.5 % (v/v) glycerol and 12.5 % (v/v) MPD, and flash-cooled in liquid nitrogen.

For the same mutant in complex with a 12-mer/16-mer duplex, crystals grew in a reservoir solution comprising 1.2 % cholic-acid derivative mix (3 % w/v each of CHAPS, CHAPSO, sodium glycocholate hydrate, and taurocholic acid sodium salt hydrate), 0.1 M Buffer System 1 (1.0 M imidazole, pH 6.5, and MES adjusted to pH 6.5), and a 30 % precipitant mix 3 (40 % v/v glycerol and 20 % w/v PEG 4000). Plate-like crystals were

observed after 3-5 days, harvested, cryoprotected with the same glycerol/MPD supplement, and flash-cooled in liquid nitrogen for subsequent diffraction analysis.

6.11. AlphaFold prediction of Efa as a molecular replacement model

The three-dimensional structure of the Efa DNA polymerase was predicted using ColabFold v1.5.0 via Google Colab on 23 May 2022, with the default parameters (Jumper et al., 2021; Mirdita et al., 2017, 2019, 2021; Mitchell et al., 2019). The full-length amino-acid sequence of the target protein was submitted as the sole input. Predictions were performed in the ColabFold environment on Google Colaboratory, which automates the AlphaFold2 workflow. Multiple sequence alignments (MSAs) were automatically generated by the pipeline. Homologous sequences were retrieved via MMseqs2 searches that employ profile hidden Markov model (HMM) profiles to maximize the detection of distant relatives. The MSAs served as the primary input features for the AlphaFold2 neural network, which produced five structural models ranked by internal confidence metrics. Model quality was evaluated using the predicted Local Distance Difference Test (pLDDT) scores (per-residue confidence) and the Predicted Aligned Error (PAE) matrix (inter-domain reliability). The model with the highest overall pLDDT and the most favorable PAE profile was selected for downstream crystallographic analyses. Predicted structures were visualized using UCSF ChimeraX (v1.8).

6.12. X-ray diffraction data collection and structure determination

Diffraction data were recorded at two synchrotron facilities: Elettra (Trieste, Italy) and the Deutsches Elektronen-Synchrotron (DESY, Hamburg, Germany), using monochromatic X-rays ($\lambda = 1.00$ Å). The raw images were automatically processed using the Xia2 pipeline, which performed indexing, integration, and scaling.

6.12.1. Apoenzyme structure determination

The apo form of the Efa polymerase crystallized in space group $P3_1$ with one monomer present in the asymmetric unit. The structure was determined at 2.3 Å resolution (completeness 92.2%). Initial phases were obtained by molecular replacement using Phaser

(PHENIX), with a search model generated by ColabFold (accelerated AlphaFold2) from the Efa amino acid sequence using default settings. The solution was refined through iterative cycles in Phenix.refine and manual rebuilding in Coot, yielding final refinement statistics of R_{work} = 0.217 and R_{free} = 0.239.

6.12.2. Holoenzyme complex structures

Ternary complexes containing Efa, Mg^{2+}, dATP and primer-template DNA were solved by molecular replacement using the refined apoenzyme as the search model. The complex with a 12-mer primer and an 18-mer template bearing a 3′-dideoxy-terminated primer crystallized in space group $P2_1\ 2_1\ 2_1$ and was refined to 2.15 Å resolution (completeness 99.8%, R_{work} = 0.177, and R_{free} = 0.223). A second complex, with a 16-mer template and a primer-template duplex containing a four-nucleotide 5′ overhang, crystallized in space group $P1\ 2_1\ 1$ and was refined at 2.21 Å resolution (completeness 99.2 %, R_{work} = 0.212 and R_{free} = 0.261). Data collection and processing followed the same protocol as for the apoenzyme.

6.12.3. Model building, refinement and validation

For both ternary complexes, the apoenzyme backbone served as the initial protein model. DNA, Mg^{2+} ions, and dATP were built manually in Coot into 2Fo-Fc maps contoured at 1.0 σ. Base pairs were fitted sequentially with attention to stacking and sugar-phosphate geometry. The 3′ dideoxy terminus and 5′ overhang nucleotides were modeled only where continuous density was present. Metal ions were placed at strong positive difference peaks and refined at full occupancy. dATP was fitted as a single ligand, with partial occupancies considered where density suggested disorder. After each manual building cycle, models were refined in Phenix.refine using positional, individual isotropic B-factor, and TLS refinement with standard geometric restraints and automatic water placement, followed by manual inspection. Final models were validated with the Phenix and MolProbity tools, confirming R_{work}/ R_{free} values within acceptable ranges, bond-length and bond-angle RMSDs < 0.01 Å and < 1.5°, > 98 % residues in favored Ramachandran regions, and acceptable clashscore and rotamer statistics. The final models generated in this study have not been deposited in the Protein Data Bank.

6.13. Bioinformatic analyses of the N-terminal region

The N-terminal domain of Efa (residues 27-124) was defined from the crystal structure and isolated as an independent chain for analysis. Domain boundaries for the Palm, Thumb, Fingers, N-terminal region, and Exonuclease domain were assigned based on the holoenzyme structures, and the N-terminal region was colored separately to facilitate visualization of its position relative to the polymerase core and DNA. To quantify conformational changes, apo and DNA-bound structures were superposed on the Palm domain, and the relative rotation of the N-terminal domain between states was measured. The ~22° angular displacement was extracted from vector angles between domain principal axes in ChimeraX. For comparative structural analysis, N-terminal segments from representative viral, bacterial, archaeal, and eukaryotic proteins were extracted and superposed onto the Efa N-terminus, generating an overlay of N-terminal folds from *E. faecalis phage, P. falciparum, S. coelicolor, M. smegmatis, S. elongatus*, human RPA, *S. solfataricus, T. thermophilus, T. aquaticus* and *M. leprae*. Pairwise 3D alignments of the Efa N-terminus with each reference structure were carried out using the RCSB PDB Pairwise Structure Alignment tool (TM-align), yielding TM-scores of ~0.50-0.60 and C_α RMSD values of ~2.6- 3.0 Å over 66-78 aligned residues, despite low sequence identity (4-17 %).

6.14. Molecular graphics and analysis in ChimeraX

All structural models were visualized and analyzed using UCSF ChimeraX (v1.8). The Efa polymerase apo-structure and the holo-enzyme complexes (with 12/18-mer and 12/16-mer DNA duplexes) were opened simultaneously and aligned on the Palm domain using the “matchmaker” command. The isolated N-terminal domain (residues 27-124) was extracted as a separate model (-open -sel residues 27-124) to enable independent manipulation. Domain rotations were quantified by measuring the angle between the principal axis of the N-terminal domain and that of the Palm domain before and after DNA binding. Key residues implicated in ssDNA binding (Arg 79, Lys 55, Tyr 74, Lys 53, Ala 52, Phe 105, Thr 107) were highlighted using “label” and “show” commands. Images were captured with “view” settings (ray trace, 300 dpi) and saved as high-resolution PNG files.

7. Results

7.1. Protein overproduction and purification

The DNA fragment coding for the vB_EfaS-271 DNA polymerase (WT Efa) containing a SUMO-His_6 tag was synthesized and cloned into the pET-28 expression vector. This construct was introduced by transformation into *E. coli* Rosetta (DE3) pLysS cells for overexpression. Protein production was induced with 0.5 mM IPTG, and the recombinant enzyme was purified by Ni-NTA affinity chromatography followed by size-exclusion chromatography (SEC). The SEC profile showed a single, symmetrical peak eluting between the 158 kDa and 44 kDa calibration standards, consistent with a monomeric species of approximately 87.5 kDa (763 amino acid residues; **Fig. 6A**). SDS-PAGE analysis of the peak fractions revealed a single prominent band migrating between the 70 kDa and 100 kDa markers, and two very weak bands of smaller polypeptides (either products of partial degradation of Efa or contaminating proteins), confirming that the preparation was ~ 99 % pure (**Fig. 6B**). The purified protein was highly soluble and could be concentrated to ~50 mg/ml without visible precipitation. Far-UV circular dichroism (CD) spectra recorded between 190 and 260 nm displayed characteristic features of a predominantly α-helical protein, with a strong negative minimum near 208 nm (**Fig. 6C**). Thermal denaturation monitored by CD at 208 nm showed a cooperative unfolding transition with a melting temperature T_m of 41.41°C (**Fig. 6D**). Taken together, these data demonstrated that recombinant WT Efa polymerase is correctly folded, monomeric, highly soluble, and biophysically well behaved, providing a robust starting point for subsequent structural and kinetic analyses.

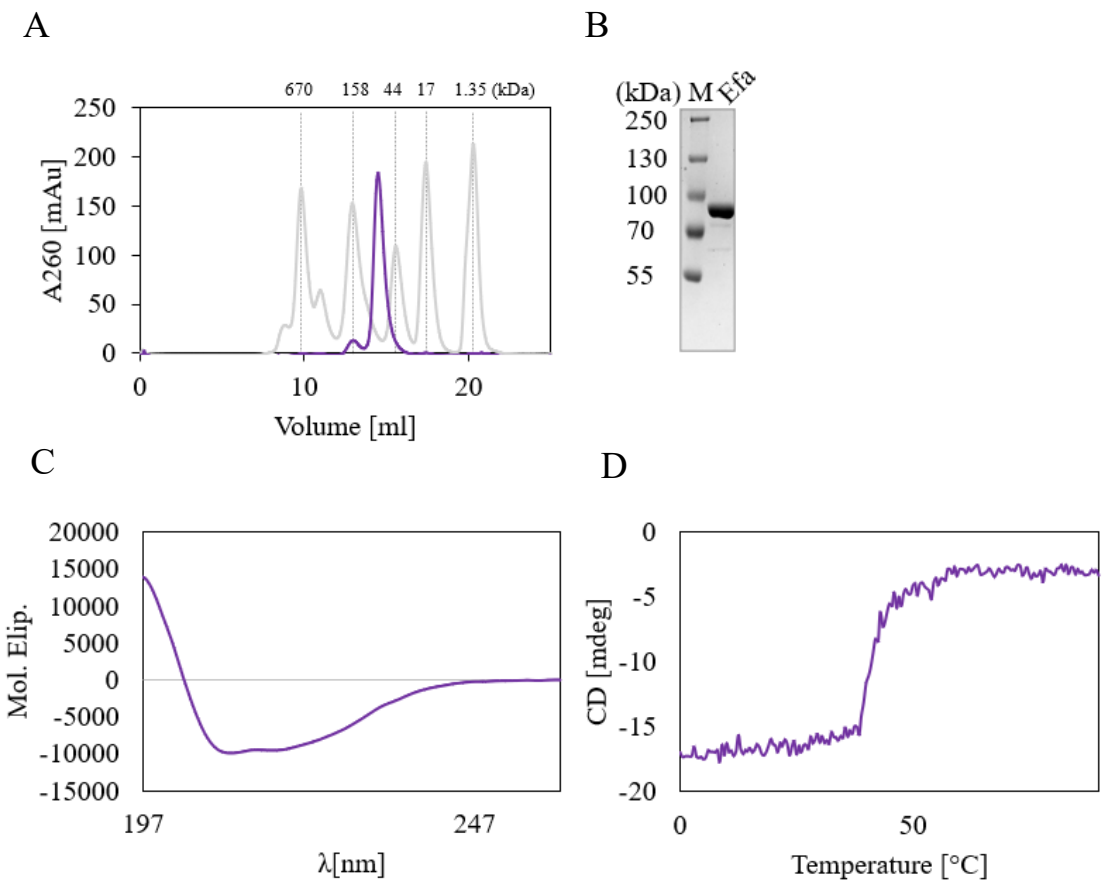


Figure 6. Biophysical characterization of the Efa WT DNA polymerase (Method section 6.3-6.4)
(A) Size-exclusion chromatography trace showing absorbance (mAu) versus elution volume (mL). The purple trace corresponds to WT Efa. The gray peaks are calibration standards of 650 kDa, 158 kDa, 44 kDa, 17 kDa, and 1.35 kDa. The Efa peak elutes at approximately 12 mL. **(B)** SDS-PAGE image of the purified protein. Lane M contains molecular-weight markers (35 to 250 kDa), and lane Efa shows a prominent band between 70 kDa and 100 kDa. **(C)** Circular dichroism (CD) spectrum of Efa. Molar ellipticity is plotted against wavelength from 197 nm to 257 nm. The spectrum shows a negative minimum near 208 nm. **(D)** Thermal denaturation monitored by CD. CD signal is recorded from 0 °C to 90 °C. The signal remains relatively constant up to approximately 40 °C, then changes as temperature increases, reaching a melting temperature of 41.41 °C.

7.2. Polymerase and exonuclease activities

Primer-extension assays were carried out with a 5′-FAM-labeled 13-nt primer annealed to a 26-nt template, with Efa concentration ranging from 0.39-100 nM, with a fixed reaction time

of 5 min. When using DNA/DNA or RNA/DNA substrates, wild-type Efa catalyzed robust 5′→3′ strand extension, yielding discrete products whose intensity increased proportionally to enzyme concentration (**Fig. 7A, B**).

However, substrate composition significantly influenced the enzymatic output. When using a DNA/RNA substrate (DNA primer paired with an RNA template), Efa failed to catalyze polymerization. Instead, the gel showed only exonucleolytic trimming of the DNA primer (**Fig. 7C**). In contrast, the enzyme was completely inactive against RNA/RNA duplexes, showing neither polymerase nor exonuclease activity under the conditions tested (**Fig. 7D**). Comparison of primer types on the same DNA template revealed that while Efa can extend both DNA and RNA primers, the DNA-primed reaction consistently generated more products than the RNA-primed reaction, suggesting a preference for DNA primers

.

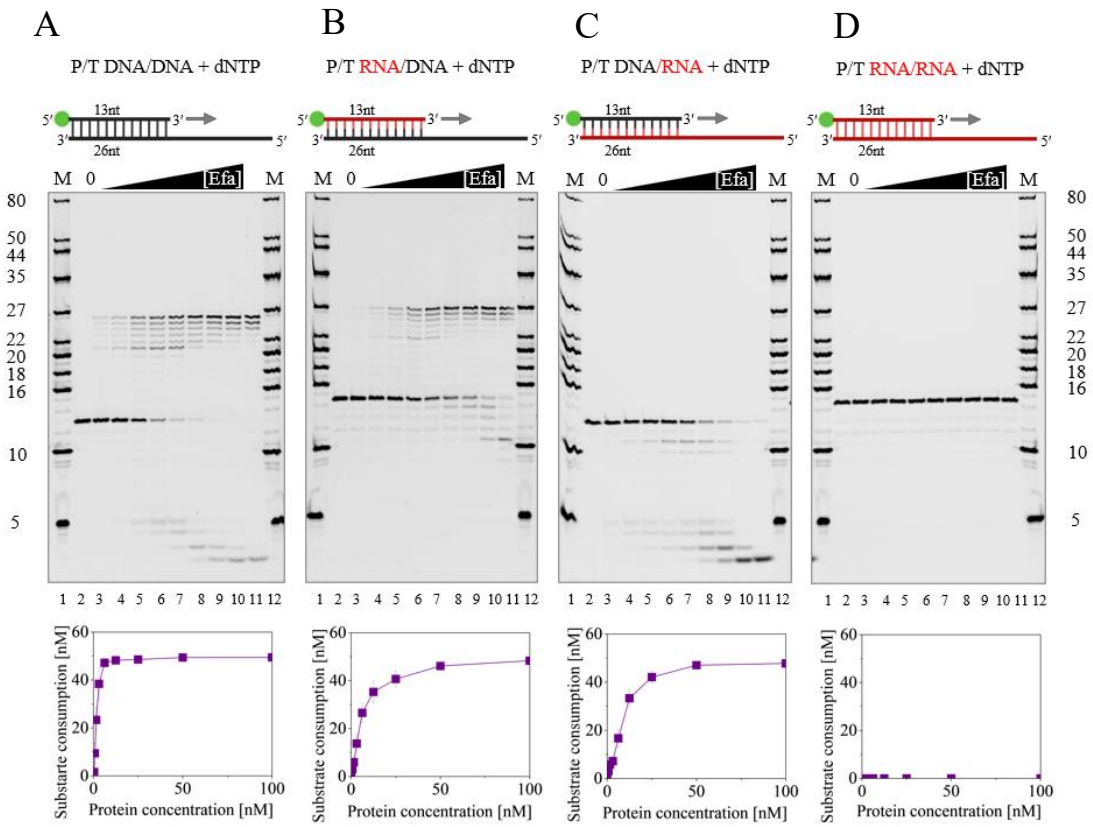


Figure 7. DNA-dependent activity of Efa in the presence of dNTPs (black- DNA, red - RNA)
Primer-extension assays using a 5′-FAM-labeled 13-nt primer annealed to a 26-nt template were performed with increasing concentrations of Efa (0.39-100 nM) in the presence of all four dNTPs. Substrate combinations were: **(A)** DNA primer/DNA template (DNA/DNA), **(B)** RNA primer/DNA template (RNA/DNA), **(C)** DNA primer/RNA template (DNA/RNA), and **(D)** RNA primer/RNA template (RNA/RNA). For each panel, the top schematic shows the primer-template configuration, the middle image shows a denaturing PAGE gel (lane M, size marker; lane 0, no enzyme; lanes 1-12, increasing Efa concentration), and the bottom graph plots substrate consumption (nM) versus Efa concentration.

Exonuclease activity was assayed in parallel reactions lacking dNTPs. Under these conditions, Efa WT hydrolyzed the 3′ ends of DNA/DNA (**Fig. 8A**) RNA/DNA (**Fig. 8B**), and DNA/RNA (**Fig. 8C**) duplexes, whereas no detectable degradation occurred on RNA/RNA (**Fig. 8D**) duplexes. Importantly, even when all dNTPs were present, a residual exonuclease signal persisted.

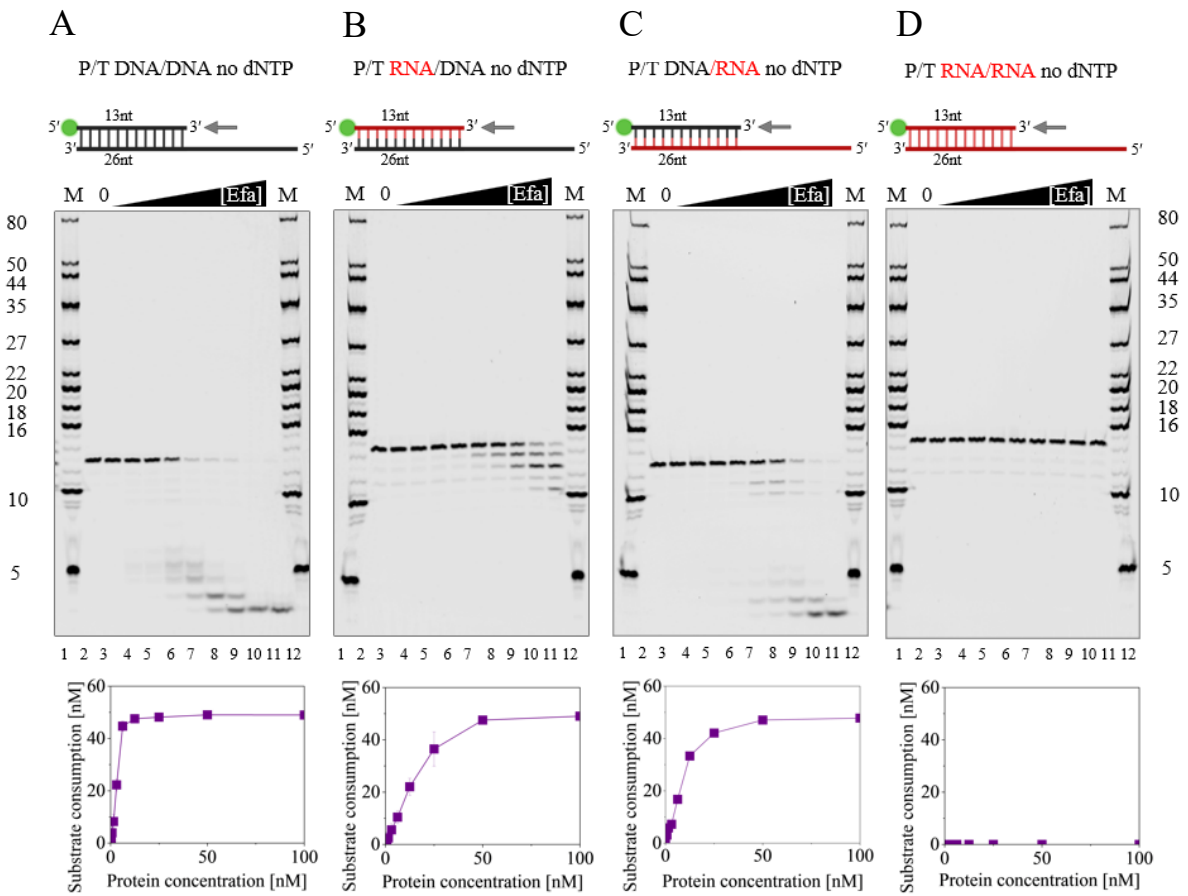


Figure 8. Exonuclease activity of Efa on different primer-template duplexes in the absence of dNTPs
Reactions were identical to those in Fig. 7, except that dNTPs were omitted to isolate 3′→5′ exonuclease activity. For DNA/DNA **(A)**, RNA/DNA **(B)**, and DNA/RNA **(C)** duplexes, the gels show progressive shortening of the primer band as Efa increases, and the corresponding plots show a saturable increase in substrate consumption with enzyme concentration. In contrast, no substrate shift is detected for RNA/RNA **(D)** duplexes.

7.3. Cold-adapted activity

The temperature dependence of WT Efa polymerase was examined by monitoring primer extension using a 13-mer/41-mer duplex over a range of temperatures from -5°C to 70°C (**Fig. 9**). The gel in Figure 9 demonstrates that WT Efa polymerase remained highly active at low temperatures. Even at 0°C, the primer-extension product was essentially identical in intensity to that observed at 10°C, indicating the presence of near-maximal activity well below the physiological range. The activity declined only modestly when the temperature was raised above 45°C and then dropped sharply beyond 55°C. The temperature-dependent decline in Efa polymerase activity correlated with the thermal instability of the protein rather than substrate destabilization. The melting temperature (T_m) of the protein, as determined by circular dichroism, was approximately 42°C, indicating that global unfolding begins near the temperature at which a sharp decrease in activity was observed.

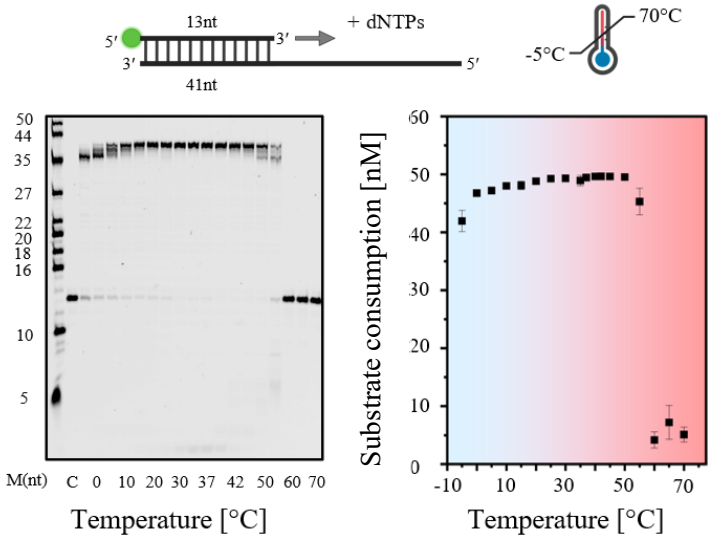


Figure 9. Temperature dependence of Efa DNA polymerase.
Primer extension on a 13-mer/41-mer duplex was monitored between -5 °C and 70 °C. A schematic of the reaction (top) shows a 13-nt primer annealed to a 41-nt template. The gel image below shows extension products at the indicated temperatures. Quantification of the results is shown in the right panel.

To assess whether the cold activity is unique among DNA polymerases with the 5′→3′ polymerase function, WT Efa was compared with three widely used enzymes: T4 DNA polymerase, T7 DNA polymerase, and the *E. coli* DNA polymerase I, under identical buffer conditions. All enzymes were first assayed at 30°C in a buffer containing 40 % glycerol (required to prevent freezing at sub-zero temperatures) (**Fig. 10**). Each polymerase displayed activity under these conditions, demonstrating that the higher glycerol concentration does not abolish enzymatic activity. All enzymes generated the expected 41-nt extension product (**Fig. 10A**), while the kinetic plot (**Fig. 10B)** reveals large differences in product formation: T4 attains the highest yield (~40 nM), Efa is intermediate (~20 nM), and T7 and Pol I produce only trace amounts of the final product after 15 min.

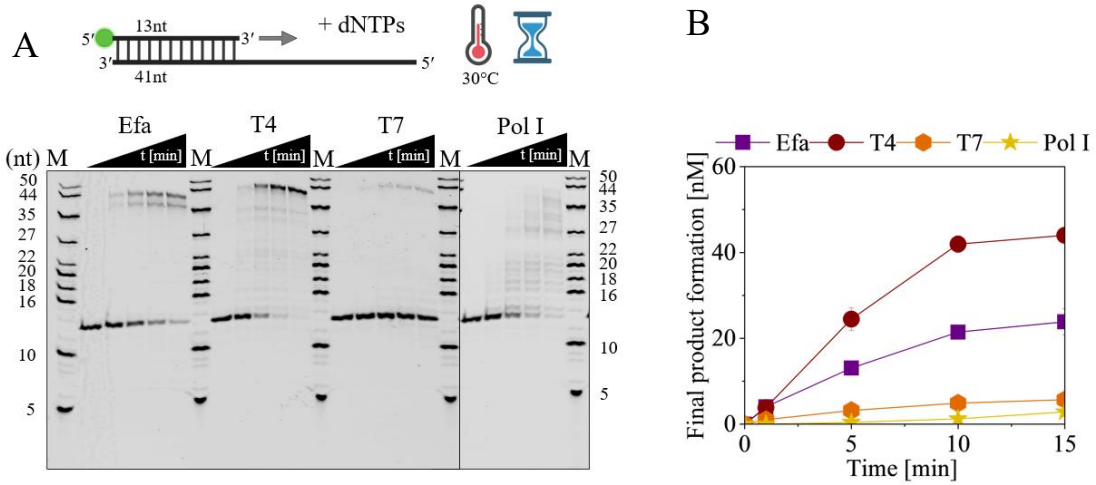


Figure 10. Activities of DNA polymerase at 30°C in 40% glycerol.
Activity of four DNA polymerases, Efa, T4, T7, and Pol I, at 30 °C in 40% glycerol. **(A)** Representative gel showing the expected 41-nt extension product formed by each enzyme. **(B)** Quantification of product formation over 15 min.

When reactions were repeated at -10°C with the same buffer composition and a 13-mer/41-mer primer-template substrate (**Fig. 11A**), WT Efa produced full-length extension products with 20 nM yield after 15 min, whereas T4, T7 and Pol I generated only trace amounts of extended primer (**Fig. 11B**). These data support the conclusion that Efa is cold-active under the assay conditions tested.

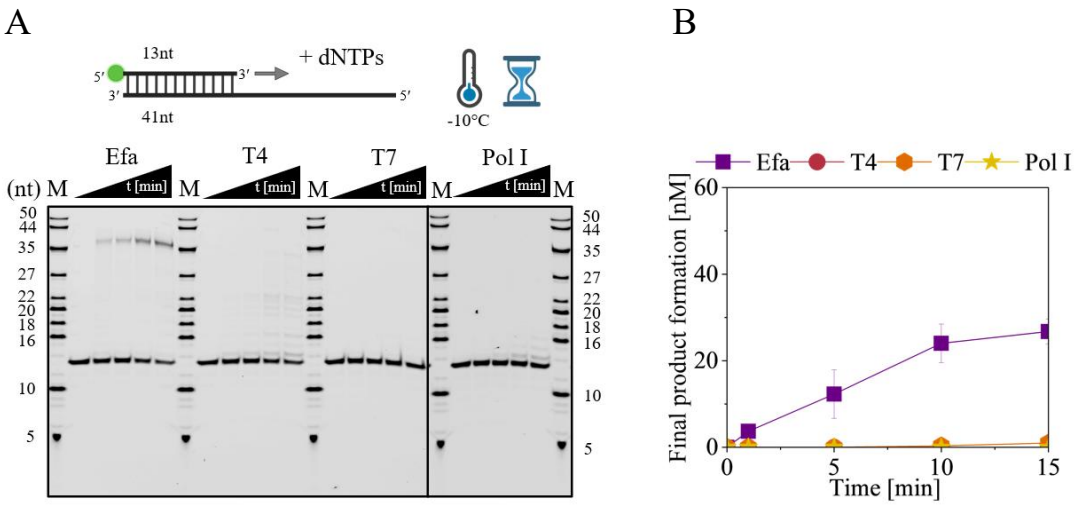


Figure 11. Comparison of Efa activity with those of T4, T7 and Pol I at -10 °C.
(A) Denaturing PAGE analysis of time-dependent primer extension at -10 °C by Efa, T4, T7, and Pol I. Lanes are labeled by reaction time, with size markers shown on both sides. WT Efa shows a strong full-length product band after 15 min, whereas T4, T7, and Pol I show faint or undetectable extension products under the same conditions. **(B)** Quantification of product concentration over time for Efa, T4, T7, and Pol I.

7.4. Structural characterization

7.4.1. Apo-enzyme crystal structure

The apo form of WT Efa polymerase crystallized in space group $P3_1$ with one monomer per asymmetric unit. Diffraction data were complete to 92%, and the structure was refined to 2.30 Å resolution. The molecular-replacement solution, obtained using an AlphaFold-predicted structure as the search model, revealed the canonical right-hand architecture of B-family polymerases, comprising fingers, palm, and thumb domains. Compared with previously solved B-family enzymes (e.g., RB69, KOD, Pfu), the overall fold was conserved, but the electron-density map revealed an N-terminal segment (residues 27-124) that adopted an OB-fold as confirmed by FoldSeek and DALI structural similarity analyses (Section 7.5.1, **Table 5**.). This N-terminal segment was resolved as a compact β-rich domain, topologically separated from the palm-fingers-thumb core, suggesting that it functions as an accessory module rather than an integral part of the polymerase active site (**Fig. 12**). The active site of the apo-structure is empty. No DNA, nucleotide, or metal ions are observed in the catalytic pocket, providing a reference state for comparison with the DNA-bound ternary complexes described below.

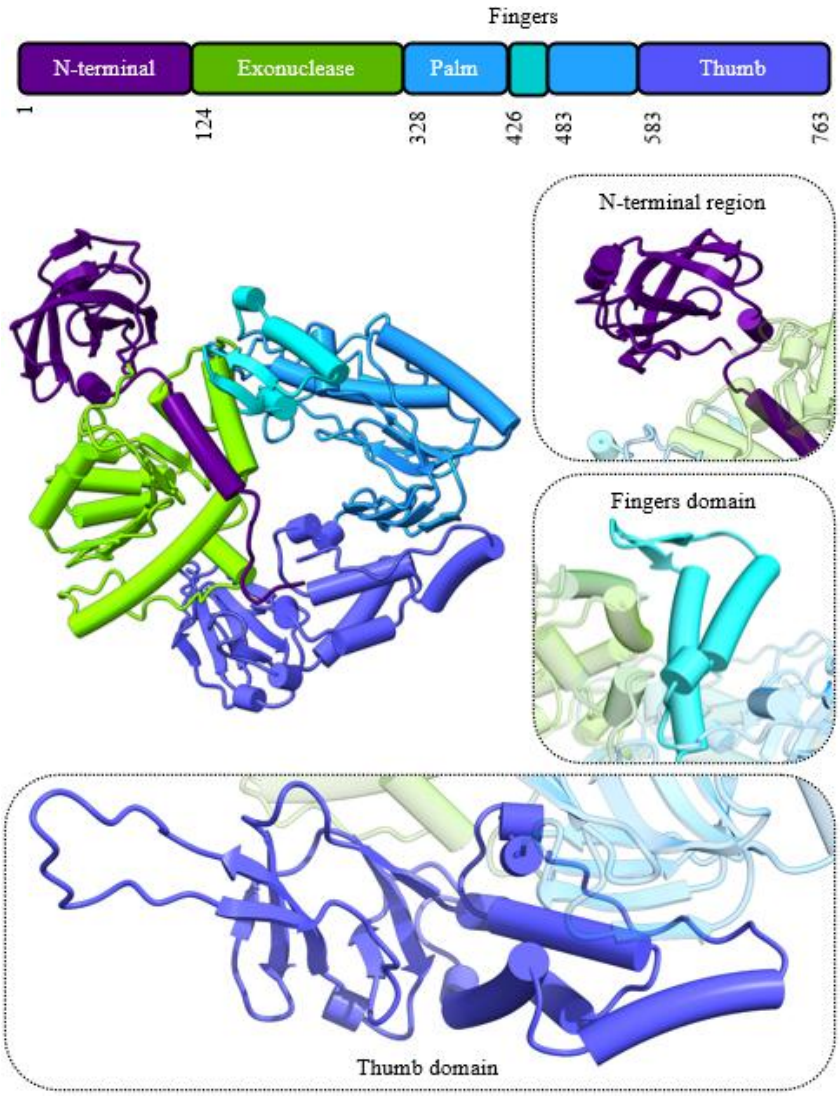


Figure 12. Overall architecture and domain organization of Efa DNA polymerase
The apo-structure of Efa DNA polymerase reveals a canonical B-family right-hand architecture with an additional N-terminal region. **(A)** linear domain organization of Efa showing the N-terminal region (residues 1-124, purple), exonuclease domain (124-328, green), palm (328-426, 483-583, teal), fingers (426-483, light blue), and thumb (583-763, dark blue). Bottom, ribbon representation of the apo-enzyme colored by domain as above, with inset views of the N-terminal, fingers, and thumb regions.

7.4.2. Prediction of residues responsible for 3′→5′ exonuclease activity

Biochemical assays demonstrated that WT Efa possesses a robust 3′→5′ exonuclease activity on DNA/DNA, RNA/DNA, and DNA/RNA duplexes, while showing no detectable degradation of RNA/RNA substrates, consistent with a canonical B-family proofreading

exonuclease domain. To identify the catalytic residues underlying this activity, the exonuclease region of Efa (residues 124-328) was aligned with three structurally characterized B-family polymerases: RB69, KOD, and Pfu, that possess well-defined exonuclease active sites (**Fig. 13**). The reference enzymes share a conserved DEDD motif (Asp-Glu-Asp-Asp) distributed across the three classical exonuclease motifs Exo I, Exo II, and Exo III. In Efa, the alignment places the DEDD motif at positions D137, E139, D188, and D281.

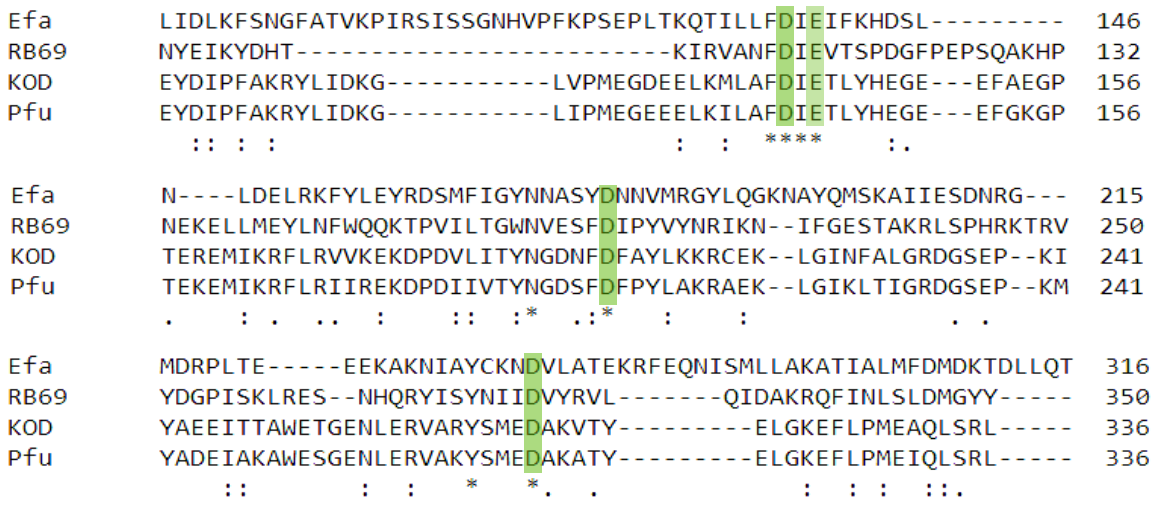


Figure 13. Multiple-sequence alignment of the exonuclease domain and the DEDD motif

Sequence alignment of the exonuclease domains of Efa and representative B-family polymerases. The Efa exonuclease region (residues 124-328) was aligned with RB69, KOD, and Pfu using Clustal Omega. The conserved DEDD catalytic tetrad is highlighted, mapping to D137, E139, D188, and D281 in Efa, which align with the Exo I, Exo II, and Exo III motifs of the reference enzymes.

Mapping of these residues onto the Efa structural model showed that they cluster within the predicted active site cleft and adopt the geometry characteristic of the B-family exonuclease center (**Fig. 14**). They superpose onto the metal-binding acidic residues of RB69, KOD and Pfu DNA polymerases, consistent with a role in binding the divalent cations required for phosphodiester-bond hydrolysis.

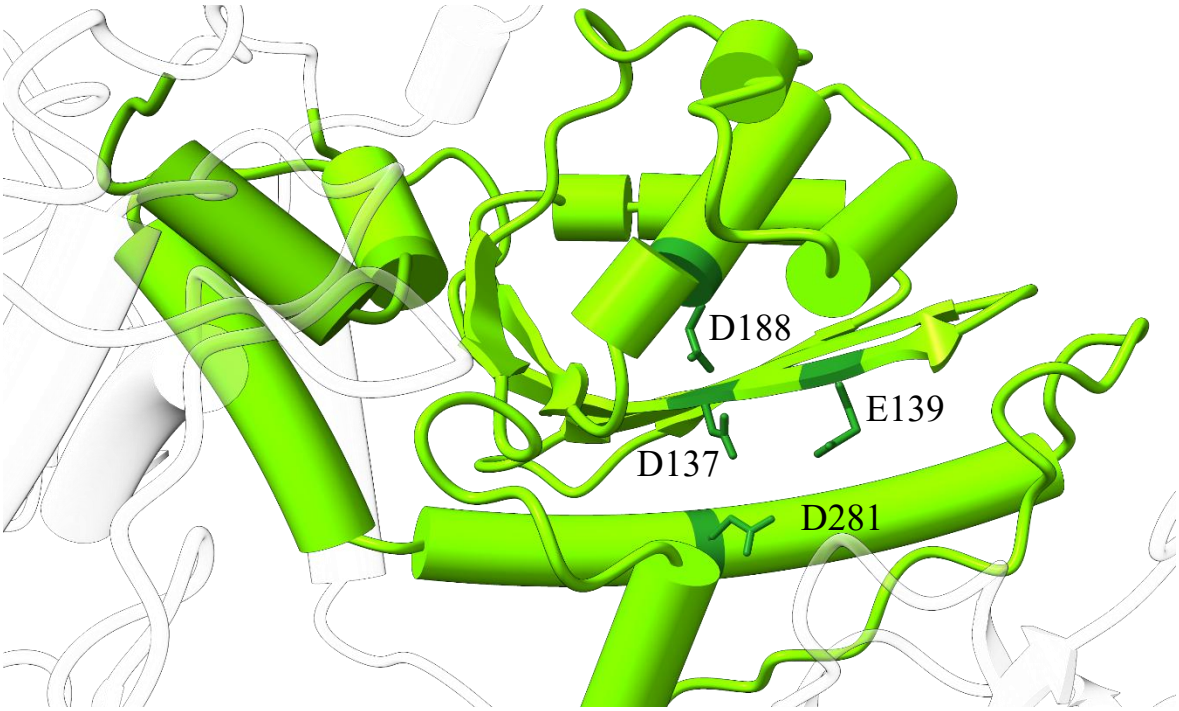


Figure 14. Structural mapping of the Efa DEDD catalytic motif
The 3D model of the exonuclease domain highlights the spatial arrangement of the DEDD catalytic residues: D137, E139, D188, and D281. These residues cluster within the exonuclease domain, forming the conserved geometry requisite for two-metal-ion phosphodiester bond hydrolysis. The background structures (faint gray) provide spatial context within the enzyme complex.

To test this assignment experimentally, we generated an exonuclease-deficient variant in which all four residues were substituted with alanine (Efa D137A/E139A/D188A/D281A; hereafter Efa DEDD). The Efa DEDD-coding gene was expressed, and the protein was purified using the same protocol as WT Efa. The mutant polymerase eluted at a similar volume on size-exclusion chromatography (**Fig. 15A**), further confirmed that the oligomeric state is unaffected by the mutation, and the band position was the same as WT Efa (**Fig. 15B**). In contrast, Efa with mutated DEDD showed a complete loss of the 3′→5′ exonuclease activity, even after 48h of incubation. It validates D137, E139, D188 and D281 as the catalytic DEDD motif of the Efa polymerase (**Fig. 15C**). To verify if the quadruple DEDD mutation compromises the protein's native structure, we analyzed far-UV CD spectra, confirming that the quadruple mutation does not perturb the overall secondary structure or

fold (**Fig. 15D**). The thermal stabilities of WT Efa and the Efa DEDD variant were investigated circular dichroism (CD), and melting curves were recorded at 208 nm. Both the wild-type and the exonuclease-deficient variant exhibited sigmoidal unfolding transitions with nearly identical melting temperatures (Efa WT: 41.41°C, Efa DEDD: 40.76°C, **Fig. 15E**). These results confirmed that the catalytic site substitutions do not significantly alter the global thermal stability or protein fold of the Efa polymerase.

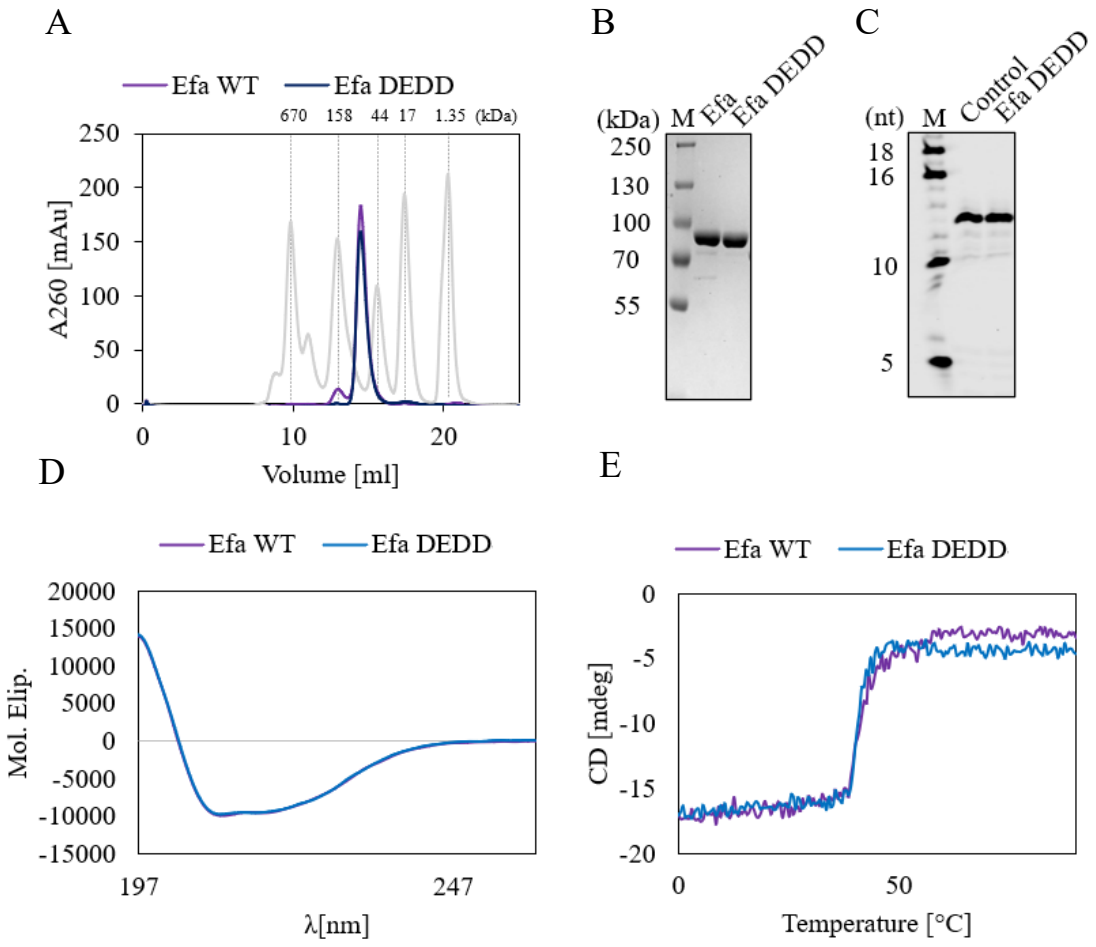


Figure 15. Biochemical characterization of the exonuclease-deficient Efa DEDD mutant **(A)** Size-exclusion chromatography profiles of Efa WT (purple) and Efa DEDD (blue), recorded as absorbance versus elution volume. **(B)** SDS-PAGE analysis of purified Efa WT and Efa DEDD. **(C)** Denaturing urea-PAGE analysis of ssDNA (Table 4. MRS#273) integrity after 48 h incubation with Efa DEDD and control. **(D)** Far-UV CD spectra of Efa WT and Efa DEDD from 197 to 257 nm. **(E).** CD melting curves recorded at 208 nm for Efa WT and Efa DEDD.

7.4.3. Ternary holo-enzyme complexes (engaged vs. loose N-terminal conformation)

To investigate how the N-terminal region interacts with DNA and contributes to catalysis, two ternary complexes of the exonuclease-deficient Efa DEDD mutant bound to primer-template duplexes of different lengths were investigated. Both structures were solved by molecular replacement using the apo-enzyme as a search model and refined to high resolution (2.15-2.21 Å), enabling precise visualization of protein-DNA contacts and N-terminal domain positioning.

In the first complex, Efa DEDD mutant was crystallized with a 12-nt primer (3′-dideoxy-terminated) annealed to an 18-nt template, dATP, and divalent metal ions. The structure was refined to 2.15 Å resolution (R_{work} = 0.18, R_{free} = 0.22). Electron density corresponding to a divalent metal ion was observed at the catalytic site. The identity of the catalytic-site metal ion was assessed by refining alternative divalent cations against the same data with identical settings. Modeling the ion as Mg^{2+} left a localized positive mFo-DFc peak at site, indicating that the observed density is stronger than expected for Mg^{2+}, whereas the Mn^{2+} model showed no residual density above 3 σ at the site. The overall active-site geometry remained consistent with two-metal catalysis. In this complex, the template strand extends beyond the primer to form a six-nucleotide 5′ single-stranded overhang (positions -6 to -1), which is clamped by the N-terminal domain (**Fig. 16**).

The N-terminal region adopts an "engaged" conformation shifted by ~4Å towards the polymerase core relative to the apo-structure. Residues Y74, R79, F105, G104, A106, and T107, together with K53, K55, and A52, form a positively charged, aromatic-rich surface that contacts template nucleotides -6 to -4, providing base-stacking and electrostatic interactions typical of OB-fold SSB modules. These contacts tether the overhang to the N-terminus, while the palm and fingers domains position the primer terminus and incoming dATP in a catalytically competent arrangement, capturing a pre-insertion or insertion-like state of the polymerase.

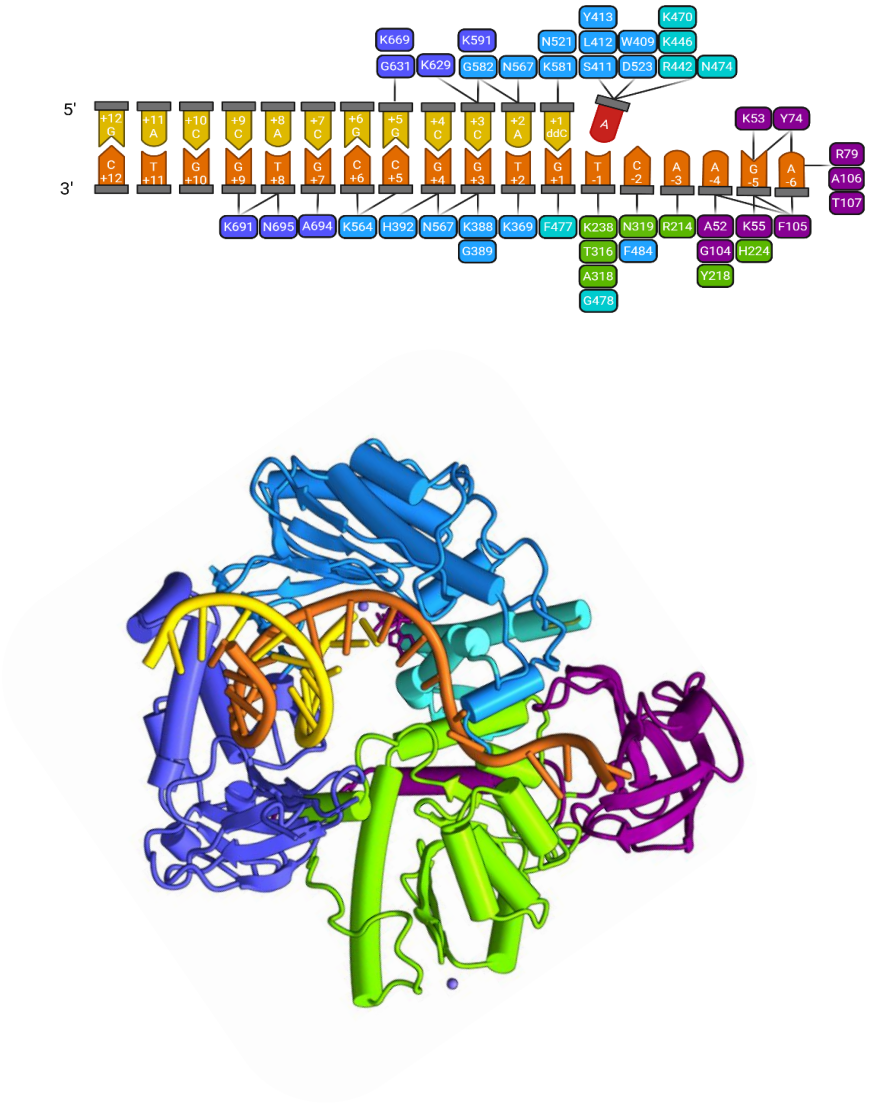


Figure 16. Ternary complex of Efa DEDD mutant with 12/18-mer template
The template is numbered relative to the primer terminus, with positions -6 to -4 forming a 5′ ssDNA overhang. N-terminal residues Y74, R79, F105, G104, A106, T107, K53, K55, and A52 are shown interacting with the overhang, while core polymerase residues are shown contacting the duplex region and the incoming nucleotide.

Complex 2 (12-mer/16-mer substrate). A second ternary complex was obtained with the same 12-nt primer but employing a shorter 16-nt template, which generates only a 4-nucleotide 5′-overhang. This structure was refined to 2.21 Å resolution (R_{work} = 0.21, R_{free} = 0.26) and

retains essentially identical interactions between the polymerase core and the duplex region. However, the N-terminal domain is displaced into a more distal “loose” conformation and makes no detectable contacts with the ssDNA overhang (**Fig. 17**). In this state, the overhang is left largely unsupported by the N-terminal region, and the N-terminal region swings away from the DNA by ~4 Å compared with the engaged complex.

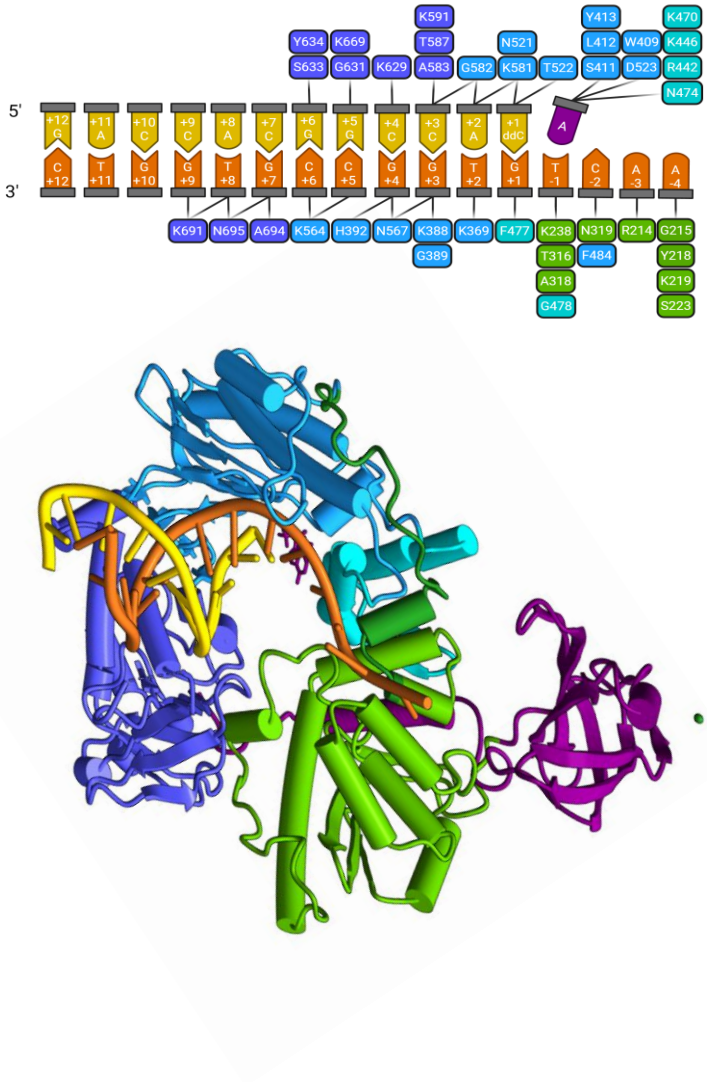


Figure 17. Ternary complex of Efa DEDD mutant with 12/16-mer template
The 16-nt template generates a 4-nt 5′ ssDNA overhang. The schematic contact map of protein-DNA interactions shows that core polymerase residues contact the duplex and the primer terminus, whereas no N-terminal residues contact the 5′ overhang.

Template-length assays. Structural superposition of Complexes 1 and 2 on the palm domain highlights a concerted rigid-body movement of the N-terminal domain between the two

states: a translation of ~4 Å combined with an overall rotation of ~22°, as quantified from principal-axis measurements in ChimeraX (**Fig. 18A**). This conformational switch correlates with template-length-dependent activity observed in solution. Primer-extension assays performed with 26-nt and 41-nt templates showed that WT Efa consistently terminates synthesis five nucleotides short of the template end for both lengths (**Fig. 18B**). In the structural context, the longer 18-nt template in Complex 1 provides sufficient 5′ overhang to engage the N-terminal domain, coinciding with a reproducible five-nucleotide premature termination.

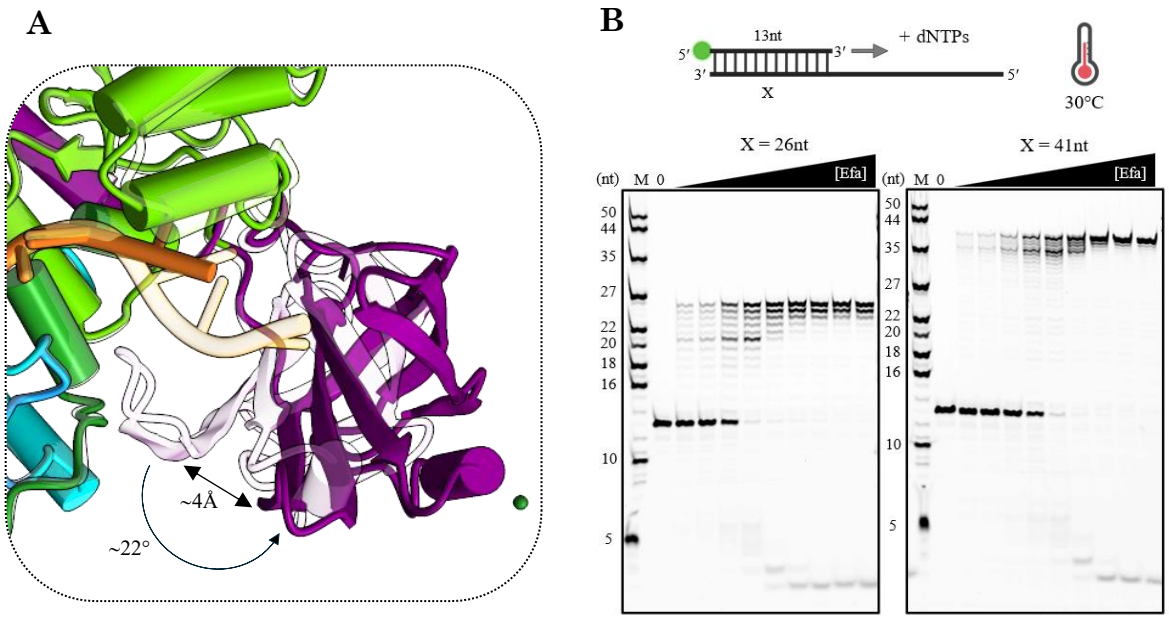


Figure 18. Template-length-dependent termination by WT Efa and domain rotation by Efa DEDD.
Template-length-dependent termination on WT Efa. **(A)** Structural comparison of short and long DNA-bound Efa DEDD, aligned on the palm domain. The two structures differ in the position of the N-terminal domain, with an approximately 22° rotation in the DNA-bound state and a 4 Å shift. **(B)** Denaturing PAGE analysis of WT Efa primer extension on 26-nt and 41-nt templates. Lanes are shown for the different reaction conditions and time points.

Together, these two crystal structures support a model in which the N-terminal region adopts distinct conformations: an engaged state that captures the single-stranded 5′-overhang and a loose state that occurs when the overhang is too short. Although it remains unclear whether this represents dynamic switching in solution, the correlation between overhang length and

N-terminal conformation provides a structural framework linking overhang length to premature termination. More broadly, these findings support a role for the N-terminal region as an accessory module that stabilizes ssDNA during synthesis and modulates efficient primer extension at low temperatures.

7.5. N-terminal domain: bioinformatic identification, creating the Efa Δ27-124 construct and functional analysis

7.5.1. Bioinformatic identification

The N-terminal segment (residues 27-124) of WT Efa polymerase was subjected to sequence-profile searches, FoldSeek, and DALI structural similarity analyses. Although the primary sequence did not match any known protein families, the top structural hits corresponded to the single-stranded DNA-binding protein (SSB) fold (**Fig. 19; Table 5**). Alignment of the N-terminal region with conserved SSB proteins suggested a potential role in stabilizing single-stranded DNA (ssDNA) during synthesis.

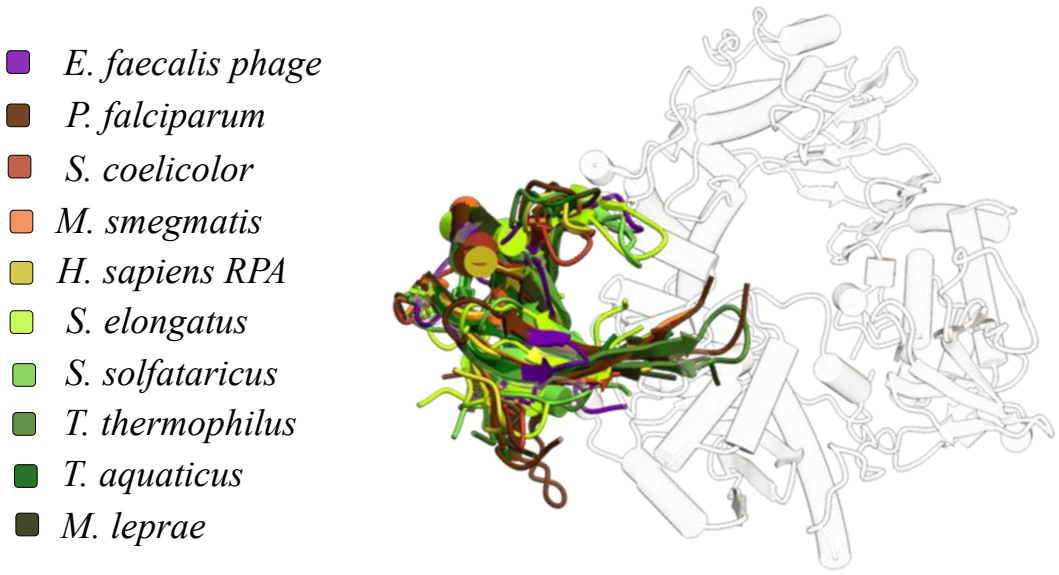


Figure 19. Structural conservation of the N-terminal SSB-like domain
Structural superposition of the Efa N-terminal domain (residues 27-124, purple) with SSB-like folds from diverse species (colored ribbons), including *P. falciparum*, *S. coelicolor*, *M. smegmatis*, *S. elongatus*, human RPA, *S. solfataricus*, *T. thermophilus*, *T. aquaticus*, and *M. leprae*.

Table 5. Structural alignment metrics for representative SSB-like/ OB-fold proteins

Entry	*Chain*	*RMSD*	*TM-score*	*Identity*	*Aligned Residues*	*Sequence Length*
N-terminus	-	-	-	-	-	97
1PFS	B	2.64	0.5	7%	67	78
1S3O	A	2.96	0.57	17%	74	132
1SE8	A	2.91	0.6	6%	78	301
1TXY	A	2.83	0.56	8%	67	104
3LGJ	A	2.97	0.54	9%	69	169
5ODP	A	2.81	0.55	5%	69	196
5YUO	B	2.99	0.53	6%	66	121
5YYU	D	2.96	0.55	4%	69	112
6CQM	A	2.63	0.57	9%	77	119

7.5.2. Construction of the Efa Δ27-124 mutant

The Efa Δ27-124 construct was obtained as described in Section 6.1. The Efa ΔN protein was expressed and purified using the same protocol as WT Efa. SDS-PAGE and analytical SEC confirmed that the Efa ΔN variant was monodisperse and >99% pure (**Fig. 20A**), with an apparent molecular mass consistent with the deletion (**Fig. 20B**). To test whether the mutation compromises the global protein fold, circular dichroism (CD) spectroscopy analysis was conducted. The far-UV spectra of Efa ΔN were nearly superimposable on WT Efa, showing characteristic α-helical signatures (**Fig. 20C**). Thermal denaturation scans further confirmed that the Efa ΔN mutation confers an increase in thermal stability, with a melting

temperature (T_m) of ~58°C compared to 41.41°C for WT (**Fig. 20D**), indicating that the core polymerase domain is structurally robust even in the absence of the N-terminal region.

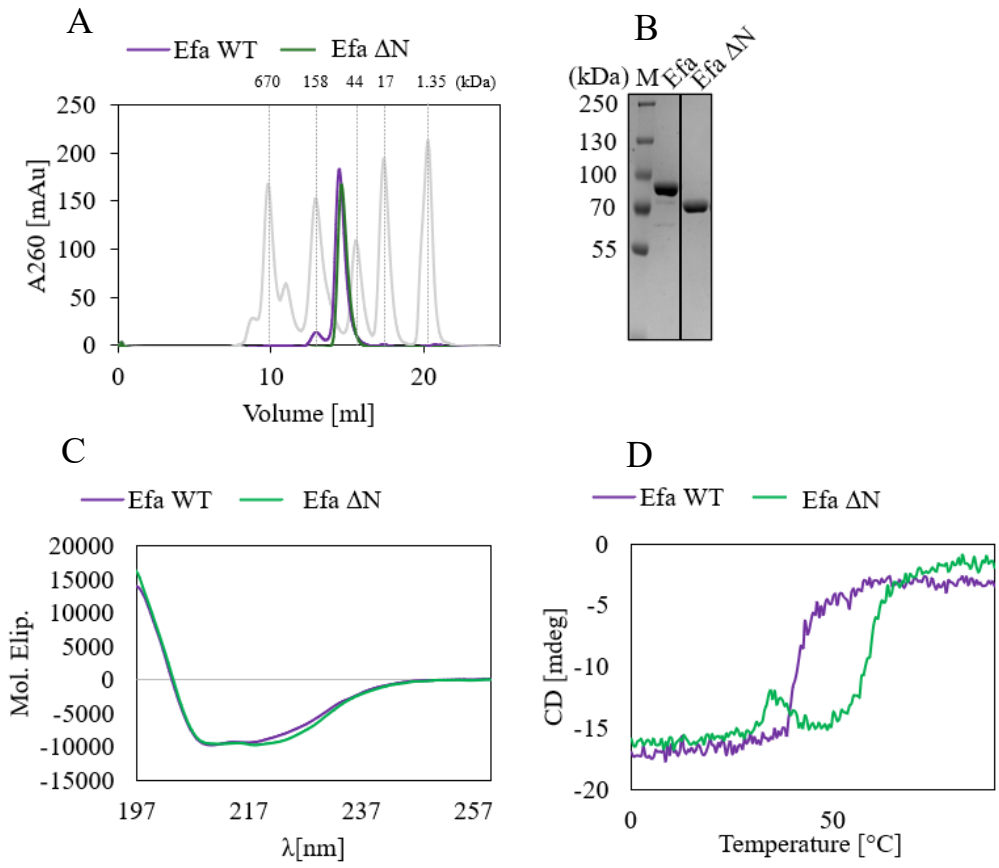


Figure 20. Biophysical validation of the Efa ΔN variant
(A) Size-exclusion chromatography profiles of WT Efa and Efa ΔN. **(B)** SDS-PAGE analysis of purified WT Efa and Efa ΔN. **(C)** Far-UV CD spectra of WT and ΔN Efa from 197 to 257 nm. **(D)** CD melting curves measured at 208 nm as a function of temperature for WT Efa and Efa ΔN.

7.5.3. Functional characterization of the Efa ΔN variant

To determine the functional role of the N-terminal region, the enzymatic activity of the WT Efa polymerase was compared with that of the Efa ΔN using primer-extension assays with linear templates at 30°C (**Fig.21A**). Denaturing PAGE analysis revealed that both WT Efa and the Efa ΔN variants efficiently converted the 13-nt primer into full-length extension

products, demonstrating that the N-terminal region is not strictly required for efficient primer extension on unstructured DNA. However, quantitative analysis of the concentration-response curves revealed that the Efa ΔN mutant achieved a higher maximal product yield (50 nM) compared to the WT enzyme (37 nM) (**Fig. 21B, C**). This enhanced efficiency suggests that, with simple linear substrates at moderate temperatures, the N-terminal domain may modulate or limit the polymerase's kinetics rather than act as a general booster of catalytic throughput.

To elucidate the role of the N-terminal domain in cold adaptation, the performance of both enzymes at -10 °C was evaluated. In contrast to its performance with linear templates at 30 °C, the Efa ΔN variant displayed a near-total loss of functionality in the cold. While the WT polymerase maintained robust catalytic activity, generating significant primer extension products, the Efa ΔN variant was virtually inactive, failing to produce detectable extension products under identical conditions (**Fig. 21D, E**).

This phenotype indicates that the N-terminal SSB-like module is required for efficient catalysis under the tested cold conditions. Although the Efa ΔN variant retained measurable activity and the domain appears to be dispensable for primer extension on linear DNA substrate at moderate temperatures, its absence was associated with a marked reduction in catalytic efficiency under sub-zero conditions. Thus, under the conditions examined, the N-terminal region appears to provide a kinetic advantage for DNA synthesis at low temperatures. Whether this effect results from direct ssDNA stabilization, altered substrate engagement, or another mechanism remains to be established.

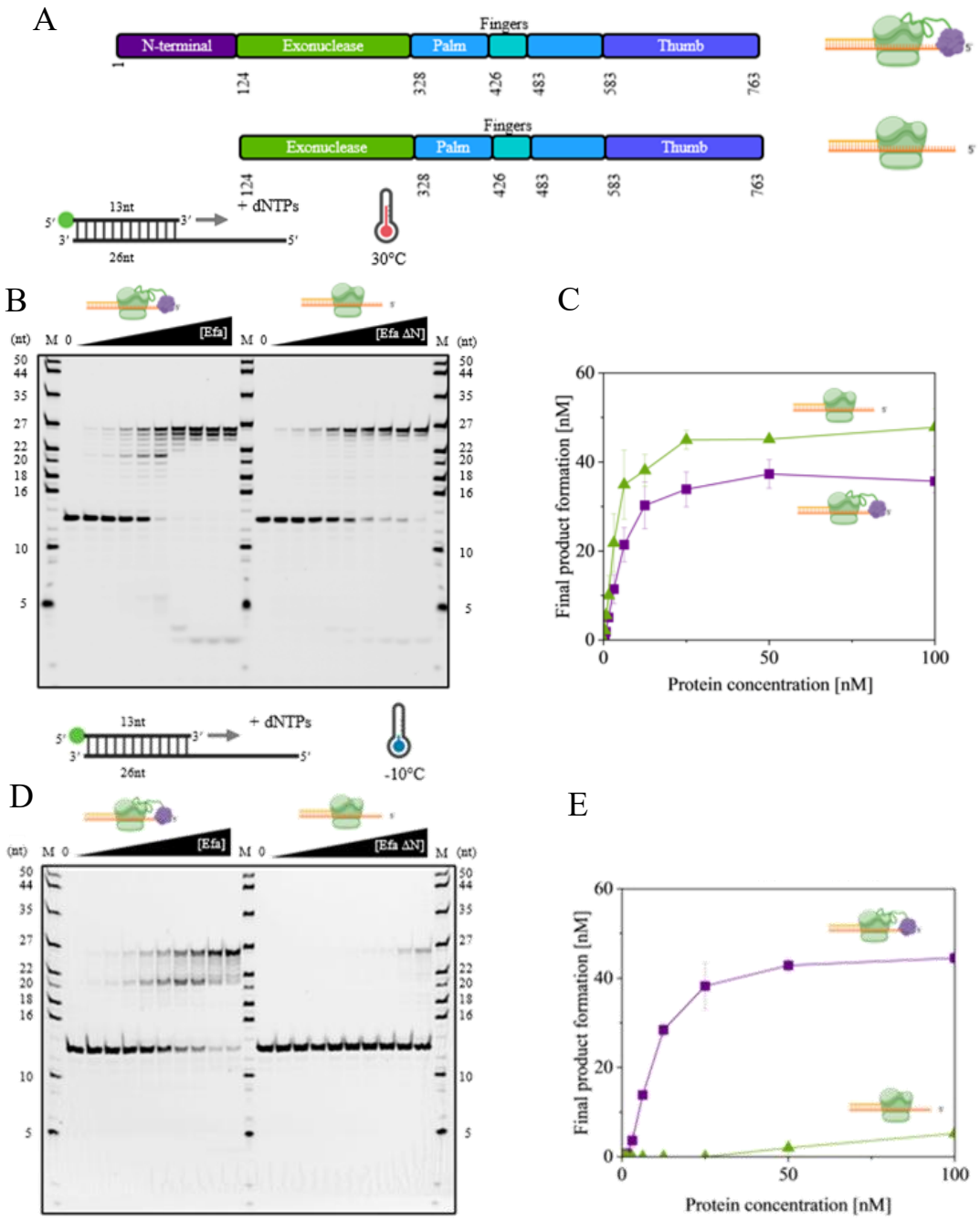


Figure 21. Functional consequences of N-terminal deletion on polymerase activity.
(A) Domain architecture of WT Efa and Efa ΔN **(B)** Denaturing PAGE analysis of reaction products for WT Efa and Efa ΔN across a protein concentration gradient, indicated by the triangle. The gel shows the starting substrate labeled 0 and the extended products. **(C)** Quantification of final product yield (nM) as a function of protein concentration (nM) for WT Efa and Efa ΔN. **(D)** Denaturing PAGE analysis of WT Efa and Efa ΔN reactions showing the product bands observed under the tested conditions. **(E)** Quantification of the gel shown in D, plotted as product yield versus enzyme concentration.

7.5.4. Performance on structured hairpin templates

To assess how the N-terminal SSB-like domain influences DNA synthesis with substrates of increasing structural complexity, efficiency of primer extension by WT Efa polymerase and the Efa ΔN truncated variant was compared using a simple linear duplex and an otherwise similar template but bearing a terminal hairpin. In the linear 13-mer/58-mer duplex assay, both WT Efa and Efa ΔN enzymes efficiently converted the 13-nt primer into full-length product across the tested enzyme concentrations (**Fig. 22A**), indicating that the N-terminal region is not required for efficient primer extension on unstructured DNA.

When the same primer was paired with the hairpin-containing template, WT Efa polymerase was able to traverse the stem-loop and generate full-length products, but with a characteristic pause approximately 5 nt upstream of the template terminus that gave rise to a prominent intermediate band. In contrast, the Efa ΔN variant stalled at the base of the hairpin, producing a discrete intermediate corresponding to the position immediately before the secondary structure and failed to yield detectable full-length product under the same reaction conditions (**Fig. 22B**). Together, these results suggest that the N-terminal OB-fold promotes efficient primer extension on hairpin-containing templates, whereas it is not required for synthesis on linear DNA. The accumulation of products near the hairpin indicates an association between the N-terminal region and the ability to extend through the structured template.

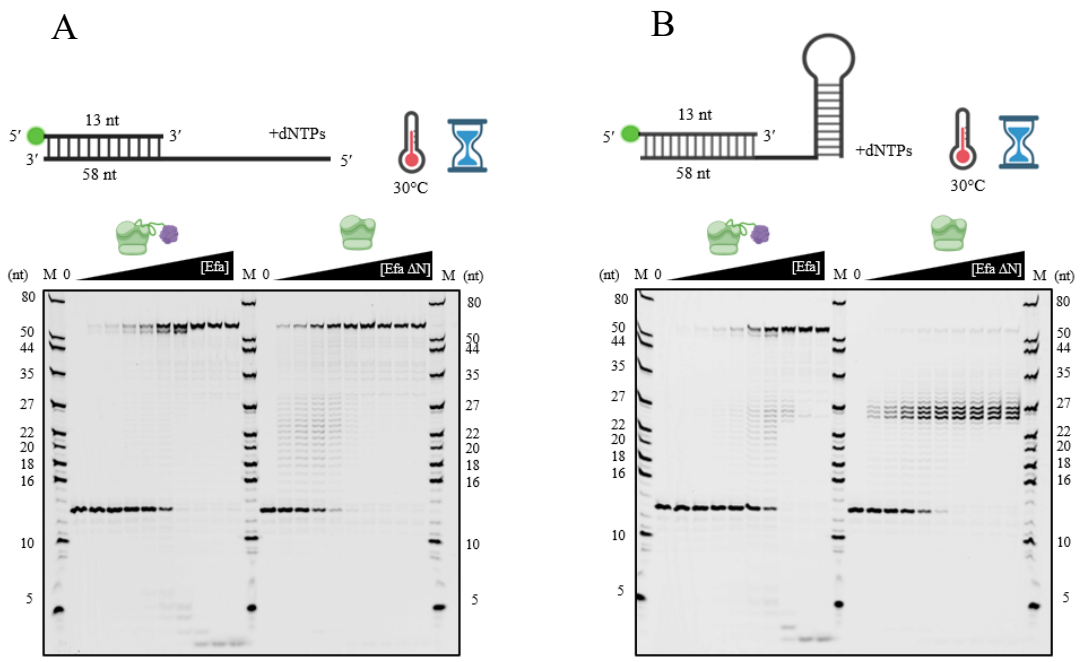


Figure 22. The N-terminal SSB-like domain on linear and structured DNA templates
(A) A 13-nt primer annealed to a 58-nt template strand extended by Efa polymerase in the presence of dNTPs at 30°C. The lower panel shows denaturing polyacrylamide gels with a size marker lane (M) followed by lanes containing increasing concentrations of polymerase. The lanes show the 13-nt primer band and a series of extension products, including the full-length product, for WT Efa and Efa ΔN on the linear substrate. **(B)** The same 13-nt primer annealed to a 58-nt template strand containing a stem-loop near the terminus. The gels below show primer extension by WT Efa and the Efa ΔN variant across an enzyme titration, with molecular size markers (M) as in panel A. The lanes show a pause product approximately 5 nt short of the full-length band and the full-length extension product for WT polymerase, whereas the Efa ΔN mutant shows the pause product predominantly.
.

7.6. Kinetic analysis

To dissect how the N-terminal SSB-like domain contributes to catalysis and cold adaptation, three complementary kinetic approaches were employed. Pre-steady-state burst experiments were used to estimate the apparent rate of rapid product formation during the initial catalytic phase and to determine the burst amplitude. Under appropriate assumptions, the burst amplitude can provide an estimate of the fraction of active enzyme. Because these experiments focused on the initial turnover, they did not resolve product release or subsequent cycles. Single-turnover kinetics were performed with enzyme in excess over the

DNA substrate to minimize contributions from multiple turnovers, substrate rebinding, and subsequent catalytic cycles. These experiments were used to characterize the apparent time course of product formation under conditions in which most substrate molecules were associated with enzymes. However, the observed rate constant cannot necessarily be assigned exclusively to the chemical step of nucleotide incorporation, because other kinetic steps may also contribute to the measured signal. Arrhenius analysis was used to estimate the apparent temperature dependence of the observed rate constants over a temperature range in which the protein remained stable. The analysis assumes that the kinetic mechanism and the rate-limiting step remain sufficiently similar over the temperature range examined. Consequently, the resulting activation energies should be interpreted as apparent values that reflect the temperature dependence of the observed process, rather than as direct measurements of the activation energy of nucleotide incorporation alone. Together, these approaches provided complementary information about the early catalytic behavior, substrate processing, and temperature dependence of Efa and its variants. Reactions were performed predominantly with a 13-nt/26-nt primer-template duplex, using dCTP as the first incoming nucleotide, and comparing WT Efa with Efa ΔN. Under enzyme-limiting conditions, burst behavior was characterized, and the single-turnover rate constant (k_{obs}) was measured under enzyme-excess conditions, as a function of temperature and nucleotide concentration. These datasets were then analyzed using the Arrhenius formalisms to extract activation energies and hyperbolic fitting of k_{obs} versus nucleotide concentration to obtain apparent dissociation constants ($K_{D,app}$) for nucleotide-binding affinities. Because Efa exhibits high 3′→5′ exonuclease activity under standard conditions, primer degradation was minimized, and the polymerization step was enriched by increasing the monovalent salt concentration to 300 mM and by employing a 3′-terminal phosphorothioate-modified primer in all kinetic assays. The phosphorothioate modification at the 3′ primer terminus renders the phosphodiester bond resistant to exonuclease hydrolysis (Eckstein, 1985), a standard approach for isolating polymerase kinetics from proofreading activity. The elevated salt concentration further suppresses exonuclease activity, though both conditions may modestly alter kinetic parameters. Accordingly, the values reported here should be considered within the context of these optimized assay conditions.

7.6.1. Pre-steady-state burst kinetics

To characterize the early phases of nucleotide incorporation and compare the kinetic behavior of WT Efa and Efa ΔN, pre-steady-state polymerization assays were performed using a rapid-quench flow apparatus. Reactions were monitored for both the WT Efa and the Efa ΔN at 30°C (**Fig. 23A, B**) and 10°C (**Fig. 23C, D**). In contrast to the wild-type enzyme, the Efa ΔN mutant failed to exhibit pre-steady-state burst kinetics under the same experimental conditions (**Fig. 23B)**. For the WT enzyme, time-course data displayed clear biphasic "burst" kinetics, characterized by an initial rapid phase followed by a slower, approximately linear steady-state phase. The data were globally fit to the burst equation:

$$P(t) = A(1 - e^{-k_{obs}t}) + k_{ss}t$$

Where:

A:	burst amplitude
k_{obs} [s^{-1}]:	the apparent rate constant of the fast phase
k_{ss} [s^{-1}]:	the apparent rate constant of the steady-state phase

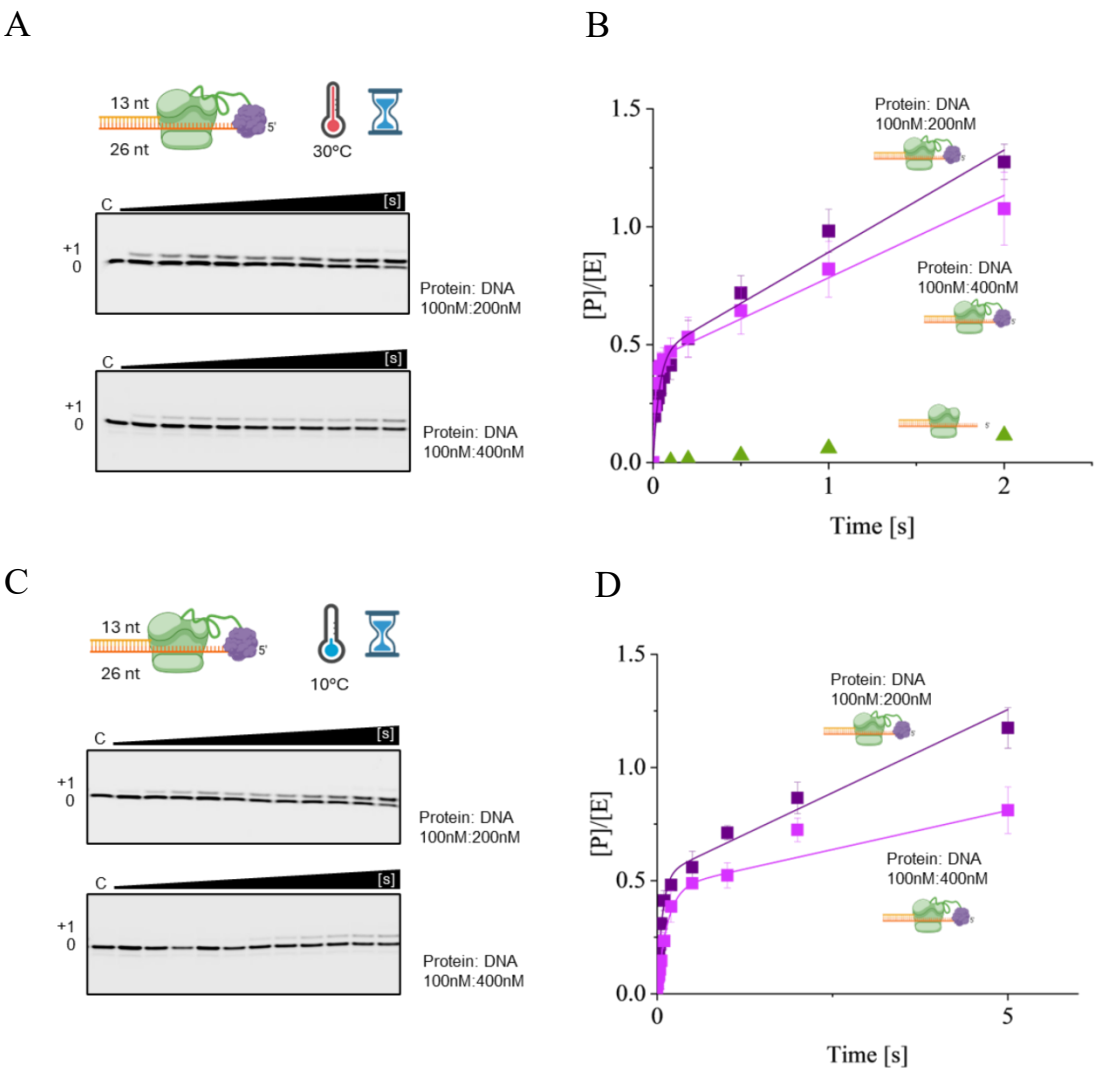


Figure 23. Pre-steady-state burst analysis of WT Efa at 30°C and 10°C
The rapid-quench-flow setup and representative gels for WT Efa reacting with a 13-nt/26-nt primer-template duplex at 30 °C **(A)** and 10 °C **(C)** in the presence of 200 μM dCTP and 300 mM salt at enzyme: DNA ratios of 1:2 and 1:4. Panels **B** and **D** plot product formation as [P]/[E] versus time for the corresponding conditions. Closed black and purple symbols denote WT Efa at 1:2 and 1:4 enzyme: DNA, respectively, and were globally fit to a burst-plus-linear model. Green triangles denote the N-terminally truncated Efa ΔN construct measured under identical conditions.

In a homogeneous active population, a pre-steady-state burst with A ~ *1* would be expected, provided that the active-site concentration is accurately determined, the DNA substrate is saturating, and all enzyme-DNA complexes are productive. The consistently reduced amplitudes (~0.5) at both 30°C and 10°C, could reflect a substoichiometric fraction of catalytically active enzyme or a population of enzyme-DNA complexes that are nonproductive or turn over slowly. This interpretation assumes that the enzyme and DNA formed a saturating complex, and that the bound complexes were fully productive. However, these assumptions were not independently established, and alternative explanations include DNA heterogeneity, incomplete substrate binding, or the formation of partially productive enzyme-DNA complexes. The SEC and CD analyses support the monomeric and well-folded character of Efa, but they do not exclude kinetic heterogeneity or incomplete productive binding. The steady-state slope is correspondingly slower at 10°C, but a distinct burst phase is still observed, confirming that the basic polymerization mechanism operates even at near-freezing temperatures (**Table 6)**.

Table 6. Pre-steady-state kinetic parameters for WT Efa polymerase at 30°C and 10°C using two protein-to-DNA ratios

Temperature (°C)	*Protein: DNA ratio*	*A*	k_{obs} (s^{-1})	k_{ss} (s^{-1})
30	1:2	0.46 ±0.04	28.17±7.02	0.43±0.04
	1:4	0.43± 0.01	73.54±5.29	0.35±0.02
10	1:2	0.52±0.03	13.71±1.53	0.15±0.02
	1:4	0.47±0.01	7.01±0.43	0.07±0.004

7.6.2. Single-turnover kinetics at low temperature

To examine how the N-terminal region influences product formation under enzyme-excess conditions, single-turnover kinetics were measured using a 13-nt primer annealed to a 26-nt template and dCTP as the first incoming nucleotide. The enzyme was used in excess over the

DNA substrate to minimize contributions from multiple turnovers and substrate rebinding. Reactions were performed in rapid-quench flow at 10°C with 1 μM polymerase, 100 nM DNA, and 200 μM dCTP. Under these conditions, the observed rate constant describes the apparent time course of product formation but cannot be assigned exclusively to the chemical step of nucleotide incorporation.

WT Efa is strongly favored over Efa ΔN at 10°C. Under these conditions, WT Efa displayed rapid product formation that was well described by a single-exponential fit, yielding an observed rate constant k_{obs} = 27.32 s^{-1} at 10 °C. In contrast, Efa ΔN displayed a lower observed incorporation rate on the same substrate, with k_{obs} = 0.05 s^{-1} (**Table 7, 8; Fig. 24**). These data establish that the N-terminal region is critical for efficient single-nucleotide incorporation at 10 °C, whereas the polymerase core of Efa ΔN displayed substantially lower observed incorporation rate under these conditions. Consistent with the ternary complexes, in which the N-terminal OB-fold clamps a 6-nt 5′ overhang but disengages when only a 4-nt overhang is available, WT Efa shows a ~540-fold acceleration at 10°C with long-overhang templates.

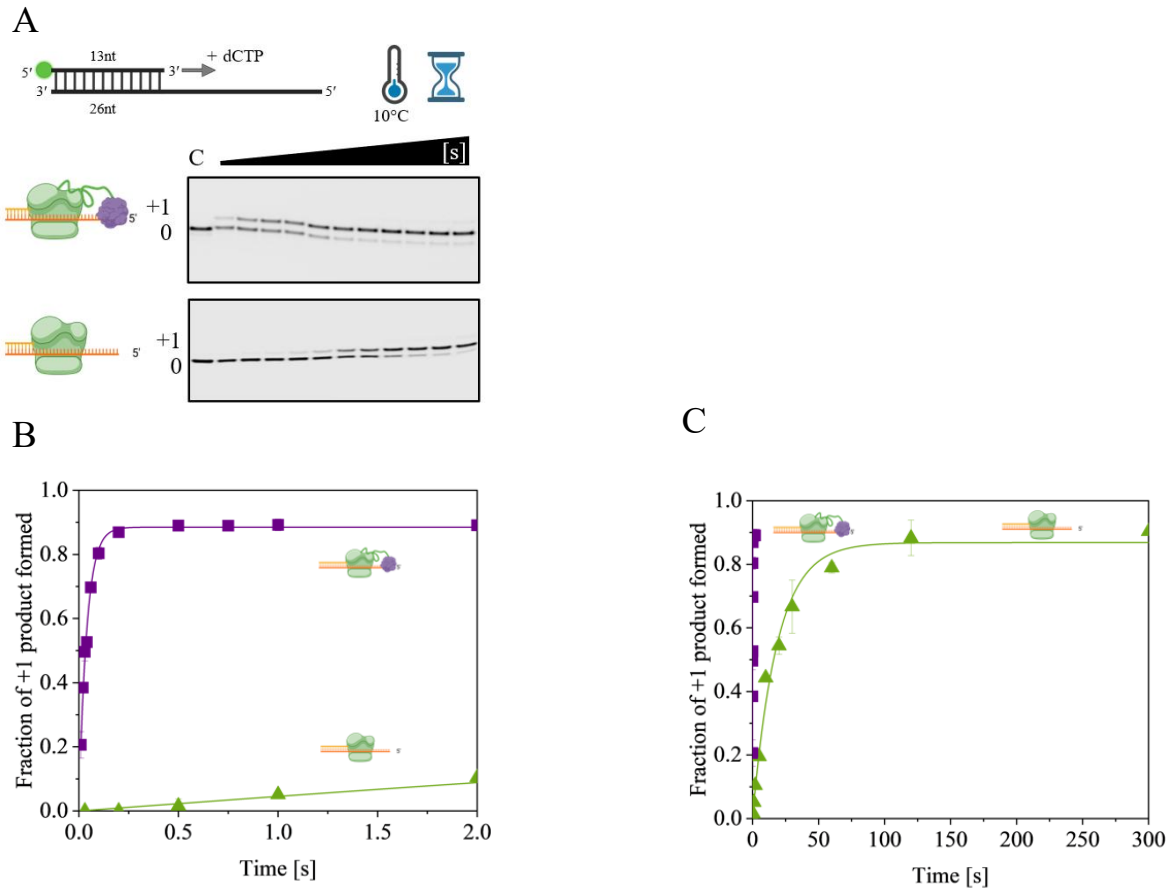


Figure 24. dCTP incorporation at 10 °C
(A) A scheme and results of experiments with the 13-nt primer/26-nt template duplex with added dCTP. **(B)** Fraction of +1 product vs. time (0-2 s) for WT Efa (purple squares) and Efa ΔN (green triangles). **(C)** Same data plotted over 0-300 s to illustrate the slower kinetic profile of Efa ΔN.

N-terminal engagement is required for the low-temperature advantage. Structural analyses indicated that the isolated N-terminal domain contacts the single-stranded 5′ overhang only when the template provides a sufficiently long stretch of ssDNA (**Fig. 25A, B, C**). To test whether this engagement is required for the high polymerization rate at 10 °C, the single-turnover measurements were repeated on a "short" template carrying a 4-nt 5′ overhang, which is too short to support stable N-terminal binding within the holoenzyme complex. With this short substrate, k_{obs} for WT at 10°C dropped to 0.2 s^{-1}, representing a ~130-fold reduction relative to the longer-template condition (**Fig. 25A, B, C**). Thus, loss of productive N-terminal engagement substantially slows nucleotide incorporation at low temperature. In contrast, Efa ΔN, which lacks the entire SSB-like module, showed no appreciable difference in rate between long and short overhangs under the same conditions. It indicates that the length-dependent acceleration is specifically mediated by the N-terminal domain rather than by the polymerase core (**Fig. 25D, E**). Taken together, these results show that, at 10 °C, WT Efa is much more efficient than Efa ΔN only when the N-terminal region can engage the template overhang. When this contact is prevented by shortening the overhang, WT collapses to ΔN-like behavior. These data show that, at 10°C, the observed rate of product formation by WT Efa increased when N-terminal region could engage a sufficiently long 5′ overhang.

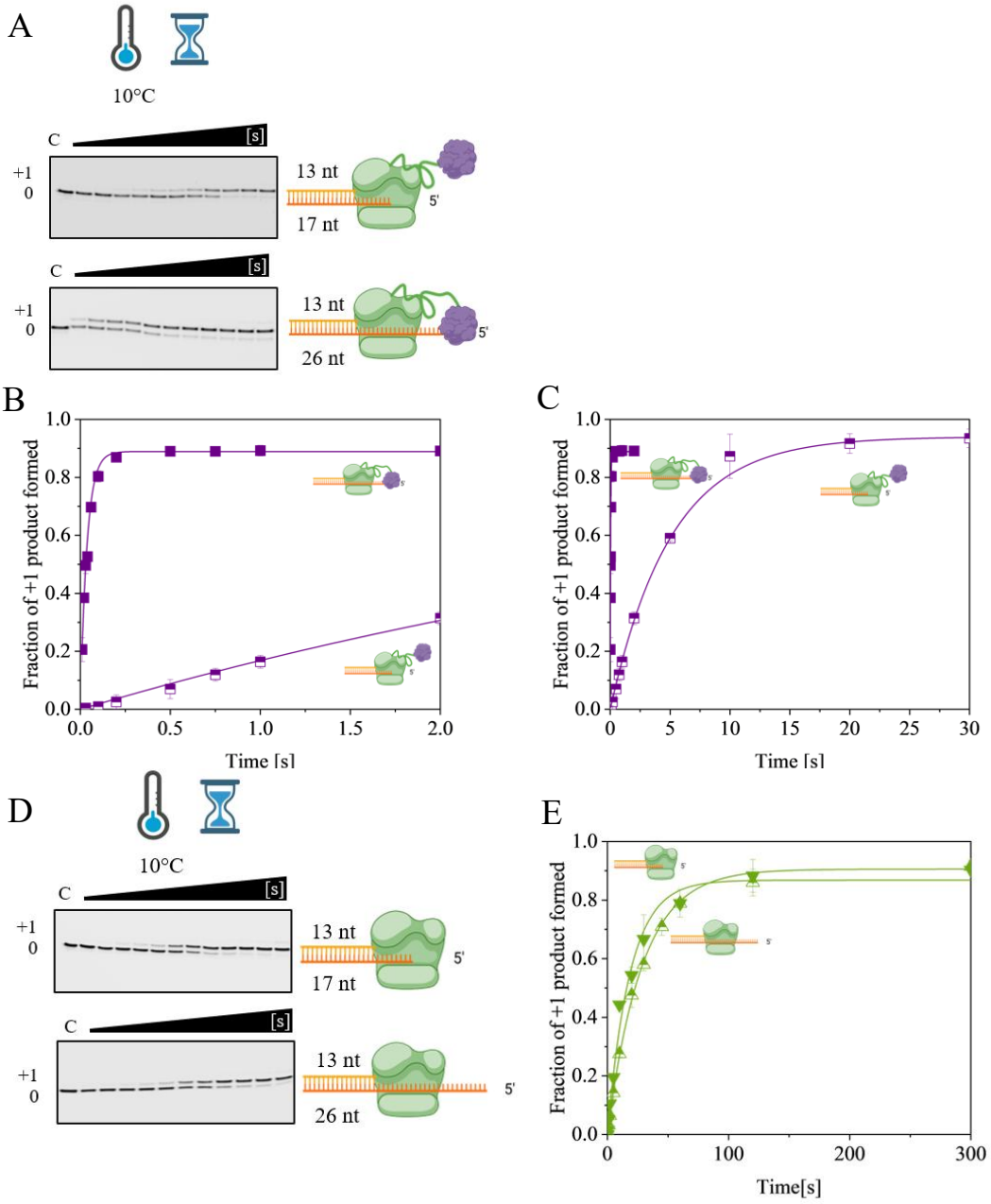


Figure 25. Substrate length-dependence of DNA synthesis by WT Efa and the Efa ΔN
(A) Representative denaturing PAGE analysis of primer extension assays performed with WT Efa polymerase using a short linear template and a long template. Lanes indicate increasing reaction time. **(B)** Kinetic analysis of WT Efa showing the fraction of +1 product formed over time for short vs. long templates. **(C)** Extended time-course kinetic analysis of WT Efa on the same templates, illustrating differences in reaction completion. **(D)** Representative PAGE analysis of primer extension assays performed with the Efa ΔN using short vs. long templates. **(E)** Kinetic analysis of the Efa ΔN mutant showing the fraction of +1 product formed over time for short vs. long templates.

Temperature dependence of WT Efa and Efa ΔN. To place these low-temperature effects in a broader thermodynamic context, single-turnover assays were repeated at 20°C for WT Efa (**Fig. 26A, B, C; Table 7)** and Efa ΔN (**Fig. 27A, B; Table 8),** and 30°C for WT Efa (**Fig. 26D, E, F; Table 7)** and Efa ΔN (**Fig. 27C, D; Table 8)** with the long and short templates.

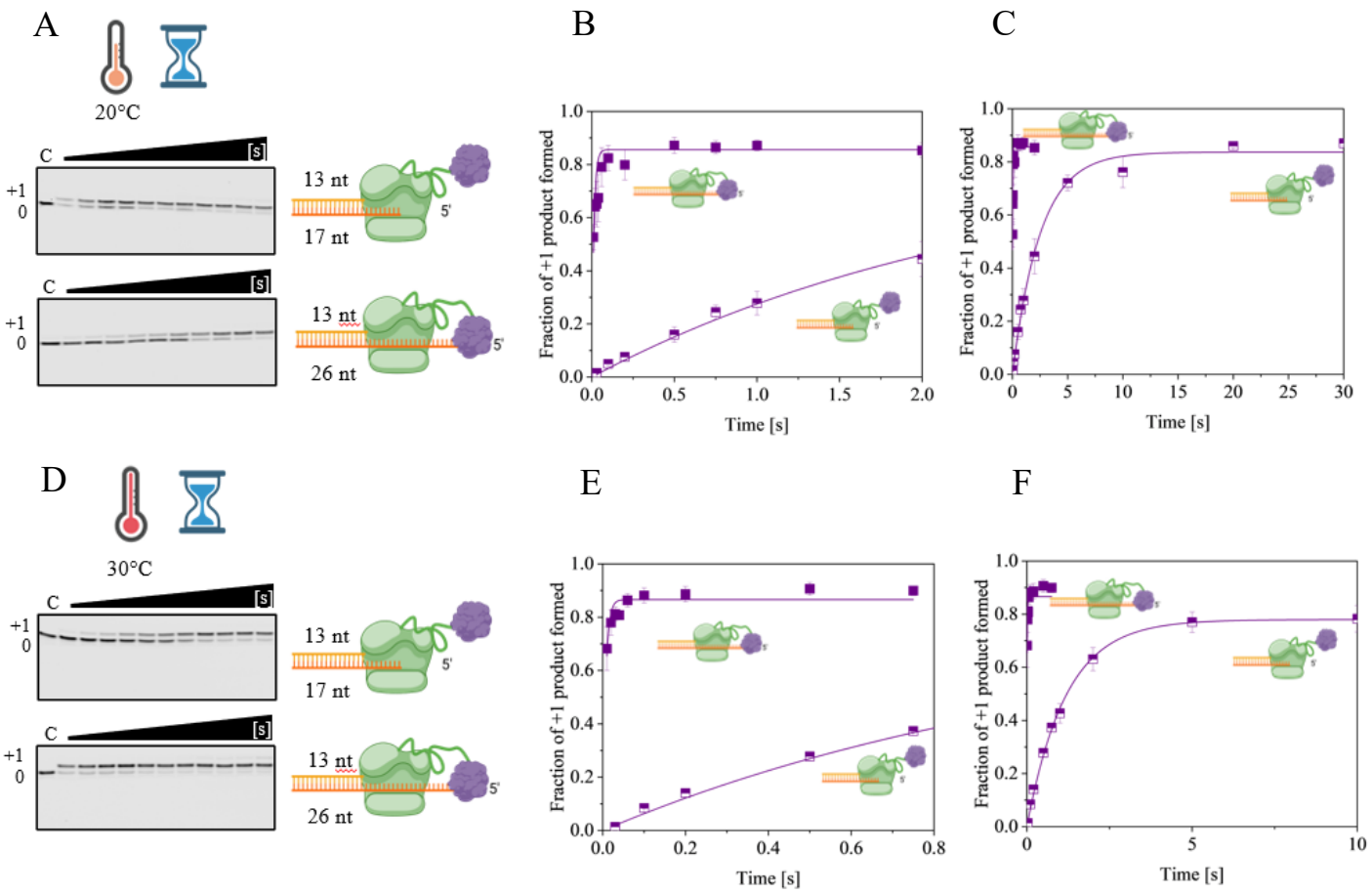


Figure 26. Temperature- and substrate-length dependence of single-turnover +1 product formation by WT Efa polymerase **(A)** WT polymerase reactions at 20 °C with a short (17 nt) or long (26 nt) primer-template duplex. Reactions contained 200 µM dCTP, 300 mM salt, 1000 nM protein, and 100 nM substrate. **(B)** Kinetic traces from panel A over the 0 to 2 s time range. **(C)** The same data shown in panel B, plotted over an extended time range. **(D)** Replication of panel A was performed at 30 °C under the same experimental conditions. **(E)** Kinetic traces from panel D over the 0 to 0.8 s time range. **(F)** The same data shown in panel E, plotted over an extended time range.

Table 7. Kinetic parameters of Efa DNA polymerase primer extension as a function of temperature and overhang length.

Temperature (°C)	*Overhang length (nt)*	*A*	*k_{obs} (s^{-1})*
30	4	0.78±0.01	0.85±0.03
	13	0.86±0.02	138.88±15.26
20	4	0.84±0.01	0.4±0.03
	13	0.86±0.01	79.45±10.45
10	4	0.94±0.01	0.2±0.005
	13	0.88±0.004	27.32±0.77

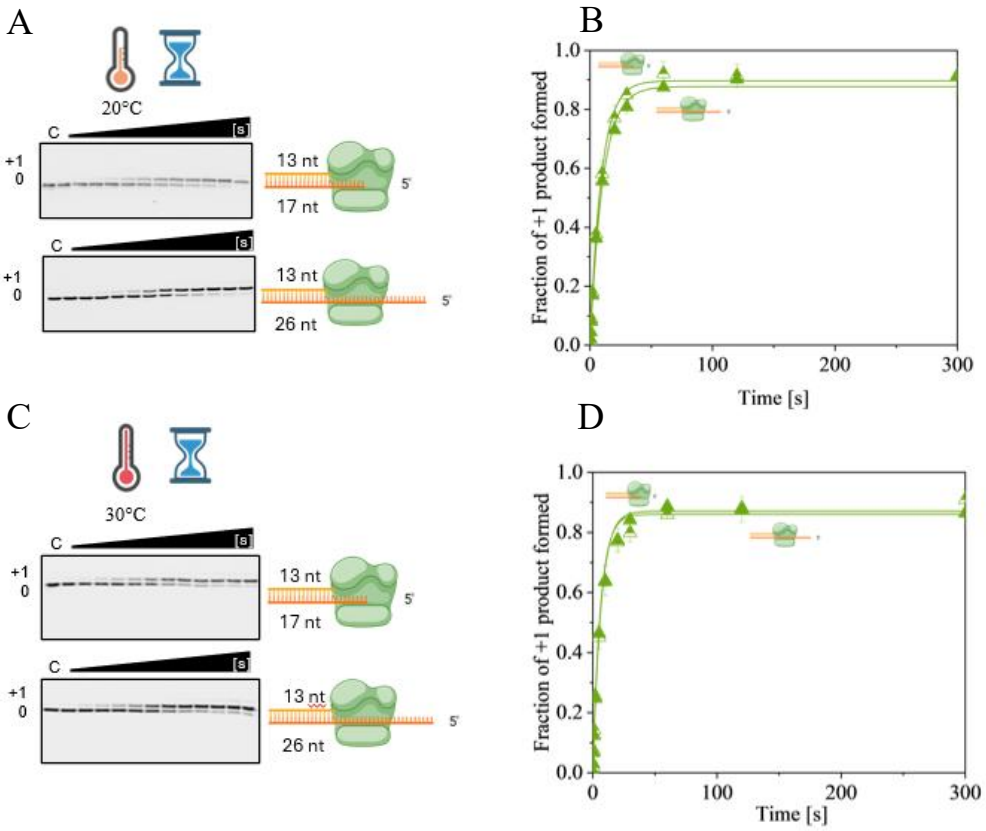


Figure 27. Temperature-dependent activity of the Efa ΔN truncation of Efa polymerase with short and long primer-template substrates.
(A) Representative denaturing PAGE of Efa ΔN reactions carried out at 20°C with a short (17 nt) and a long (26 nt) template. **(B)** Quantitative time course at 20°C. The fraction of +1 product versus time is plotted for the short (green-white triangle) and long (green triangle) templates. **(C)** Gel analysis of the same Efa ΔN reactions performed at 30°C. **(D)** Corresponding kinetic traces at 30°C. The fraction of +1 product vs time is plotted for the short substrate (green-white triangle) and the long substrate (green triangle).

Table 8. Kinetic parameters of Efa ΔN DNA polymerase primer extension as a function of temperature and overhang length.

Temperature (°C)	*Overhang length (nt)*	*A*	k_{obs} (s^{-1})
30	4	0.87±0.01	0.15±0.01
	13	0.86±0.01	0.16±0.01
20	4	0.88±0.01	0.1±0.004
	13	0.9±0.01	0.11±0.001
10	4	0.9±0.01	0.04±0.001
	13	0.87±0.02	0.05±0.004

The resulting k_{obs} values (**Table 7, 8**) were analyzed by Arrhenius plots of ln(k_{obs}) versus $1/T$ (**Fig. 28**).

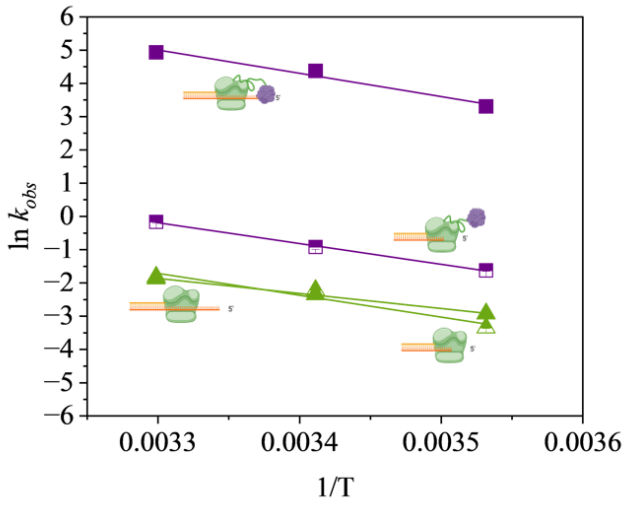


Figure 28. Arrhenius plots of ln(k_{obs}) versus $1/T$ for the two primer-template combinations examined for WT Efa and Efa DN.

For each enzyme-overhang combination, the natural logarithm of the observed rate constant was plotted against the reciprocal of the absolute temperature ($1/T$) to generate an Arrhenius plot (**Table 9**). Linear regression of the data gave a slope (m) and intercept (b):

$$lnk_{obs} = m\left(\frac{1}{T}\right) + b$$

It should be noted that the Arrhenius analysis was performed using only three temperature points (10, 20 and 30°C), which limits the statistical confidence in the derived slope and intercept. The activation energies reported here should therefore be considered as estimates rather than precise determinations.

The activation energy follows from the slope via

$$E_a = -mR$$

where R = 8.314 J mol^{-1} K^{-1}

The pre-exponential factor is obtained by exponentiating the intercept,

$$A = e^b$$

Table 9. Linear-regression parameters (intercept and slope) for WT Efa and Efa ΔN polymerases as a function of 5′-overhang length.

Efa DNA polymerase	*Overhang length (nt)*	*Intercept*	*Slope*
WT	4	20.44±0.88	-6250±257
	13	28.1±3.84	-7000±1124
ΔN	4	20±5.73	-6584±1677
	13	13.06±0.56	-4523±165

For the long-overhang substrate, WT Efa exhibited an activation energy E_a= 58.2 kJ mol^{-1}, whereas Efa ΔN showed a lower activation energy of 38.1 kJ mol^{-1}. Despite this higher E_a, WT Efa remains significantly faster than Efa ΔN at 10°C because the pre-exponential factor A is orders of magnitude larger for the full-length enzyme (WT Efa long: A ~ 1.6 × 10^{12} s^{-1}; Efa ΔN long: A 4.7 × 10^5 s^{-1}). WT Efa exhibits a somewhat higher activation energy than Efa ΔN with the long-overhang substrate, whereas its pre-exponential factor is ~10^6-fold larger. The higher fitted pre-exponential factor for WT Efa indicates a different temperature dependence of the observed rate relative to Efa ΔN. However, the pre-exponential factor may be influenced by several features of the measured reaction, including the population of productive complexes, conformational equilibria, and other kinetic steps. This large A factor, together with the N-terminally mediated overhang engagement, may explain why WT remains orders of magnitude faster than ΔN at 10 °C. When the overhang was shortened to 4 nt, the activation energy for WT decreased to 52 kJ mol^{-1}, whereas Efa ΔN displayed E_a = 54 kJ mol^{-1} with the corresponding short template (**Table 10**). Consistent with the 10°C rates, this condition abolishes the kinetic distinction between WT Efa and Efa ΔN: both constructs now exhibit similar barriers and low k_{obs} values, indicating that the advantage of the N-terminal domain depends on its physical engagement with the single-stranded overhang.

Table 10. Arrhenius-derived kinetic parameters for WT Efa and Efa ΔN DNA polymerases

Efa DNA polymerase	*Overhang length(nt)*	*Activation Energy (kJ/mol)*	*Pre-exponential factor (s^{-1})*	*A range (s^{-1})*
WT	4	52±2	7.5×10^{8}	3.1×10^{8}-1.8×10^{9}
	13	58.2±9.3	1.6×10^{12}	3.48×10^{10}-7.39×10^{13}
ΔN	4	54±14	4.9×10^{8}	1.6×10^{6}-1.5×10^{11}
	13	38±1	4.7×10^{5}	2.6×10^{5}-8.3×10^{5}

7.6.3. Apparent dCTP dependence and the role of the N-terminus

To assess how N-terminus engagement affects the observed rate of nucleotide addition and its dependence on dCTP concentration, the observed rate constant k_{obs} was measured as a function of dCTP concentration under single-turnover conditions at 10°C for WT Efa (**Fig. 29A, B**) and Efa ΔN (**Fig. 29C, D)**.

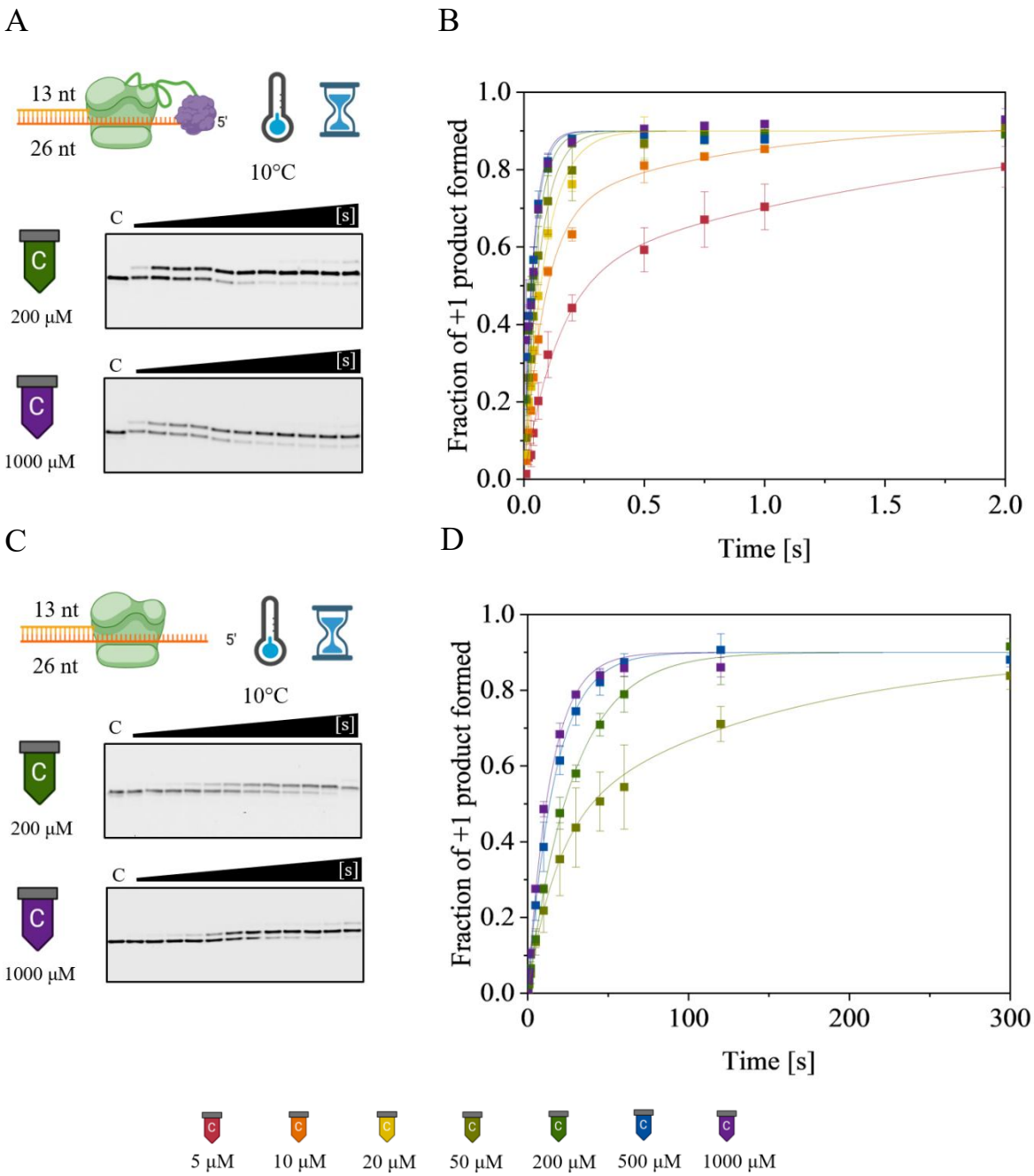


Figure 29. Nucleotide-dependent kinetics and the apparent dCTP binding affinity of the Efa DNA polymerase.
The kinetics of the dCTP-dependent primer extension reaction for the Efa polymerase at 10°C. Panels **A** and **C** present schematic representations of the primer-extension assays and the corresponding gel-based analysis of the +1 incorporation product by WT Efa **(A)** and Efa ΔN **(C)**. Panels **B** and **D** display the fraction of the +1 product formed over time across a range of dCTP concentrations, from 5 to 1000 µM, for WT Efa **(B)** and 50 to 1000µM for Efa ΔN **(D)**.

The data were fitted to a hyperbolic dependence according to the following equation:

$$k_{obs} = \frac{k_{max} \cdot [dNTP]}{K_D + [dNTP]}$$

where k_{max} represents the maximal observed incorporation rate, and $K_{D,app}$ is the apparent dissociation constant for the incoming dNTP (**Table 11**).

Table 11. Kinetic parameters (A_1, A_2, k_{obs}, k_{obs2}) of WT and ΔN Efa DNA polymerase across a range of dCTP concentrations

Efa DNA polymerase	*dCTP (μM)*	*A1*	*A2*	k_{obs}	k_{obs2}
WT	5	0.53±0.15	0.439±0.36	6.99±1.97	0.51±1.16
	10	0.68±0.13	0.24±0.1	11.92±2.82	1.33±1.18
	20	0.9		11.65±0.54	
	50	0.9		15.39±0.93	
	200	0.9		26.79±0.9	
	500	0.9		24.91±2.38	
	1000	0.9		20.76±1.62	
ΔN	50	0.47±0.06	0.43±0.1	0.007±0.003	0.055±0.01
	200	0.9		0.035±0.0005	
	500	0.9		0.06±0.001	
	1000	0.9		0.07±0.001	

Values were obtained from single-or double-exponential fits of time course. The model selection criterion is described in Section 6.7. Where only A_1 and k_{obs1} are reported, a single exponential was sufficient. The amplitude was constrained to A_1 = 0.9 during fitting, therefore no fitting error is reported for these values. k_{obs} denotes the rate constant of the first phase and was used for the dCTP-dependence analysis in Fig. 30

For the WT Efa, this analysis yielded a k_{max} of 26.75 ± 2.49 s^{-1} and an apparent $K_{D,app}$ for dCTP of 26.0 ± 7.34 μM. The dependence of k_{obs} on dCTP was not strictly monotonic. Above 200 μM the observed rate decreased slightly (26.79, 24.91 and 20.76 s^{-1} at 200, 500 and 1000μM). The hyperbolic fit therefore does not adequately describes the complete dataset, and the derived parameters should be regarded as apparent values (**Fig. 30A**). In contrast, the Efa ΔN variant displayed a markedly reduced k_{max} of 0.1 ± 0.005 s^{-1} and an elevated $K_{D,app}$ of 333.78 ± 37.64 μM (**Fig. 30B**).

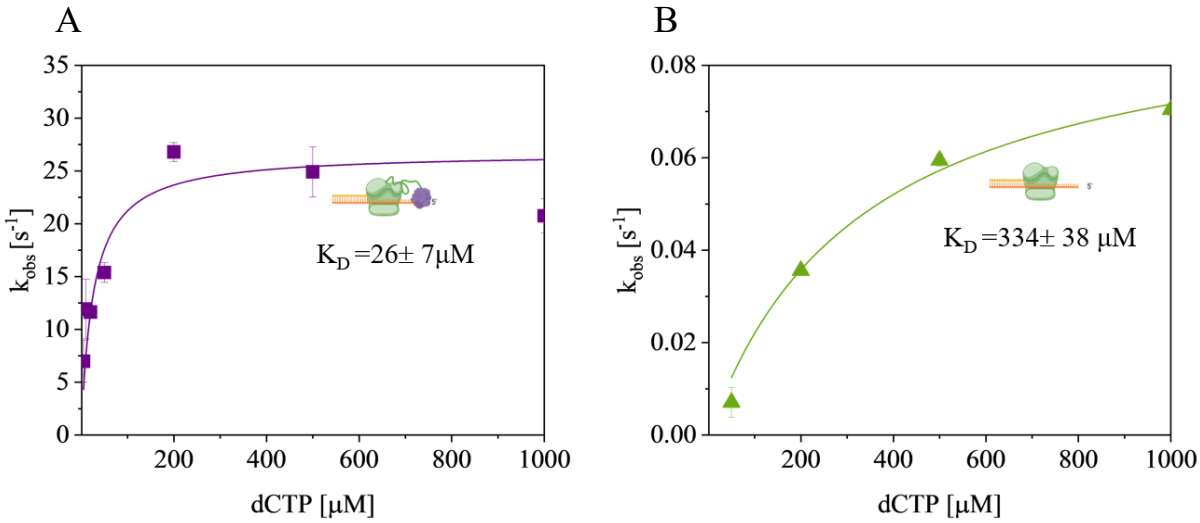


Figure 30. Kinetic analysis and determination of the apparent nucleotide binding affinity for WT Efa and the Efa ΔN mutant.
The dependence of the observed reaction rate (k_{obs}) on dCTP concentration fitted to a hyperbolic model to derive kinetic parameters for the polymerase. **(A)** Graph for wild-type (WT) Efa polymerase. **(B)** Graph for the Efa ΔN mutant.

These results demonstrate that the removal of the N-terminal SSB-like domain reduces the apparent affinity for dCTP by approximately 13-fold (as indicated by an increase in apparent $K_{D,app}$) and simultaneously lowers the maximal observed incorporation rate of the catalytic step by ~268 times (**Table 12**). The N-terminal domain, therefore, appears to influence both the apparent dCTP dependence and the observed rate of incorporation. Because these parameters are apparent, this may reflect effects on nucleotide binding, on conformational steps preceding chemistry, or on the chemical step itself, which cannot be distinguished in these experiments. One interpretation is that the N-terminal domain helps organize the single-stranded DNA overhang and accurately positioning the template within the catalytic active site, consistent with the structural evidence from the ternary complexes.

Table 12. Maximal catalytic rate (k_{max}) and apparent dissociation constant ($K_{D,app}$) for WT and Efa ΔN DNA polymerase

Efa DNA polymerase	k_{max}	$K_{D,app}$
WT	26.75±2.49	26±7.34
ΔN	0.1±0.005	333.78±37.64

8. Discussion

This thesis presented, to our knowledge, the first integrated biochemical, kinetic, and structural characterization of a cold-active B-family DNA polymerase from a bacteriophage source. The work established that Efa achieved efficient DNA synthesis at sub-zero temperatures through a mechanism that couples a conventional polymerase core with an N-terminal OB-fold domain that functions as a built-in SSB module. This N-terminal domain engages single-stranded overhangs ahead of the replication fork and is associated with a favorable temperature dependence of the observed polymerization rate. The structural and kinetic data further suggest that the domain contributes to efficient synthesis on structured templates at low temperatures, although the individual kinetic step affected by this interaction remains unresolved.

8.1. Biotechnological relevance of a cold-active polymerase

From a practical perspective, the most striking feature of Efa is its broad and unusually low temperature activity window. Primer extension assays demonstrated efficient DNA synthesis from approximately -5°C to 50 °C, with maximal substrate consumption maintained across a wide sub-ambient range and a sharp activity drop only at higher temperatures. This profile contrasts with most enzymes used in current isothermal amplification platforms (e.g., in RPA, LAMP, HDA), which typically operate optimally between 37°C and 65°C and rapidly lose activity at low temperatures (Cao et al., 2013; Gunasegar & Neela, 2021; Munawar et al., 2020).

From a translational perspective, Efa's activity profile addresses a specific bottleneck in POC molecular diagnostics. Current isothermal kits based on RPA or LAMP require heat blocks or chemical heating packs to maintain reaction temperatures, adding weight, cost, and logistical complexity that constrain deployment in remote or austere environments (Niemz et al., 2011; Urdea et al., 2006). Efa's ability to function at or below 10°C suggests that diagnostic assays designed around this enzyme could operate at ambient temperature across a wide geographic range, including temperate and cold climates, and could be integrated into paper-based or microfluidic platforms that lack active temperature control (Maffert et al., 2017). Furthermore, the compatibility of Efa with high-glycerol and cryo-protective conditions raises the possibility of formulating liquid reagent mixes that remain

viable without cold-chain logistics, a major practical advantage for global health applications (Xu et al., 2024).

Direct comparisons with classical DNA polymerases highlight Efa's advantage in the cold. At 30°C in 40 % glycerol, Efa generates substantial full-length product and final product formation, approaching the performance of T4 DNA polymerase and far exceeding that of T7 and Pol I under identical conditions. At -10 °C, Efa maintains robust extension, whereas T4, T7, and Pol I show negligible product formation, underscoring Efa's unique suitability for low-temperature synthesis.

These properties position Efa as a promising catalyst for isothermal nucleic acid amplification in the 0-10°C range. Reactions at such low temperatures could reduce or eliminate the need for active heating, enabling simpler point-of-care or field-deployable devices. Operating near 0°C may also help preserve DNA integrity in samples containing active nucleases or labile analytes, as many contaminating enzymes are strongly attenuated at low temperatures, whereas Efa remains active (Oliveira et al., 2021). In addition, the tolerance of Efa to viscous, cryo-protective conditions (e.g. high glycerol) suggests compatibility with formulations designed for cold-chain-independent storage and transport.

8.2. Comparative assessment with classical polymerase

Efa retains hallmark features of B-family polymerases, including a right-hand architecture comprising exonuclease, palm, fingers, and thumb domains, and a conserved DEDD motif in the exonuclease active site. The engineered DEDD mutant abolishes 3′→5′ exonuclease activity while preserving overall folding, oligomeric state, and secondary structure, confirming that the quadruple D137A E139A D188A D281A substitutions selectively inactivate proofreading without destabilizing the protein.

Substrate profiling shows that Efa behaves as a DNA-dependent polymerase with a broad capacity for DNA and RNA primers with DNA templates. It supports efficient primer extension with DNA/DNA and RNA/DNA duplexes, with substrate consumption saturating at low nanomolar enzyme concentrations, while displaying minimal extension with DNA/RNA and no detectable activity with RNA/RNA duplexes. In the absence of dNTPs, Efa exhibits strong 3′→5′ exonuclease activity with DNA/DNA, RNA/DNA, and DNA/RNA duplexes, but not with RNA/RNA, demonstrating a clear preference for

substrates containing at least one DNA strand. This pattern mirrors the behavior of many replicative B-family polymerases, which couple high-fidelity synthesis with proofreading on DNA-containing substrates.

In terms of thermal behavior, CD spectroscopy and thermal melting indicate that WT Efa is folded and predominantly α-helical, with a modest melting temperature of around 41 °C. This relatively low T_m is consistent with psychrophilic adaptation, in which increased flexibility at low temperature often comes at the expense of thermal stability. Compared with thermostable archaeal B-family enzymes used in PCR (Gavrilov et al., 2022; Kermekchiev et al., 2009), Efa therefore offers superior cold activity but reduced tolerance to high temperatures. That implies, it is best suited to applications that do not require cycling or prolonged incubation above ~40-45 °C.

Altogether, Efa combines a conventional B-family catalytic core with substrate preferences and exonuclease behavior similar to classical replicative polymerases but shifted toward low-temperature operation and lower thermal stability. This places it in a distinct niche within the current toolbox of polymerases: complementary rather than competitive with high-temperature enzymes such as Taq or archaeal Pol B.

8.3. Mechanistic insight: N-terminal SSB-like function

A central mechanistic insight of this study concerns the role of the Efa N-terminal region (residues 27-124). Bioinformatic and structural analyses showed that this segment adopts an OB fold reminiscent of single-stranded DNA-binding (SSB) proteins, despite limited primary sequence conservation. In the apo structure, the N-terminal region forms an additional domain appended to the canonical polymerase core.

Ternary complexes with primer-template DNA revealed two distinct N-terminal conformational states. In a complex with a 12-mer primer and 18-mer template (6-nt 5′ overhang), the N-terminal OB-fold engages the single-stranded overhang through a network of contacts involving residues such as K53, Y74, R79, and F105, effectively clamping the ssDNA. In a second complex with a shorter 16-nt template (4-nt overhang), the N-terminal domain swings away by ~4 Å and rotates by ~22°, adopting a “loose” conformation with no detectable contacts to the overhang. Structural superposition thus supports a model in which overhang length dictates whether the N-terminus can productively bind ssDNA.

Solution assays corroborate this structural switching. Primer extension experiments on 26- and 41-nt templates revealed that WT Efa consistently terminates synthesis 5 nucleotides before the template end, generating a pronounced intermediate band that correlates with N-terminal engagement in the long-overhang structure. On hairpin-containing templates, WT Efa produces substantial full-length product, whereas the Efa ΔN mutant accumulates almost exclusively at the stall site and fails to efficiently extend through the secondary structure. These data indicate that the N-terminal OB fold acts as an accessory SSB module that stabilizes the single-stranded region ahead of the polymerase, allowing the enzyme to overcome secondary-structure barriers during synthesis.

Kinetic analyses further illuminate how this domain contributes to cold adaptation. WT Efa exhibits clear pre-steady-state burst kinetics at both 30°C and 10°C, consistent with a rapid product-formation phase followed by a slower step, such as product release or DNA translocation. In contrast, Efa ΔN shows no detectable burst but instead displays a simple linear time course indicative of rate-limiting incorporation or a conformational step. Single-turnover experiments at 10°C underscore this difference. WT Efa incorporates the first nucleotide with $k_{obs} \sim 27.3\ s^{-1}$, whereas Efa ΔN is ~546 times slower on the same substrate, with $k_{obs} \sim 0.05\ s^{-1}$.

Importantly, this low-temperature advantage of WT Efa depends on the presence of a sufficiently long 5′ overhang. On a long overhang, WT displays rapid incorporation at 10 °C, while shortening the overhang to 4 nt reduces k_{obs} by ~130-fold, effectively collapsing its behavior to that of the ΔN mutant. In contrast, Efa ΔN shows similar, uniformly low rates with long and short overhangs, indicating that the length-dependent acceleration is mediated specifically by the N-terminal module. Arrhenius analysis showed that N-terminal engagement was associated with a different apparent temperature dependence of the observed reaction rate. However, these data do not establish that N-terminal engagement lowers the activation barrier specifically for the chemical step or identify which individual kinetic step limits the overall reaction rate.

Nucleotide-dependence experiments reinforce this picture. At 10 °C, WT Efa displays relatively lower apparent $K_{D,app}$ for dCTP (approximately~26 μM), whereas Efa ΔN shows a higher apparent $K_{D,app}$ of ~334 μM and significantly reduced maximal rates. These differences are consistent with a model in which stable N-terminal engagement

helps position the DNA template and primer in a conformation more favorable for incorporation, although the individual microscopic step affected cannot be resolved in these experiments. When this contact is lost, the enzyme-DNA-dNTP complex may sample productive states far less frequently, potentially resulting in the absence of a detectable burst, weaker nucleotide binding, and severely diminished turnover at low temperature.

The N-terminal OB-fold of Efa thus provides a striking example of an integrated, cis-acting SSB module that functions analogously to canonical trans-acting SSB proteins such as *E. coli* SSB or eukaryotic RPA. In canonical replication systems, SSB proteins bind and protect ssDNA, prevent secondary-structure formation, and stimulate polymerase activity through direct protein-protein interactions (Flynn & Zou, 2010). Efa achieves a similar outcome through an intramolecular mechanism. The OB-fold is tethered to the polymerase core by a flexible linker and can therefore engage the emerging ssDNA without requiring a separate binding partner. This cis arrangement has two potential advantages. First, the effective local concentration of the SSB module at the primer-template junction is extremely high, ensuring rapid rebinding after transient dissociation. Second, the physical coupling links the energetic benefit of ssDNA stabilization directly to the catalytic center, consistent with the different apparent temperature dependence of the observed reaction rate described above. A similar principle of tethering accessory DNA-binding domains to polymerase cores has been exploited in engineered fusion enzymes such as the Sso7d-polymerase chimeras used in commercial PCR formulations (Sundarrajan et al., 2018), suggesting that the Efa architecture represents a naturally evolved version of a concept that protein engineers have only recently begun to explore.

Taken together, the structural, biochemical and kinetic data support a mechanistic model in which the N-terminal OB-fold functions as an integrated SSB-like accessory domain that binds sufficiently long 5′ overhangs, stabilizes single-stranded DNA ahead of the replication fork, and accelerates the observed rate of nucleotide addition at low temperatures. This domain is dispensable for synthesis on simple linear templates at moderate temperatures but becomes essential for efficient incorporation under cold conditions and in the presence of secondary structure.

8.4. Implications for engineering new isothermal enzymes

The modular architecture of Efa, a conventional B-family polymerase core coupled to an SSB-like N-terminal appendage, has important implications for enzyme engineering. The demonstration that a single OB fold module can both stabilize ssDNA and dramatically accelerate catalysis at 0-10°C suggests that similar domains could be grafted onto other polymerases to extend their operational temperature range or improve their performance on structured templates.

For example, fusing SSB-like modules to mesophilic polymerases might enhance their ability to operate at lower temperatures or in the presence of strong secondary structures, features desirable for isothermal amplification of GC-rich or highly structured genomes (D. E. Johnson & Richardson, 2003; Olszewski et al., 2017; S. Sun et al., 2006). Conversely, coupling the Efa N-terminal domain to thermostable polymerases could yield chimeric enzymes with broadened temperature profiles, combining high-temperature robustness with improved low-temperature activity.

More broadly, Efa provides a natural blueprint for designing multi-domain polymerases in which accessory modules dynamically engage or disengage from DNA depending on substrate features such as overhang length or structure, thereby tuning processivity and kinetics in response to local sequence context. This strategy may be particularly valuable for applications where amplification must proceed efficiently under variable or poorly controlled environmental conditions, such as field diagnostics.

The structural data presented in this thesis provides a foundation for structure-guided engineering of Efa itself. For instance, the resolution of the N-terminal OB-fold in both engaged and loose conformations identifies specific hinge residues and interdomain contacts that control the open-closed transition. Mutations that stabilize the engaged conformation, for example by introducing hydrogen-bond networks or salt bridges at the domain-domain interface, could shift the equilibrium toward the active state, potentially reducing the minimum overhang length required for activation and broadening the range of substrates that Efa can amplify efficiently. Conversely, mutations that destabilize the engaged state could be used to tune processivity downward for applications requiring short amplicons or controlled termination. The availability of high-resolution structures also enables computational docking and molecular dynamics simulations to predict the effects of point mutations on domain motion and DNA binding, thereby creating a rational

design cycle that could be substantially faster than directed evolution alone (Bromberg & Rost, 2008; Korendovych, 2018).

8.5. Study limitations

Despite the depth of the biochemical and structural characterization, several limitations must be acknowledged. First, most functional assays employed relatively short, defined primer-template substrates, which provide precise kinetic and structural insights but may not fully capture Efa's activity with long, complex genomes or under conditions of high processivity. Second, a limitation of the current study is that the functional contributions of specific N-terminal residues (K53, Y74, R79, F105) identified in the ternary complexes have not been directly tested by site directed mutagenesis. While the structural and kinetic data are consistent with a model in which these contacts mediate ssDNA binding and kinetic acceleration, this interpretation remains to be validated by alanine or charge-reversal substitutions at these positions.

Third, all experiments were performed in vitro with purified components. The in vivo performance of Efa during phage replication, including its interactions with other viral or host factors, remains unexplored.

Fourth, while the work focused on catalytic efficiency and cold adaptation, a comprehensive analysis of replication fidelity, error spectra, and lesion bypass capacity was beyond the scope of this thesis. Such properties are critical for evaluating suitability in applications where accuracy is paramount, such as sequencing library preparation or high-fidelity amplification.

Fifth, the kinetic characterization of the dCTP dependence was limited by the titration range used. The dependence of k_{obs} on dCTP was not strictly monotonic above ~200µM, which may indicate substrate inhibition at high nucleotide concentrations. The current dataset does not include intermediate concentrations between 200 and 1000µM, so this behavior could not be fully characterized, and the fitted parameters (k_{max}, $K_{D,app}$) should be regarded as apparent values describing the ascending portion of the titration. Confirming the origin of this effect would require additional titration points and, ideally, testing whether the same nonmonotonic behavior occurs with other dNTPs.

Finally, the current study did not integrate Efa into fully developed diagnostic workflows (e.g. LAMP or RPA formats), so its practical performance in real-world sample matrices, in the presence of inhibitors or contaminants, remains to be established.

8.6. Future directions

Future work should build on these findings in several directions. High-resolution structures of additional catalytic states, such as mismatched termini or translocation intermediates, would provide further insight into fidelity and exonuclease coupling.

At the engineering and application levels, incorporating Efa into prototypical low-temperature isothermal amplification schemes and testing its performance on clinically relevant targets will be essential for assessing its translational potential. Such studies should include comparisons with established enzymes, evaluation of robustness to inhibitors, and optimization of buffer systems compatible with field-deployable devices. Parallel efforts in thermostability engineering, for example, introducing disulfide bridges or modulating surface charge, could seek to raise Efa's melting temperature without compromising its cold activity, thereby expanding its usable temperature window.

Finally, the modular concept demonstrated by Efa invites the design and testing of chimeric polymerases in which SSB-like modules from different sources are fused to diverse polymerase cores. These chimeras could be screened for improved performance at low temperature, on structured templates, or in challenging sample environments, potentially yielding a new generation of tailored isothermal enzymes with significant industrial potential.

Beyond the immediate biochemical and engineering goals, the Efa system offers opportunities for computational and evolutionary studies. The unique domain architecture makes Efa an excellent model for investigating how multi-domain proteins acquire new functions through domain acquisition and interface evolution. Ancestral sequence reconstruction and phylogenetic analysis of phage B-family polymerases could reveal the evolutionary history of N-terminal OB-fold acquisition and whether similar modules exist in other uncharacterized phage genomes (Hochberg & Thornton, 2017; Merkl & Sterner, 2016).

8.7. Concluding remarks

Taken together, this work identifies Efa as a cold-active B-family DNA polymerase from a bacteriophage source. Its conventional catalytic core is linked to an N-terminal OB-fold domain that functions as a built-in SSB module. Structural and biochemical analyses indicate that this domain engages sufficiently long single-stranded overhangs and supports primer extension through secondary structures, whereas its deletion has a more limited effect on synthesis from simple linear substrates under moderate-temperature conditions. The kinetic data further show that productive N-terminal engagement is associated with faster observed nucleotide incorporation at low temperature.

Beyond its specific contribution to understanding phage enzyme cold adaptation, this study illustrated a broader principle. Nature has evolved modular solutions to the challenge of DNA replication under extreme conditions, and these solutions can be discovered through systematic exploration of environmental bacteriophage genomes. The Efa architecture, a polymerase core with an accessory DNA-binding domain, provides a natural blueprint for engineering multi-domain polymerases with tailored temperature profiles, substrate preferences, and kinetic properties. As the demand for low-cost equipment-minimal molecular diagnostics continues to grow, enzymes such as Efa represent a promising path toward truly field-deployable nucleic acid amplification technologies.

9. References

Analytical Methods Committee. (2014). PCR – the polymerase chain reaction. *Analytical Methods*, *6*(2), 333–336. https://doi.org/10.1039/C3AY90101G

Aoi, T. (2016). Biology of lung cancer: Genetic mutation, epithelial-mesenchymal transition, and cancer stem cells. *General Thoracic and Cardiovascular Surgery*, *64*(9), 517–523. https://doi.org/10.1007/s11748-016-0682-8

Åqvist, J., Isaksen, G. V., & Brandsdal, B. O. (2017). Computation of enzyme cold adaptation. *Nature Reviews Chemistry*, *1*(7), 0051. https://doi.org/10.1038/s41570-017-0051

Bebenek, K., & Kunkel, T. A. (2004). Functions of DNA Polymerases. In *Advances in Protein Chemistry* (Vol. 69, pp. 137–165). Elsevier. https://doi.org/10.1016/S0065-3233(04)69005-X

Benkovic, S. J., Valentine, A. M., & Salinas, F. (2001). Replisome-Mediated DNA Replication. *Annual Review of Biochemistry*, *70*(1), 181–208. https://doi.org/10.1146/annurev.biochem.70.1.181

Bertolin, A. P., Canal, B., Yekezare, M., Early, A., Zeng, J., Instrell, R., Howell, M., & Diffley, J. F. X. (2025). The DNA replication checkpoint prevents PCNA/RFC depletion to protect forks from HLTF-induced collapse in human cells. *Molecular Cell*, *85*(13), 2474-2486.e6. https://doi.org/10.1016/j.molcel.2025.06.002

Betancurt-Anzola, L., O'Connell, K. C., Potapov, V., Ong, J. L., Tanner, N. A., Sauguet, L., & Zatopek, K. M. (2025). The A, B, C, D's of replicative DNA polymerase fidelity: Utilizing high-throughput single-molecule sequencing to understand the molecular basis for DNA polymerase accuracy. *Nucleic Acids Research*, *53*(21), gkaf1143. https://doi.org/10.1093/nar/gkaf1143

Blanca, G., Shevelev, I., Ramadan, K., Villani, G., Spadari, S., Hübscher, U., & Maga, G. (2003). Human DNA Polymerase λ Diverged in Evolution from DNA Polymerase β toward Specific Mn^{++} Dependence: A Kinetic and Thermodynamic Study. *Biochemistry*, *42*(24), 7467–7476. https://doi.org/10.1021/bi034198m

Blanco, L., Bernad, A., Lázaro, J. M., Martín, G., Garmendia, C., & Salas, M. (1989). Highly Efficient DNA Synthesis by the Phage ϕ 29 DNA Polymerase. *Journal*

of Biological Chemistry, *264*(15), 8935–8940. https://doi.org/10.1016/S0021-9258(18)81883-X

Boonbanjong, P., Treerattrakoon, K., Waiwinya, W., Pitikultham, P., & Japrung, D. (2022). Isothermal Amplification Technology for Disease Diagnosis. *Biosensors*, *12*(9), 677. https://doi.org/10.3390/bios12090677

Braithwaite, D. K., & Ito, J. (1993). Compilation, alignment, and phylogenetic relationships of DNA polymerases. *Nucleic Acids Research*, *21*(4), 787–802. https://doi.org/10.1093/nar/21.4.787

Brautigam, C. A., & Steitz, T. A. (1998). Structural and functional insights provided by crystal structures of DNA polymerases and their substrate complexes. *Current Opinion in Structural Biology*, *8*(1), 54–63. https://doi.org/10.1016/S0959-440X(98)80010-9

Bromberg, Y., & Rost, B. (2008). Comprehensive *in silico* mutagenesis highlights functionally important residues in proteins. *Bioinformatics*, *24*(16), i207–i212. https://doi.org/10.1093/bioinformatics/btn268

Brown, H. S., & LiCata, V. J. (2013). Enthalpic switch-points and temperature dependencies of DNA binding and nucleotide incorporation by Pol I DNA polymerases. *Biochimica et Biophysica Acta (BBA) - Proteins and Proteomics*, *1834*(10), 2133–2138. https://doi.org/10.1016/j.bbapap.2013.06.021

Buchel, G., Nayak, A. R., Herbine, K., Sarfallah, A., Sokolova, V. O., Zamudio-Ochoa, A., & Temiakov, D. (2023). Structural basis for DNA proofreading. *Nature Communications*, *14*(1), 8501. https://doi.org/10.1038/s41467-023-44198-8

Cao, Y., Kim, H., Li, Y., Kong, H., & Lemieux, B. (2013). Helicase-Dependent Amplification of Nucleic Acids. *Current Protocols in Molecular Biology*, *104*(1). https://doi.org/10.1002/0471142727.mb1511s104

Cobzariu, M. A., Lobo-Castañón, M. J., & Miranda-Castro, R. (2023). Enzyme-assisted isothermal amplification of nucleic acids on the electrode surface. *Current Opinion in Electrochemistry*, *40*, 101322. https://doi.org/10.1016/j.coelec.2023.101322

Cohan, B., & Frappier, L. (2021). Herpesvirus DNA polymerase processivity factors: Not just for DNA synthesis. *Virus Research*, *298*, 198394. https://doi.org/10.1016/j.virusres.2021.198394

Collins, T., & Feller, G. (2023). Psychrophilic enzymes: Strategies for cold-adaptation. *Essays in Biochemistry*, *67*(4), 701–713. https://doi.org/10.1042/EBC20220193

Cui, F., Sun, L., Qiao, J., Li, J., Li, M., Chen, S., Sun, B., & Huang, X. (2020). Genetic mutation analysis of hereditary spastic paraplegia: A retrospective study. *Medicine*, *99*(23), e20193. https://doi.org/10.1097/MD.0000000000020193

Czarnecki, M. W., & Traktman, P. (2017). The vaccinia virus DNA polymerase and its processivity factor. *Virus Research*, *234*, 193–206. https://doi.org/10.1016/j.virusres.2017.01.027

Diffley, J. F. (1994). Eukaryotic DNA replication. *Current Opinion in Cell Biology 6*, 368–372.

Dodd, T., Botto, M., Paul, F., Fernandez-Leiro, R., Lamers, M. H., & Ivanov, I. (2020). Polymerization and editing modes of a high-fidelity DNA polymerase are linked by a well-defined path. *Nature Communications*, *11*(1), 5379. https://doi.org/10.1038/s41467-020-19165-2

Eckert, K. A., & Kunkel, T. A. (1991). DNA polymerase fidelity and the polymerase chain reaction. *Genome Research*, *1*(1), 17–24. https://doi.org/10.1101/gr.1.1.17

Eckstein, F. (1985). Nucleoside Phosphorothioates. *Annual Review of Biochemistry*, (54), 367–402.

Ekundayo, B., & Bleichert, F. (2019). Origins of DNA replication. *PLOS Genetics*, *15*(9), e1008320. https://doi.org/10.1371/journal.pgen.1008320

Esteban, J. A., Salas, M., & Blanco, L. (1993). Fidelity of phi 29 DNA polymerase. Comparison between protein-primed initiation and DNA polymerization. *Journal of Biological Chemistry*, *268*(4), 2719–2726. https://doi.org/10.1016/S0021-9258(18)53833-3

Feller, G., & Gerday, C. (2003). Psychrophilic enzymes: Hot topics in cold adaptation. *Nature Reviews Microbiology*, *1*(3), 200–208. https://doi.org/10.1038/nrmicro773

Feng, X., Liu, X., Xu, R., Zhao, R., Feng, W., Liao, J., Han, W., & She, Q. (2020). A Unique B-Family DNA Polymerase Facilitating Error-Prone DNA Damage Tolerance in Crenarchaeota. *Frontiers in Microbiology*, *11*, 1585. https://doi.org/10.3389/fmicb.2020.01585

Flynn, R. L., & Zou, L. (2010). Oligonucleotide/oligosaccharide-binding fold proteins: A growing family of genome guardians. *Critical Reviews in Biochemistry and Molecular Biology*, *45*(4), 266–275. https://doi.org/10.3109/10409238.2010.488216

Gao, Y., & Yang, W. (2016). Capture of a third Mg^{2+} is essential for catalyzing DNA synthesis. *Science*, *352*(6291), 1334–1337. https://doi.org/10.1126/science.aad9633

Garcia-Diaz, M., & Bebenek, K. (2007). Multiple Functions of DNA Polymerases. *Critical Reviews in Plant Sciences*, *26*(2), 105–122. https://doi.org/10.1080/07352680701252817

Gavrilov, M., Yang, J. Y. C., Zou, R. S., Ma, W., Lee, C.-Y., Mohapatra, S., Kang, J., Liao, T.-W., Myong, S., & Ha, T. (2022). Engineered helicase replaces thermocycler in DNA amplification while retaining desired PCR characteristics. *Nature Communications*, *13*(1), 6312. https://doi.org/10.1038/s41467-022-34076-0

Gayet-Ageron, A., Lautenschlager, S., Ninet, B., Perneger, T. V., & Combescure, C. (2013). Sensitivity, specificity and likelihood ratios of PCR in the diagnosis of syphilis: A systematic review and meta-analysis. *Sexually Transmitted Infections*, *89*(3), 251–256. https://doi.org/10.1136/sextrans-2012-050622

González-Magaña, A., & Blanco, F. J. (2020). Human PCNA Structure, Function and Interactions. *Biomolecules*, *10*(4), 570. https://doi.org/10.3390/biom10040570

Gunasegar, S., & Neela, V. K. (2021). Evaluation of diagnostic accuracy of loop-mediated isothermal amplification method (LAMP) compared with polymerase chain reaction (PCR) for Leptospira spp. in clinical samples: A systematic review and meta-analysis. *Diagnostic Microbiology and Infectious Disease*, *100*(3), 115369. https://doi.org/10.1016/j.diagmicrobio.2021.115369

Han, P., Fan, H., & Tong, Y. (2023). Identification of a novel family B DNA polymerase from Enterococcus phage IME199 and its overproduction in Escherichia coli BL21(DE3). *Microbial Cell Factories*, *22*(1), 217. https://doi.org/10.1186/s12934-023-02228-6

Hochberg, G. K. A., & Thornton, J. W. (2017). Reconstructing Ancient Proteins to Understand the Causes of Structure and Function. *Annual Review of Biophysics*, *46*(1), 247–269. https://doi.org/10.1146/annurev-biophys-070816-033631

Hoeben, R. C., & Uil, T. G. (2013). Adenovirus DNA Replication. *Cold Spring Harbor Perspectives in Biology*, *5*(3), a013003–a013003. https://doi.org/10.1101/cshperspect.a013003

Inata, K., Miyazaki, D., Uotani, R., Shimizu, D., Miyake, A., Shimizu, Y., & Inoue, Y. (2018). Effectiveness of real-time PCR for diagnosis and prognosis of varicella-

zoster virus keratitis. *Japanese Journal of Ophthalmology*, *62*(4), 425–431. https://doi.org/10.1007/s10384-018-0604-7

Ishino, Y., Komori, K., Cann, I. K. O., & Koga, Y. (1998). A Novel DNA Polymerase Family Found in *Archaea*. *Journal of Bacteriology*, *180*(8), 2232–2236. https://doi.org/10.1128/JB.180.8.2232-2236.1998

Johnson, D. E., & Richardson, C. C. (2003). A Covalent Linkage between the Gene 5 DNA Polymerase of Bacteriophage T7 and Escherichia coli Thioredoxin, the Processivity Factor. *Journal of Biological Chemistry*, *278*(26), 23762–23772. https://doi.org/10.1074/jbc.M301366200

Johnson, K. A. (2010). The kinetic and chemical mechanism of high-fidelity DNA polymerases. *Biochimica et Biophysica Acta (BBA) - Proteins and Proteomics*, *1804*(5), 1041–1048. https://doi.org/10.1016/j.bbapap.2010.01.006

Joyce, C. M., & Benkovic, S. J. (2004). DNA Polymerase Fidelity: Kinetics, Structure, and Checkpoints. *Biochemistry*, *43*(45), 14317–14324. https://doi.org/10.1021/bi048422z

Jumper, J., Evans, R., Pritzel, A., Green, T., Figurnov, M., Ronneberger, O., Tunyasuvunakool, K., Bates, R., Z'idek, A., Potapenko, A., Bridgland, A., Meyer, C., Kohl, S. A. A., Ballard, A. J., Cowie, A., Romera-Paredes, B., Nikolov, S., Jain, R., Adler, J., … Hassabis, D. (2021). Highly accurate protein structure prediction with AlphaFold. *Nature*. https://doi.org/10.1038/s41586-021-03819-2

Kannan, S., Gillespie, S. W., Picking, W. L., Picking, W. D., Lorson, C. L., & Singh, K. (2024). Inhibitors against DNA Polymerase I Family of Enzymes: Novel Targets and Opportunities. *Biology*, *13*(4), 204. https://doi.org/10.3390/biology13040204

Kaszubowski, J. D., & Trakselis, M. A. (2022). Beyond the Lesion: Back to High Fidelity DNA Synthesis. *Frontiers in Molecular Biosciences*, *8*, 811540. https://doi.org/10.3389/fmolb.2021.811540

Kaunitz, J. D. (2015). The Discovery of PCR: ProCuRement of Divine Power. *Digestive Diseases and Sciences*, *60*(8), 2230–2231. https://doi.org/10.1007/s10620-015-3747-0

Kelman, L. M., & Kelman, Z. (2014). Archaeal DNA Replication. *Annual Review of Genetics*, *48*(1), 71–97. https://doi.org/10.1146/annurev-genet-120213-092148

Keown, R. A., Dums, J. T., Brumm, P. J., MacDonald, J., Mead, D. A., Ferrell, B. D., Moore, R. M., Harrison, A. O., Polson, S. W., & Wommack, K. E. (2022). Novel Viral DNA Polymerases From Metagenomes Suggest Genomic Sources of Strand-Displacing Biochemical Phenotypes. *Frontiers in Microbiology*, *13*, 858366. https://doi.org/10.3389/fmicb.2022.858366

Kermekchiev, M. B., Kirilova, L. I., Vail, E. E., & Barnes, W. M. (2009). Mutants of Taq DNA polymerase resistant to PCR inhibitors allow DNA amplification from whole blood and crude soil samples. *Nucleic Acids Research*, *37*(5), e40–e40. https://doi.org/10.1093/nar/gkn1055

Kitao, H., Iimori, M., Kataoka, Y., Wakasa, T., Tokunaga, E., Saeki, H., Oki, E., & Maehara, Y. (2018). DNA replication stress and cancer chemotherapy. *Cancer Science*, *109*(2), 264–271. https://doi.org/10.1111/cas.13455

Korendovych, I. V. (2018). Rational and Semirational Protein Design. In U. T. Bornscheuer & M. Höhne (Eds.), *Protein Engineering* (Vol. 1685, pp. 15–23). Springer New York. https://doi.org/10.1007/978-1-4939-7366-8_2

Kumar, K., Choudhary, H., Ahmad, H., Muthu, V., Gupta, P., Rudramurthy, S. M., Agnihotri, S., Agarwal, R., Chakrabarti, A., & Kaur, H. (2025). Diagnostic performance of an in-house real-time polymerase chain reaction (PCR) assay and antigen detection from respiratory samples for the diagnosis of pulmonary cryptococcosis. *Diagnostic Microbiology and Infectious Disease*, *113*(2), 116924. https://doi.org/10.1016/j.diagmicrobio.2025.116924

Kuznetsova, A. A., Fedorova, O. S., & Kuznetsov, N. A. (2022). Structural and Molecular Kinetic Features of Activities of DNA Polymerases. *International Journal of Molecular Sciences*, *23*(12), 6373. https://doi.org/10.3390/ijms23126373

Lai, M. Y., Ponnampalavanar, S. S. L. S., Omar, S. F. S., & Lau, Y. L. (2024). A visualized hybrid PCR-LAMP assay for the detection of human Plasmodium species. *Acta Tropica*, *251*, 107120. https://doi.org/10.1016/j.actatropica.2024.107120

Leonardo, S., Toldrà, A., & Campàs, M. (2021). Biosensors Based on Isothermal DNA Amplification for Bacterial Detection in Food Safety and Environmental Monitoring. *Sensors*, *21*(2), 602. https://doi.org/10.3390/s21020602

Lobato, I. M., & O'Sullivan, C. K. (2018). Recombinase polymerase amplification: Basics, applications and recent advances. *TrAC Trends in Analytical Chemistry*, *98*, 19–35. https://doi.org/10.1016/j.trac.2017.10.015

Lonhienne, T., Gerday, C., & Feller, G. (2000). Psychrophilic enzymes: Revisiting the thermodynamic parameters of activation may explain local flexibility.*Biochimica et Biophysica Acta 1543*, 1–10.

Mabey, D., Peeling, R. W., Ustianowski, A., & Perkins, M. D. (2004). Diagnostics for the developing world. *Nature Reviews Microbiology*, *2*(3), 231–240. https://doi.org/10.1038/nrmicro841

Maffert, P., Reverchon, S., Nasser, W., Rozand, C., & Abaibou, H. (2017). New nucleic acid testing devices to diagnose infectious diseases in resource-limited settings. *European Journal of Clinical Microbiology & Infectious Diseases*, *36*(10), 1717–1731. https://doi.org/10.1007/s10096-017-3013-9

Mannier, C., & Yoon, J.-Y. (2022). Progression of LAMP as a Result of the COVID-19 Pandemic: Is PCR Finally Rivaled? *Biosensors*, *12*(7), 492. https://doi.org/10.3390/bios12070492

Martinez, A. N., Talhari, C., Moraes, M. O., & Talhari, S. (2014). PCR-Based Techniques for Leprosy Diagnosis: From the Laboratory to the Clinic. *PLoS Neglected Tropical Diseases*, *8*(4), e2655. https://doi.org/10.1371/journal.pntd.0002655

Matinja, A. I., Kamarudin, N. H. A., Leow, A. T. C., Oslan, S. N., & Ali, M. S. M. (2022). Cold-Active Lipases and Esterases: A Review on Recombinant Overexpression and Other Essential Issues. *International Journal of Molecular Sciences*, *23*(23), 15394. https://doi.org/10.3390/ijms232315394

Merkl, R., & Sterner, R. (2016). Ancestral protein reconstruction: Techniques and applications. *Biological Chemistry*, *397*(1), 1–21. https://doi.org/10.1515/hsz-2015-0158

Mirdita, M., Schütze, K., Moriwaki, Y., Heo, L., Ovchinnikov, S., & Steinegger, M. (2021). ColabFold—Making Protein folding accessible to all. *bioRxiv*. https://doi.org/10.1101/2021.08.15.456425v2

Mirdita, M., Steinegger, M., & Soding, J. (2019). MMseqs2 desktop and local web server app for fast, interactive sequence searches. *Bioinformatics*, *35*(16), 2856–2858. https://doi.org/10.1093/bioinformatics/bty1057

Mirdita, M., von den Driesch, L., Galiez, C., Martin, M. J., Soding, J., & Steinegger, M. (2017). Uniclust databases of clustered and deeply annotated protein sequences and alignments. *Nucleic Acids Res.*, *45*(D1), D170–D176. https://doi.org/10.1093/nar/gkw1081

Mitchell, A. L., Almeida, A., Beracochea, M., Boland, M., Burgin, J., Cochrane, G., Crusoe, M. R., Kale, V., Potter, S. C., Richardson, L. J., Sakharova, E., Scheremetjew, M., Korobeynikov, A., Shlemov, A., Kunyavskaya, O., Lapidus, A., & Finn, R. D. (2019). MGnify: The microbiome analysis resource in 2020. *Nucleic Acids Res.* https://doi.org/10.1093/nar/gkz1035

Morcinek-Orłowska, J., Zdrojewska, K., & Węgrzyn, A. (2022). Bacteriophage-Encoded DNA Polymerases—Beyond the Traditional View of Polymerase Activities. *International Journal of Molecular Sciences*, *23*(2), 635. https://doi.org/10.3390/ijms23020635

Munawar, M. A., Martin, F., Toljamo, A., Kokko, H., & Oksanen, E. (2020). RPA-PCR Couple: An Approach to Expedite Plant Diagnostics and Overcome PCR Inhibitors. *BioTechniques*, *69*(4), 270–280. https://doi.org/10.2144/btn-2020-0065

Nasko, D. J., Chopyk, J., Sakowski, E. G., Ferrell, B. D., Polson, S. W., & Wommack, K. E. (2018). Family A DNA Polymerase Phylogeny Uncovers Diversity and Replication Gene Organization in the Virioplankton. *Frontiers in Microbiology*, *9*, 3053. https://doi.org/10.3389/fmicb.2018.03053

Nicolini, U., Lalatta, F., Natacci, F., Curcio, C., & Bui, T.-H. (2004). The introduction of QF-PCR in prenatal diagnosis of fetal aneuploidies: Time for reconsideration. *Human Reproduction Update*, *10*(6), 541–548. https://doi.org/10.1093/humupd/dmh046

Niemz, A., Ferguson, T. M., & Boyle, D. S. (2011). Point-of-care nucleic acid testing for infectious diseases. *Trends in Biotechnology*, *29*(5), 240–250. https://doi.org/10.1016/j.tibtech.2011.01.007

Nowak, J. S., & Otzen, D. E. (2024). Helping proteins come in from the cold: 5 burning questions about cold-active enzymes. *BBA Advances*, *5*, 100104. https://doi.org/10.1016/j.bbadva.2023.100104

Oliveira, B. B., Veigas, B., & Baptista, P. V. (2021). Isothermal Amplification of Nucleic Acids: The Race for the Next "Gold Standard." *Frontiers in Sensors*, *2*, 752600. https://doi.org/10.3389/fsens.2021.752600

Olszewski, M., Śpibida, M., Bilek, M., & Krawczyk, B. (2017). Fusion of Taq DNA polymerase with single-stranded DNA binding-like protein of Nanoarchaeum equitans—Expression and characterization. *PLOS ONE*, *12*(9), e0184162. https://doi.org/10.1371/journal.pone.0184162

Paez, J. G., Ming, L., Beroukhim, R., Lee, C. J., Zhao, X., Richter, J. D., Gabriel, S., Herman, P., Saski, H., Altshuler, D., Li, C., Meyerson, M., Sellers, R. W. (2004). Genome coverage and sequence fidelity of 29 polymerase-based multiple strand displacement whole genome amplification. *Nucleic Acids Research*, *32*(9), e71–e71. https://doi.org/10.1093/nar/gnh069

Park, J.-W. (2022). Principles and Applications of Loop-Mediated Isothermal Amplification to Point-of-Care Tests. *Biosensors*, *12*(10), 857. https://doi.org/10.3390/bios12100857

Parvizpour, S., Hussin, N., Shamsir, M. S., & Razmara, J. (2021). Psychrophilic enzymes: Structural adaptation, pharmaceutical and industrial applications. *Applied Microbiology and Biotechnology*, *105*(3), 899–907. https://doi.org/10.1007/s00253-020-11074-0

Raia, P., Carroni, M., Henry, E., Pehau-Arnaudet, G., Brûlé, S., Béguin, P., Henneke, G., Lindahl, E., Delarue, M., & Sauguet, L. (2019). Structure of the DP1–DP2 PolD complex bound with DNA and its implications for the evolutionary history of DNA and RNA polymerases. *PLOS Biology*, *17*(1), e3000122. https://doi.org/10.1371/journal.pbio.3000122

Reha-Krantz, L. J. (2010). DNA polymerase proofreading: Multiple roles maintain genome stability. *Biochimica et Biophysica Acta (BBA) - Proteins and Proteomics*, *1804*(5), 1049–1063. https://doi.org/10.1016/j.bbapap.2009.06.012

Rentergent, J., Driscoll, M. D., & Hay, S. (2016). Time Course Analysis of Enzyme-Catalyzed DNA Polymerization. *Biochemistry*, *55*(39), 5622–5634. https://doi.org/10.1021/acs.biochem.6b00442

Roske, J. J., & Yeeles, J. T. P. (2024). Structural basis for processive daughter-strand synthesis and proofreading by the human leading-strand DNA polymerase Pol ε. *Nature Structural & Molecular Biology*, *31*(12), 1921–1931. https://doi.org/10.1038/s41594-024-01370-y

Sale, J. E., Lehmann, A. R., & Woodgate, R. (2012). Y-family DNA polymerases and their role in tolerance of cellular DNA damage. *Nature Reviews Molecular Cell Biology*, *13*(3), 141–152. https://doi.org/10.1038/nrm3289

Sauguet, L., Raia, P., Henneke, G., & Delarue, M. (2016). Shared active site architecture between archaeal PolD and multi-subunit RNA polymerases revealed by X-ray crystallography. *Nature Communications*, *7*(1), 12227. https://doi.org/10.1038/ncomms12227

Schleper, C., Swanson, R. V., Mathur, E. J., & DeLong, E. F. (1997). Characterization of a DNA polymerase from the uncultivated psychrophilic archaeon Cenarchaeum symbiosum. *Journal of Bacteriology*, *179*(24), 7803–7811. https://doi.org/10.1128/jb.179.24.7803-7811.1997

Shukla, J. L., Husain, A. A., Bhan, S., Singh, L. R., & Kashyap, R. S. (2023). Diagnostic utility of LAMP PCR targeting bcsp-31 gene for human brucellosis infection. *Indian Journal of Medical Microbiology*, *44*, 100354. https://doi.org/10.1016/j.ijmmb.2023.01.012

Siddiqui, K. S., & Cavicchioli, R. (2006). Cold-Adapted Enzymes. *Annual Review of Biochemistry*, *75*(403–33).10.1146/ annurev.biochem.75.103004.142723

Simonsen, S., Søgaard, C. K., Olsen, J. G., Otterlei, M., & Kragelund, B. B. (2024). The bacterial DNA sliding clamp, β-clamp: Structure, interactions, dynamics and drug discovery. *Cellular and Molecular Life Sciences*, *81*(1), 245. https://doi.org/10.1007/s00018-024-05252-w

Sočan, J., Isaksen, G. V., Brandsdal, B. O., & Åqvist, J. (2019). Towards Rational Computational Engineering of Psychrophilic Enzymes. *Scientific Reports*, *9*(1), 19147. https://doi.org/10.1038/s41598-019-55697-4

Soroka, M., Wasowicz, B., & Rymaszewska, A. (2021). Loop-Mediated Isothermal Amplification (LAMP): The Better Sibling of PCR? *Cells*, *10*(8), 1931. https://doi.org/10.3390/cells10081931

Steitz, T. A. (1999). DNA Polymerases: Structural Diversity and Common Mechanisms. *Journal of Biological Chemistry*, *274*(25), 17395–17398. https://doi.org/10.1074/jbc.274.25.17395

Sun, S., Geng, L., & Shamoo, Y. (2006). Structure and enzymatic properties of a chimeric bacteriophage RB69 DNA polymerase and single-stranded DNA binding protein with increased processivity. *Proteins: Structure, Function, and Bioinformatics*, *65*(1), 231–238. https://doi.org/10.1002/prot.21088

Sun, Y., Fu, K., Lin, W., Gao, J., Zhao, X., He, Y., & Tian, H. (2025). Characterization and Engineering of Two Novel Strand-Displacing B Family DNA Polymerases

from Bacillus Phage SRT01hs and BeachBum. *Biomolecules*, *15*(8), 1126. https://doi.org/10.3390/biom15081126

Sun, Y., Ko, D. H., Gao, J., Fu, K., Mao, Y., He, Y., & Tian, H. (2024). Engineering psychrophilic polymerase for nanopore long-read sequencing. *Frontiers in Bioengineering and Biotechnology*, *12*, 1406722. https://doi.org/10.3389/fbioe.2024.1406722

Sundarrajan, S., Parambath, S., Suresh, S., Rao, S., & Padmanabhan, S. (2018). Novel properties of recombinant Sso7d-Taq DNA polymerase purified using aqueous two-phase extraction: Utilities of the enzyme in viral diagnosis. *Biotechnology Reports*, *19*, e00270. https://doi.org/10.1016/j.btre.2018.e00270

Suther, C., Stoufer, S., Zhou, Y., & Moore, M. D. (2022). Recent Developments in Isothermal Amplification Methods for the Detection of Foodborne Viruses. *Frontiers in Microbiology*, *13*, 841875. https://doi.org/10.3389/fmicb.2022.841875

Tabor, S., & Richardson, C. C. (1989). Effect of manganese ions on the incorporation of dideoxynucleotides by bacteriophage T7 DNA polymerase and Escherichia coli DNA polymerase I. *Proceedings of the National Academy of Sciences*, *86*(11), 4076–4080. https://doi.org/10.1073/pnas.86.11.4076

Tahirov, T. H., Makarova, K. S., Rogozin, I. B., Pavlov, Y. I., & Koonin, E. V. (2009). Evolution of DNA polymerases: An inactivated polymerase-exonuclease module in Pol ε and a chimeric origin of eukaryotic polymerases from two classes of archaeal ancestors. *Biology Direct*, *4*(1), 11. https://doi.org/10.1186/1745-6150-4-11

Tan, M., Liao, C., Liang, L., Yi, X., Zhou, Z., & Wei, G. (2022). Recent advances in recombinase polymerase amplification: Principle, advantages, disadvantages and applications. *Front. Cell. Infect. Microbiol.* doi: 10.3389/fcimb.2022.1019071

Topilow, J. S., Ospina Cardona, D., Beck, D. B., Ferrada, M. A., McMahan, Z. H., & Paik, J. J. (2022). Novel genetic mutation in myositis-variant of VEXAS syndrome. *Rheumatology*, *61*(12), e371–e373. https://doi.org/10.1093/rheumatology/keac356

Topka-Bielecka, G., Bloch, S., Nejman-Faleńczyk, B., Grabski, M., Jurczak-Kurek, A., Górniak, M., Dydecka, A., Necel, A., Węgrzyn, G., & Węgrzyn, A. (2020). Characterization of the Bacteriophage vB_EfaS-271 Infecting Enterococcus

faecalis. *International Journal of Molecular Sciences*, *21*(17), 6345. https://doi.org/10.3390/ijms21176345

Topka-Bielecka, G., Nejman-Faleńczyk, B., Bloch, S., Dydecka, A., Necel, A., Węgrzyn, A., & Węgrzyn, G. (2021). Phage–Bacteria Interactions in Potential Applications of Bacteriophage vB_EfaS-271 against Enterococcus faecalis. *Viruses*, *13*(2), 318. https://doi.org/10.3390/v13020318

Urdea, M., Penny, L. A., Olmsted, S. S., Giovanni, M. Y., Kaspar, P., Shepherd, A., Wilson, P., Dahl, C. A., Buchsbaum, S., Moeller, G., & Hay Burgess, D. C. (2006). Requirements for high impact diagnostics in the developing world. *Nature*, *444*(S1), 73–79. https://doi.org/10.1038/nature05448

Wang, M., Liu, H., Ren, J., Huang, Y., Deng, Y., Liu, Y., Chen, Z., Chow, F. W.-N., Leung, P. H.-M., & Li, S. (2023). Enzyme-Assisted Nucleic Acid Amplification in Molecular Diagnosis: A Review. *Biosensors*, *13*(2), 160. https://doi.org/10.3390/bios13020160

Wang, Y. (2004). A novel strategy to engineer DNA polymerases for enhanced processivity and improved performance in vitro. *Nucleic Acids Research*, *32*(3), 1197–1207. https://doi.org/10.1093/nar/gkh271

Weigel, C., & Seitz, H. (2006). Bacteriophage replication modules. *FEMS Microbiology Reviews*, *30*(3), 321–381. https://doi.org/10.1111/j.1574-6976.2006.00015.x

Wommack, K. E., Nasko, D. J., Chopyk, J., & Sakowski, E. G. (2015). Counts and sequences, observations that continue to change our understanding of viruses in nature. *Journal of Microbiology*, *53*(3), 181–192. https://doi.org/10.1007/s12275-015-5068-6

Wu, E. Y., Walsh, A. R., Materne, E. C., Hiltner, E. P., Zielinski, B., Miller, B. R., Mawby, L., Modeste, E., Parish, C. A., Barnes, W. M., & Kermekchiev, M. B. (2015). A Conservative Isoleucine to Leucine Mutation Causes Major Rearrangements and Cold Sensitivity in KlenTaq1 DNA Polymerase. *Biochemistry*, *54*(3), 881–889. https://doi.org/10.1021/bi501198f

Xu, H., Xu, D., & Liu, Y. (2024). Molecular Biology Applications of Psychrophilic Enzymes: Adaptations, Advantages, Expression, and Prospective. *Applied Biochemistry and Biotechnology*, *196*(9), 5765–5789. https://doi.org/10.1007/s12010-023-04810-5

Xue, Y., Braslavsky, I., & Quake, S. R. (2021). Temperature effect on polymerase fidelity. *Journal of Biological Chemistry*, *297*(5), 101270. https://doi.org/10.1016/j.jbc.2021.101270

Yager, P., Domingo, G. J., & Gerdes, J. (2008). Point-of-Care Diagnostics for Global Health. *Annual Review of Biomedical Engineering*, *10*(1), 107–144. https://doi.org/10.1146/annurev.bioeng.10.061807.160524

Yamtich, J., & Sweasy, J. B. (2010). DNA polymerase Family X: Function, structure, and cellular roles. *Biochimica et Biophysica Acta (BBA) - Proteins and Proteomics*, *1804*(5), 1136–1150. https://doi.org/10.1016/j.bbapap.2009.07.008

Yang, N., Zhang, H., Han, X., Liu, Z., & Lu, Y. (2024). Advancements and applications of loop-mediated isothermal amplification technology: A comprehensive overview. *Frontiers in Microbiology*, *15*, 1406632. https://doi.org/10.3389/fmicb.2024.1406632

Yang, W. (2005). Portraits of a Y-family DNA polymerase. *FEBS Letters*, *579*(4), 868–872. https://doi.org/10.1016/j.febslet.2004.11.047

Yang, W. (2011). Nucleases: Diversity of structure, function and mechanism. *Quarterly Reviews of Biophysics*, *44*(1), 1–93. https://doi.org/10.1017/S0033583510000181

Zecchinon, L., Claverie, P., Collins, T., D'Amico, S., Delille, D., Feller, G., Georlette, D., Gratia, E., Hoyoux, A., Meuwis, M.-A., Sonan, G., & Gerday, C. (2001). Did psychrophilic enzymes really win the challenge? *Extremophiles*, *5*(5), 313–321. https://doi.org/10.1007/s007920100207

Zhao, Y., Chen, F., Li, Q., Wang, L., & Fan, C. (2015). Isothermal Amplification of Nucleic Acids. *Chemical Reviews*, *115*(22), 12491–12545. https://doi.org/10.1021/acs.chemrev.5b00428

Zhou, Z.-X., & Kunkel, T. A. (2022). Extrinsic proofreading. *DNA Repair*, *117*, 103369. https://doi.org/10.1016/j.dnarep.2022.103369

10. Scientific Meetings and Trainings

2025 Joanna Morcinek-Orłowska, **Karolina Zdrojewska**, Alicja Węgrzyn, Grzegorz Węgrzyn, Michał R. Szymański, Hold on tight: N-terminal region enables low-temperature activity of phage-derived Efa DNA polymerase,6th BIO Life Science Congress (54th Meeting of the Polish Biochemical Society), 17-20 September 2025, Poznań, Poland

Roksana Dosz, **Karolina Zdrojewska**, Joanna Morcinek-Orłowska, Alicja Węgrzyn, Michał R. Szymański, Szczególne cechy polimerazy DNA Efa pochodzącej z bakteriofaga vB_EfaS-271, IV Sympozjum Bakteriofagowe, 4-6 September 2025, Gdańsk, Poland

Joanna Morcinek-Orłowska, **Karolina Zdrojewska**, Alicja Węgrzyn, Michał R. Szymański, Domena N-terminalna fagowej polimerazy DNA Efa umożliwia aktywność w ujemnych temperaturach, IV Sympozjum Bakteriofagowe, 4-6 September 2025, Gdańsk, Poland

2024 Roksana Dosz, **Karolina Zdrojewska**, Alicja Węgrzyn, Michał R. Szymański, Mechanistic study of Efa DNA polymerase: balancing speed and accuracy, III Sympozjum Bakteriofagowe, 5-7 September 2024, Gdańsk, Poland

Joanna Morcinek-Orłowska, **Karolina Zdrojewska**, Grzegorz Węgrzyn, Alicja Węgrzyn, Michał R. Szymański, Functional studies on the DNA polymerase from vB_EfaS-271 bacteriophage-the role of N-terminal domain in handling secondary structures on DNA template, III Sympozjum Bakteriofagowe, 5-7 September 2024, Gdańsk, Poland

Karolina Zdrojewska, Joanna Morcinek-Orłowska, Roksana Dosz, Grzegorz Węgrzyn, Alicja Węgrzyn, Michał R. Szymański, Structural Insights into Efa DNA Polymerase, 7th DNA polymerases meeting, 27 August- 01 September 2024, Warsaw, Poland

2023 **Karolina Zdrojewska**, Joanna Morcinek-Orłowska, Alicja Węgrzyn, Grzegorz Węgrzyn, Michał R. Szymański, Unlocking the secrets of phage DNA polymerase: A structural analysis of the Efa, EMBO Workshop-Computational Structural Biology, 06-09 December 2023, Heidelberg, Germany

XXVI Biotechnology Summer School: RNA in Biology and Medicine, 11-15 September 2023, Kościerzyna, Poland, Participant

Karolina Zdrojewska, Joanna Morcinek-Orłowska, Alicja Węgrzyn, Grzegorz Węgrzyn, Michał R. Szymański, Biochemiczne I strukturalne badania nowo odkrytej polimerazy DNA, II Sympozjum Bakteriofagowe 07-09 September, 2023, Gdańsk, Poland

2022 Helmholtz Training Workshop on integrative structural Biology, 8-14 October 2022, Berlin-Adlershof & Berlin-Buch, Germany

Karolina Zdrojewska, Joanna Morcinek-Orłowska, Alicja Węgrzyn, Grzegorz Węgrzyn, Michał R. Szymański, Ciekawy przypadek EfaS-271, I Sympozjum bakteriofagowe, 08-10 September 2022, Gdańsk, Poland

Karolina Zdrojewska, Joanna Morcinek-Orłowska, Alicja Węgrzyn, Grzegorz Węgrzyn, Michał R. Szymański, The EfaS-271 will expand our knowledge of bacteriophage genome DNA replication, iNEXT-Discovery 2nd Annual Scientific Meeting, 29-30 August 2022, Warsaw, Poland

Karolina Zdrojewska, Joanna Morcinek-Orłowska, Alicja Węgrzyn, Grzegorz Węgrzyn, Michał R. Szymański, Biochemical and structural studies of newly discovered phage DNA polymerase EfaS-271, Viruses of Microbes Conference, 17-23 July 2022, Guimaraes, Portugal

11. Scholarships and Fellowships

2025 Unrevealing the mysteries of newly discovered DNA polymerase: Kinetics and conformational dynamics, The NAWA Bekker Programme, Washington University in Saint Louis, Supervisor: prof. Roberto Galletto, 01 October 2024-30 September 2025, Saint Louis, USA

12. Lists of Publications

2022 Katarzyna Kosznik-Kwaśnicka, Małgorzata Stasiłojć, Łukasz Grabowski, **Karolina Zdrojewska,** Grzegorz Węgrzyn, Alicja Węgrzyn, Efficacy and Safety of Phage Therapy against Salmonella enterica Serovars Typhimurium and Enteritidis estimated by using a Battery of in vitro Tests and the Galleria mellonella Animal Model, Microbiological Research, 2022, 10.1016/j.micres.2022.127052

Joanna Morcinek-Orłowska, **Karolina Zdrojewska**, Alicja Węgrzyn, Bacteriophage-encoded DNA Polymerase-Beyond the Traditional View of Polymerase Activities, International Journal of Molecular Sciences, 2022, 10.3390/ijms23020635

13. List of patent applications

Joanna Morcinek-Orłowska, Michał Szymański, **Karolina Zdrojewska**, Alicja Węgrzyn, Grzegorz Węgrzyn *Polimeraza DNA Efa, kodująca ją sekwencja kwasu nukleinowego, wektor ekspresyjny zawierający sekwencję nukleotydową kodującą fuzyjną polimerazę DNA Efa, sposób otrzymywania polimerazy DNA Efa oraz zastosowanie polimerazy DNA Efa do izotermicznej amplifikacji DNA w niskich temperaturach* Polish patent application No. P.449897, filed 26 September 2024. Applicant: University of Gdańsk. Published 30 March 2026 (PL449897 A1).

Joanna Morcinek-Orłowska, Michał Szymański, **Karolina Zdrojewska**, Alicja Węgrzyn, Grzegorz Węgrzyn *N-terminal fragment of DNA polymerase, DNA polymerase, method for producing the same, and use thereof for isothermal DNA amplification at low temperatures.* International patent application No. PCT/PL2025/050073, filed 26 September 2025, claiming priority from Polish application P.449897 (26 September 2024). Applicant: University of Gdańsk. Published 2 April 2026 (WO 2026/071892).